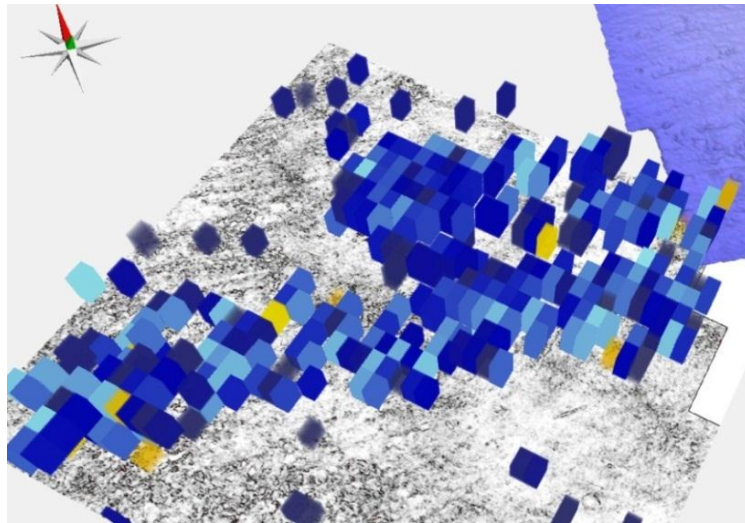




GEO-3900

MASTER'S THESIS IN GEOLOGY

RELATIONSHIP BETWEEN GLACIAL EROSION AND FLUID FLOW
INFERRED FROM 3D SEISMIC DATA, SW BARENTS SEA



Alexey Deryabin

May, 2012

FACULTY OF SCIENCE AND TECHNOLOGY
Department of Geology
University of Tromsø

GEO-3900

MASTER'S THESIS IN GEOLOGY

Relationship between glacial erosion and fluid flow
inferred from 3D seismic data, SW Barents Sea

Alexey Deryabin

May, 2012

ABSTRACT

This Master thesis investigates the relationship between glacial erosion, glaciotectonically displaced sediment blocks and indications of fluid flow and shallow gas accumulations in buried glacial sediments of the south-western Barents Sea margin. The thesis is based on two three-dimensional (3D) seismic datasets, NH98003 and EL0001, the two-dimensional (2D) seismic survey NH9702 and exploration well 7216/11-1. 3D seismic techniques have allowed mapping and visualizing of buried geomorphological features in great details within the study area. Large semi-circular depressions and fluid migration pathways are imaged, as well as glacial sediment blocks and rafts. A glacial origin is inferred for the megablocks and rafts indicating high glaciotectonic activity of the former ice streams. Six large-scale depressions are inferred to be sources for the removal of sediment mega-blocks and rafts at one particular stratigraphic level of the Plio-Pleistocene succession. Mapped fluid migration pathways and shallow gas accumulations show evidence of an active fluid migration system, and its spatial relationship with the erosional depressions is documented. Modeling of the gas hydrate stability zone has been performed for glacial and interglacial conditions and its effect on the sediment properties is discussed. A conceptual model is proposed for the formation of the depressions, where brittle glaciotectonic deformation along a weak layer at the base of gas-hydrate cementing sediments is inferred. Subsequent expulsion of gas-rich fluids is assumed to have followed deglaciation which might further have reworked the depressions.

Что касается меня,
то я знаю только то,
что я ничего не знаю.

Сократ, 410 год до н. э.

As for me, all I know is that I know nothing.

Socrates, 410 BC

ACKNOWLEDGMENTS

First and foremost, I would like to acknowledge my supervisor Professor Karin Andreassen and “GlaciBar” project for giving me the opportunity to write this Master’s Thesis. I want to thank and extend my gratitude to Karin for the technical and mental support, constructive corrections and guidance through the exiting year. I’m grateful for her contribution to my academic and personal development and for opportunity to visit the northernmost point on Earth I’ve ever been during research cruise.

I also want to thank Michael D. Max and Christine Fichler for the inspiring conversations and shearing their knowledge, as well as for input in my constant search for new ideas and publications.

I would like to show my appreciation to fellow MSc students and PhDs especially in office14 whose diversity in knowledge and skills contributed tremendously to my studying in Tromsø.

Special thanks go to Alexander, Morten, Sunil, Torgeir, Marianne, Malin and Liselott, whose untamed energy was keeping me busy aside of the studies and for their company in discovering the Polar Norway.

I am really grateful to whole my family and parents in particular for their blessings and for being supportive and encouraging throughout my education.

Finally, yet importantly, author wishes to express his love and gratitude to his fiancée Marina for inspiration, endless love and patience through these years.

Contents

1	Introduction	1
1.1	Objectives.....	1
1.2	Study area.....	2
1.3	Tectonic and stratigraphic development of the SW Barents Sea.....	4
1.4	Lithostratigraphy of the South-western Barents Sea.....	10
1.5	Glacial evolution of the Barents Sea continental margin.....	15
1.6	Glaciotectonic processes and mechanisms.....	21
1.7	Subsurface fluid migration, trapping and expulsion	24
1.8	Gas hydrate formation and stability field.....	28
2	Data and methods	32
2.1	Seismic datasets	32
2.2	Artifacts	37
2.3	Interpretation tools.....	39
2.4	Volumetric 3D Seismic attributes.....	40
2.5	Well Data.....	43
3	Results	44
3.1	Geomorphological features on the 3D seismic data	44
3.2	Interpreted seismic horizons.....	49
3.3	Buried glaciotectonic features	65
3.4	Fluid flow migration pathways.....	76
3.5	Gas hydrate stability zone (GHSZ) modeling	87
4	Discussion	91
4.1	Relationship between palaeo ice stream flow and sediment blocks.....	91
4.2	Relationship between the sediment blocks and depressions	95
4.3	Relationship between the depressions and indications of fluid migration.....	98
4.4	Hypothesis for the formation of the buried depressions.....	102
5	Conclusions	113
6	References	115

1 Introduction

1.1 Objectives

Preliminary observations suggest that glaciotectionic erosion at the SW Barents Sea margin may be associated with underlying shallow gas accumulations and fluid flow. This Master thesis aims at investigating if such a relationship can be established based on two three-dimensional (3D) datasets, several 2D lines and one well, located at the SW Barents Sea continental margin (Fig. 1.1). Large erosional depressions and glaciotectionic megablocks and rafts occur commonly in the glacial sediments of this area, and so do also indications of fluid flow and shallow gas accumulations (Andreassen et al. 2007a). Previous Master theses at University of Tromsø have studied fluid flow (Pless, 2009) and glacial features (Sanchez-Borgue, 2009) in part of the study area, but this thesis is the first study focusing on the relationship between fluid flow and glacial erosion.

It has been a main objective to visualize the spatial relationship between large glacial erosional depressions, glaciotectionically displaced sediment blocks and indications of fluid flow and shallow gas accumulations in the study area. Lithostratigraphic and structural controls on fluid migration and gas accumulations have been evaluated based on available well information and seismic data. It has also been evaluated if gas hydrates could have been involved in glacial erosion, and the gas hydrate stability field and its changes between glacial periods and interglacials has been modeled and discussed. Based on the results, a conceptual model is suggested for formation of the large depressions observed and their relationship with sediment blocks and fluid flow features.

1.2 Study area

The study area of this thesis is located in the south-western Barents Sea (*Fig.1.1*). The Barents Sea is an epicontinental sea at the north-western part of the Eurasian continent. The continental shelf area of this water body covers about 1.4×10^6 km² and has an average depth of around 250 meters with deepest parts reaching up to 500 meters (Solheim and Elverhøi, 1993).

The Barents Sea occupies the shelf area between Norway and Svalbard on western margin and between Timan-Pechora coast and Franz Joseph Land on eastern side. (Henriksen et al., 2011b). It is bounded in the west by the Norwegian-Greenland Sea and Novaya Zemlya in the east, whereas northern limit is defined by the deeper waters of the Nansen Basin in the Arctic Ocean.

Generalized bathymetry of the Barents Sea shelf is comprised of shallow banks and over-deepened troughs. The bank areas are about 200-300 m deep and troughs are around 400 m water depth. Water depth in the study area is from 280m to 500 m and the seafloor is dipping towards west-northwest. Partly large-scale bathymetric features resemble structural trends of underlying bedrocks, and in particular reflect Late-Cenozoic erosion due to uplift and more recent glacial erosion by the Quaternary ice sheets (Elverhøi et al., 1998). The ice sheets left their imprints of elongated troughs carved into the sedimentary bedrock and sediments by *ice streams* – zones of fast-flowing ice within more stagnant surrounding ice, as inferred for the Bear Island Trough (Laberg and Vorren, 1996; Vorren and Laberg, 1997; Andreassen et al., 2007,b). The most prominent morphological features are the Storfjord Trough and the larger Bear Island Trough (Bjørnøyrenna) are lying to the north and south of the Bear Island respectively (*Fig.1.1 A*). These bathymetric lows about 400 m deep lead towards large fan-shaped aprons called Trough Mouth Fans (TMF) (Vorren et al., 1988; Vorren and Laberg, 1997).

Location of the study area (*Fig.1.1*) allows to investigate the glacial history and evolution of the Barents Sea Ice Sheet (BSIS) by studying preserved sediment record on the western continental margin, located at the Bjørnøya Trough Mouth Fan (TMF). Regional seismic surveys indicate extensive shelf break progradation into the Norwegian Sea basin during Plio-Pleistocene, caused by erosion and sediment supply by ice streams draining the BSIS (Fiedler and Faleide, 1996).

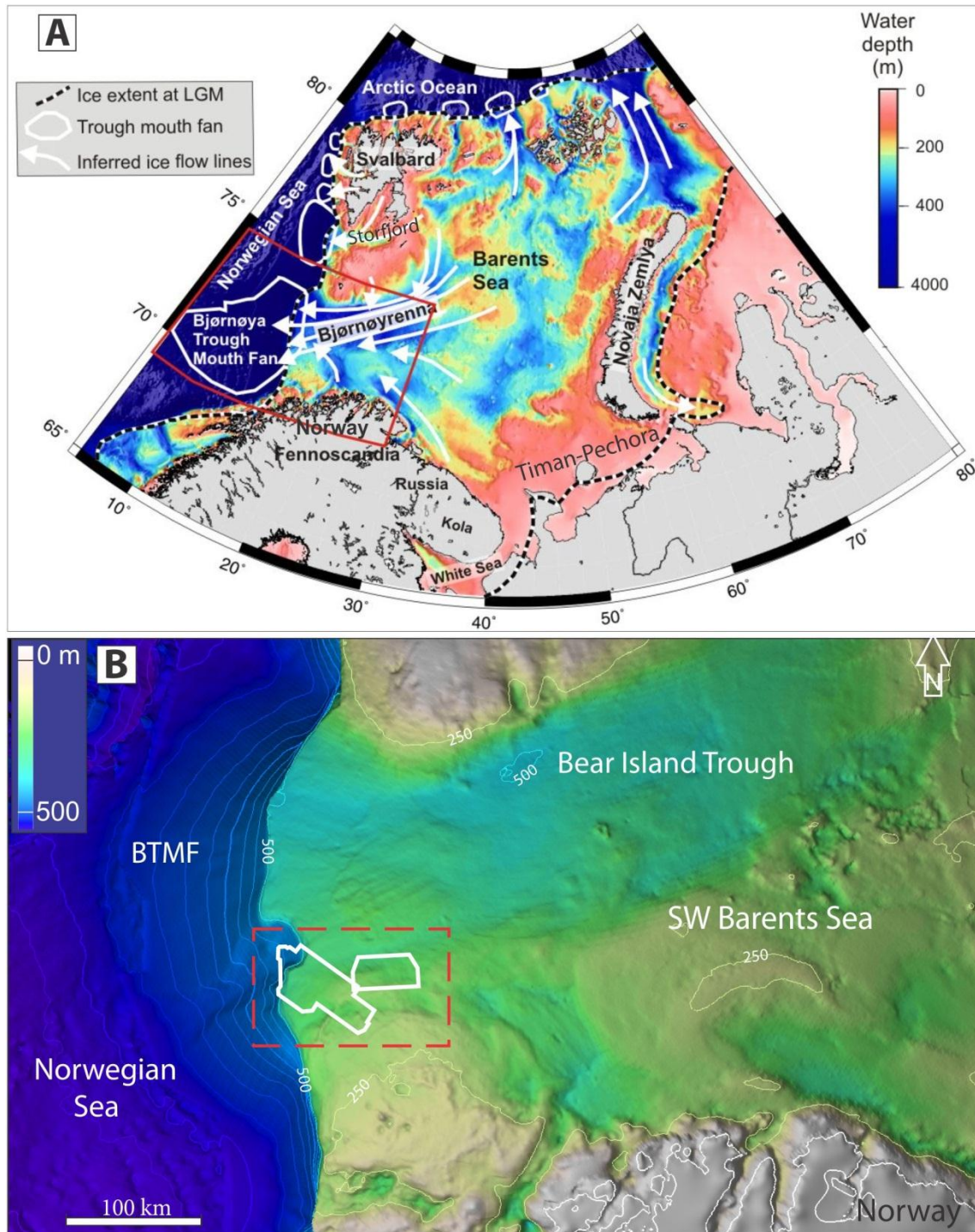


Figure 1.1 A) Map showing location of the study area (red box) and extent of the Last Glacial Maximum Barents Sea and Fennoscandian Ice Sheets. Flow lines of major ice streams are indicated by white arrows, modified from Andreassen and Winsborrow (2009). **B)** Shaded bathymetry map of the SW Barents Sea, with location of the study area indicated by the red dashed rectangle. White polygons show location of the 3D surveys used. BTMF indicates location of the Bear Island Trough Mouth Fan.

1.3 Tectonic and stratigraphic development of the SW Barents Sea

The Barents Sea continental shelf has undergone complex evolution and for convenience its history is subdivided on two sub-chapters: structural and stratigraphic development.

1.3.1 Tectonic development of the south-western Barents Sea

The study area in SW Barents Sea, belonging to the northern part of the post-Caledonian North Atlantic rift province, and it covers the southern part of the Veslemøy structural High and central part of the Sørvestsnaget Basin (Fig. 1.2).

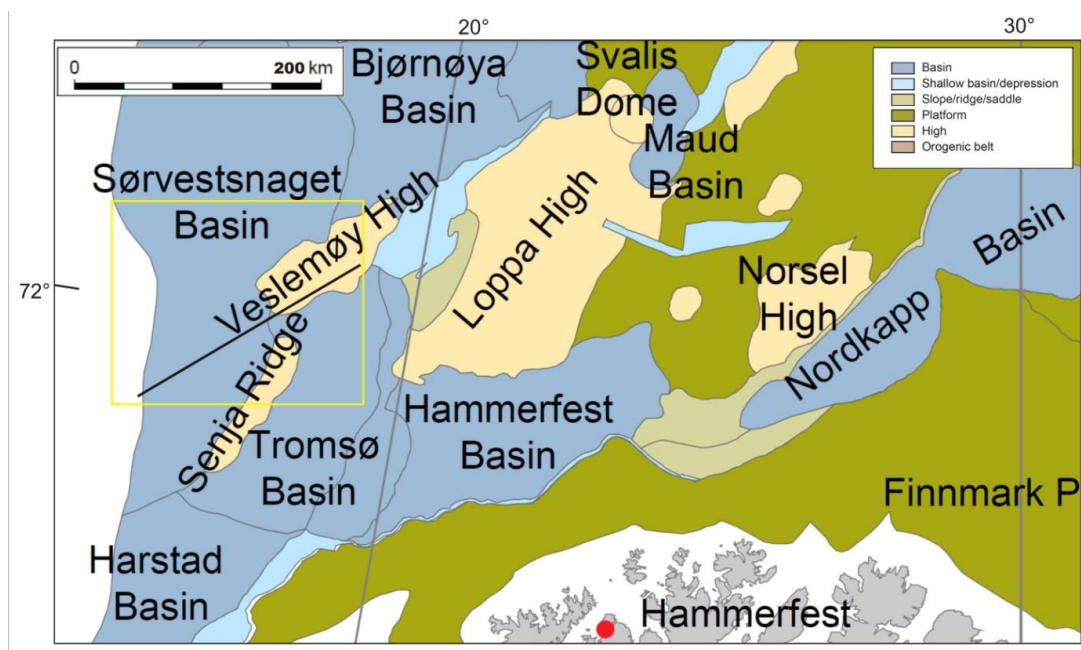


Figure 1.2 Map of general structural elements in the SW Barents Sea. Location of the study area is indicated with a yellow rectangle. The black line within study area indicates position of the profile in Fig.1.5. Modified from Henriksen et al. (2011a)

The area has a complex basin development history and has gone through several phases of tectonism since Devonian times. Figure 1.3 sheds light on the geodynamic evolution of the North-Atlantic and Arctic regions. The following basin development stages are indicated for SW Barents province: 1) Late Devonian – Middle Carboniferous rifting, 2) Late Carboniferous – Permian Carbonate platform development, 3) Triassic – Cretaceous siliciclastic shelf development, 4) Early Cenozoic crustal break-up, and 5) Late Cenozoic passive margin development (Ryseth et al., 2003).

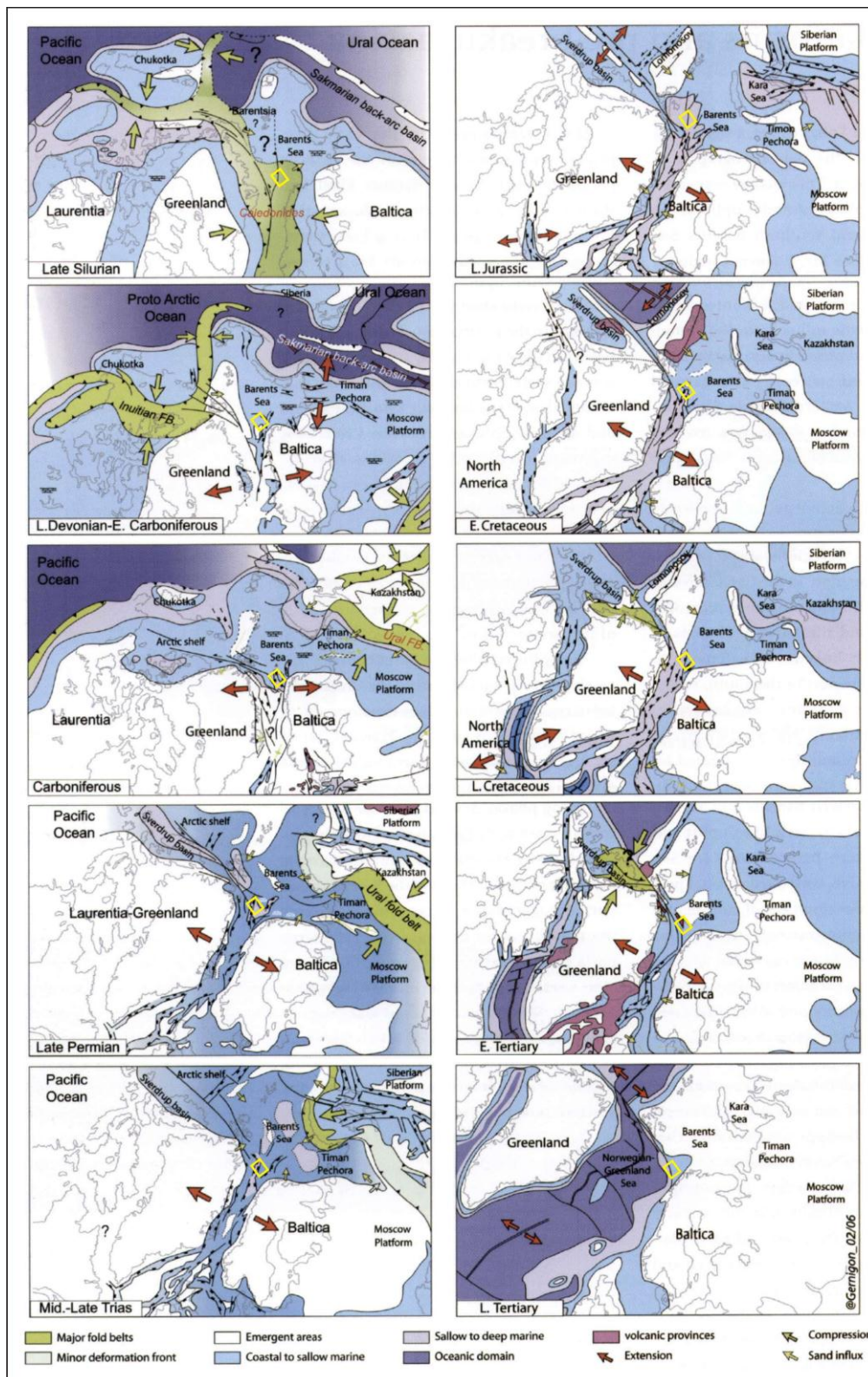


Figure 1.3 Schematic diagram of the geodynamic evolution of the Atlantic–Arctic region since Late Paleozoic until the Late Tertiary. The study area is indicated by the yellow square, modified from Smelror et al. (2009).

Late Paleozoic to Early Mesozoic

Caledonide consolidated basement is indicated to underlay Late Paleozoic strata and its structural grain has influenced formation of a Carboniferous rift system (Gudlaugsson et al., 1998). A 600 km long, fan-shaped rift zone extended in NNE direction and was direct continuation of northeast Atlantic rift system separating Fennoscandia and Greenland at that time (Fig. 1.3). This rift zone, which underlies the present day western margin, had a northerly orientation and is comprised of deep-faulted rift basins and intrabasinal highs. The Veslemøy High is interpreted to originate at this stage of Late Paleozoic development, consisting of tilted basement block at its core. Since Late Carboniferous throughout Permian, tectonic development of the area was characterized by regional subsidence and post rift sedimentation. Though tectonic reactivation took place in Permian to Early Triassic leading to North trend rift structures formation (Gudlaugsson et al., 1998).

Mesozoic era

Mesozoic tectonic development of the south-western Barents Sea is characterized by rifting and basin formation. The period is subdivided into two main tectonic phases: the Mid-Kimmerian and Late-Kimmerian (Faleide et al., 1993). The Mid-Kimmerian tectonic phase of Mid to Late Jurassic age (Faleide et al., 1984), led to formation of basins bounded by normal faults and sync-rift sedimentation.

The Late-Kimmerian phase lasted from Late Jurassic to Early Cretaceous and contributed to the tectonically induced low stand in relative sea level, resulted in a regional unconformity for entire North Atlantic (Faleide et al., 1993). Following the Kimmerian rifting epoch entire SW Barents Sea was subjected to rapid subsidence since Early Cretaceous and resulted in formation of major depocenters in Sørvestsnaget, Bjørnøya and Tromsø basins, surrounding Veslemøy high (Breivik et al., 1998). Consequent uplift of the Svalbard archipelago to the north of the area in Late Cretaceous shed sediments into deeply subsiding sag basins (Faleide et al., 1984; Ryseth et al., 2003).

Cenozoic to present

The Cenozoic tectonic development of the south-western Barents Sea margin can roughly be subdivided in two stages: i) Early Cenozoic to Miocene tectonic activity due to continental

break-up and ii) Pliocene to present passive continental margin development (Faleide et al., 1984; Gabrielsen et al., 1990; Ryseth et al., 2003).

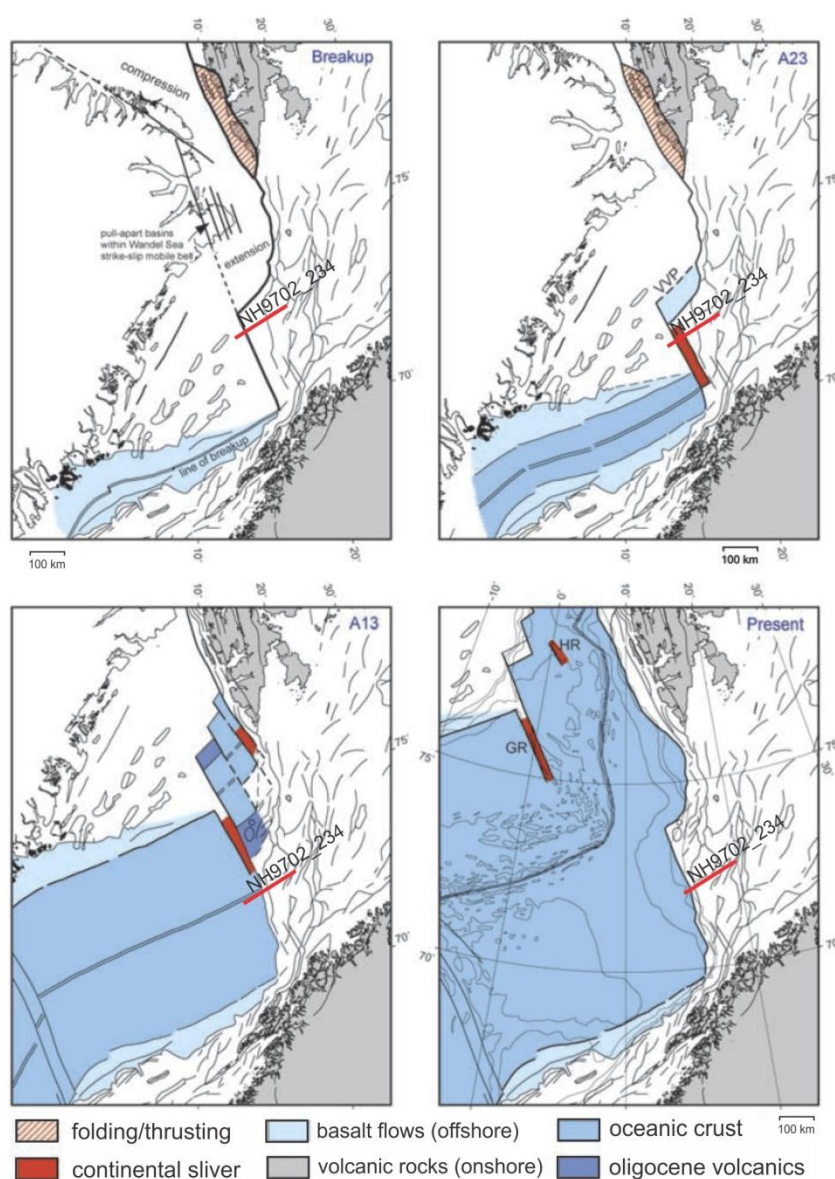


Figure 1.4 Cenozoic plate tectonics reflecting stages of the Norwegian-Greenland Sea opening from break-up until present. Red line indicates approximate position of the 2D seismic line NH9702_234 shown in Fig. 1.6. GR: Greenland Ridge, HR: Hovgaard Ridge, VVP: Vestbakken Volcanic Province, modified from Faleide et al. (2008).

During Early Paleocene – early Eocene times Sørvestnaget Basin underwent significant subsidence as an independent sedimentary basin, with Veslemøy High forming syn-phase (contemporary) bathymetrical high (Ryseth et al., 2003). The entire south-western Barents Sea was subjected to the complex transform setting with dextral shear of N–NW orientation along Senja Fracture Zone (SFZ) (Fig. 1.4) with continuation further North (Faleide et al.,

Introduction

1991; Faleide et al., 1993). During Early Eocene, associated with onset of sea floor spreading, development of strike-slip tectonic regime occurred. It led to significant extensional faulting, and was followed by the footwall uplifting formed marginal high (Fig1.5) within Sørvestsnaget Basin (Sættem et al., 1994; Ryseth et al., 2003).

Opening of the Norwegian- Greenland Sea continued to be the dominant force influencing tectonic evolution of the SW Barents margin throughout Tertiary. Shifts from extensional to compressional tectonic movement in Oligocene was likely related to the spreading poles reorganization, resulting in inversion structuring of the Veslemøy High (Gabrielsen et al., 1990; Ryseth et al., 2003). The final phase of the SW Barents Sea margin evolution is expressed in an Upper Pliocene-Pleistocene clastic sedimentary wedge attributed to subsidence of the area and passive continent-ocean boundary development (Vorren et al., 1991). However pronounced unconformity at the base of the wedge was induced by regional uplift and eustatic sea level fall related to onset of glaciations. Subsequently Sørvestsnaget Basin, Veslemøy High and areas along the western margin experienced subsidence due to sediment load supplied from still uplifted areas to the East, and affected by minor movements due to isostatic load, associated with the Plio-Pleistocene glaciations (Sættem et al., 1994; Ryseth et al., 2003). Figure 1.5 below provide diagram of vertical movement restored to the time equivalent phases, based on the seismic stratigraphy analysis (Ryseth et al., 2003).

More detailed glacial development of the SW Barents Sea margin is covered in chapter 1.5 later in this thesis.

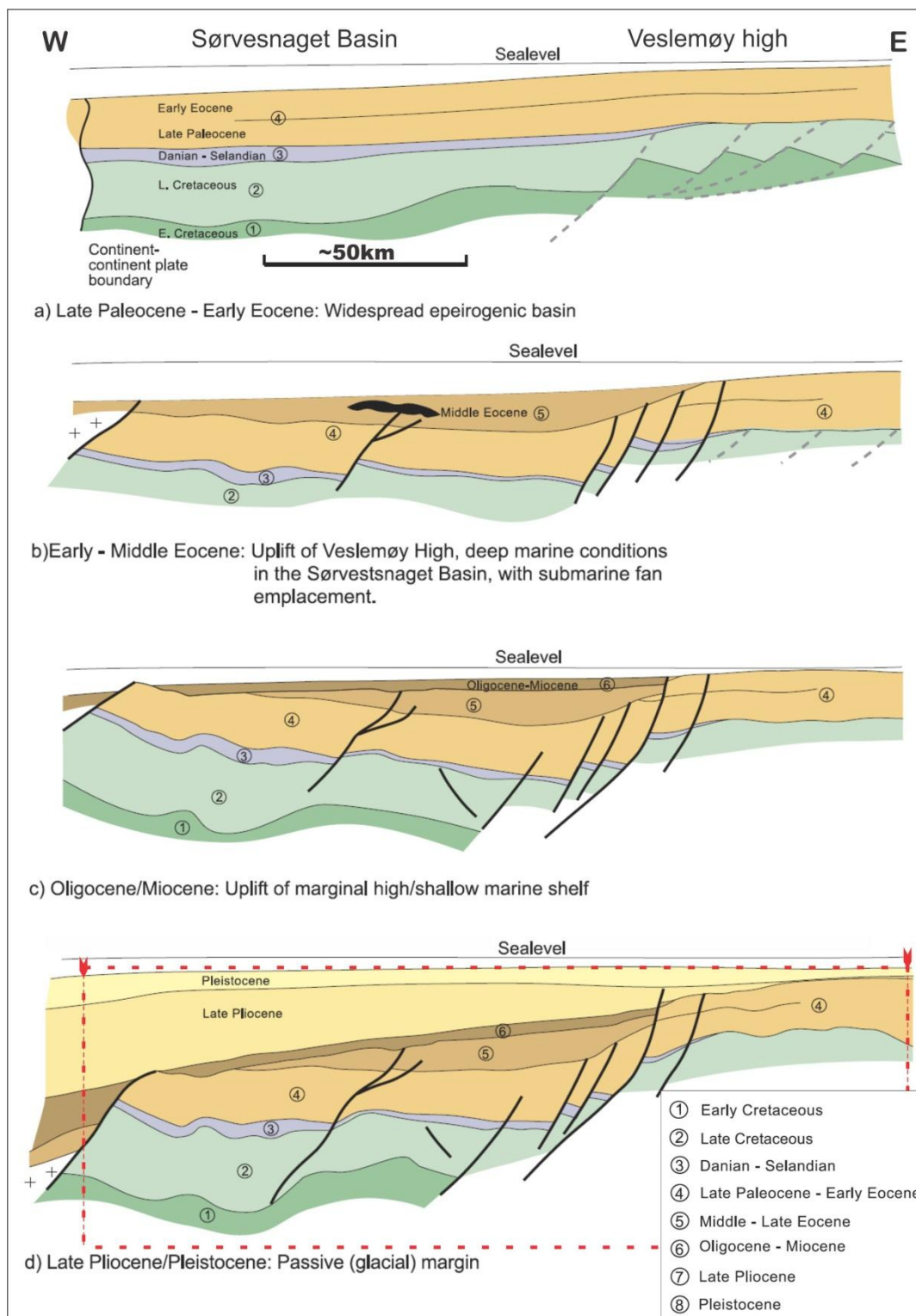


Figure 1.5 Tectonostratigraphic model showing main stages in evolution of the Sørvestsnaget Basin and Veslemøy High development during Cenozoic time. Red arrows indicate lateral extent of the two 3D surveys used in this study, modified from Ryseth et al. (2003). Location of the line is indicated in Fig. 1.2.

1.4 Lithostratigraphy of the South-western Barents Sea

Stratigraphic framework for the SW Barents Sea was established in early 90's (Gabrielsen et al., 1990) when the first well and core data became available, and were tied to seismic profiles. Later, two dimensional (2D) seismic data acquired in by the "Barents Sea Project" (1997-1998) and followed by the drilling of the well 7216/11-1S, gave a solid database for lithostratigraphic framework of the SE Barents Sea margin. The well penetrated Early Paleocene sediments and nine units were subdivided in the study area based on the stratigraphy established by Ryseth et al. (2003) (Fig.1.6). This thesis is focused on Cenozoic succession which will be covered later in this chapter.

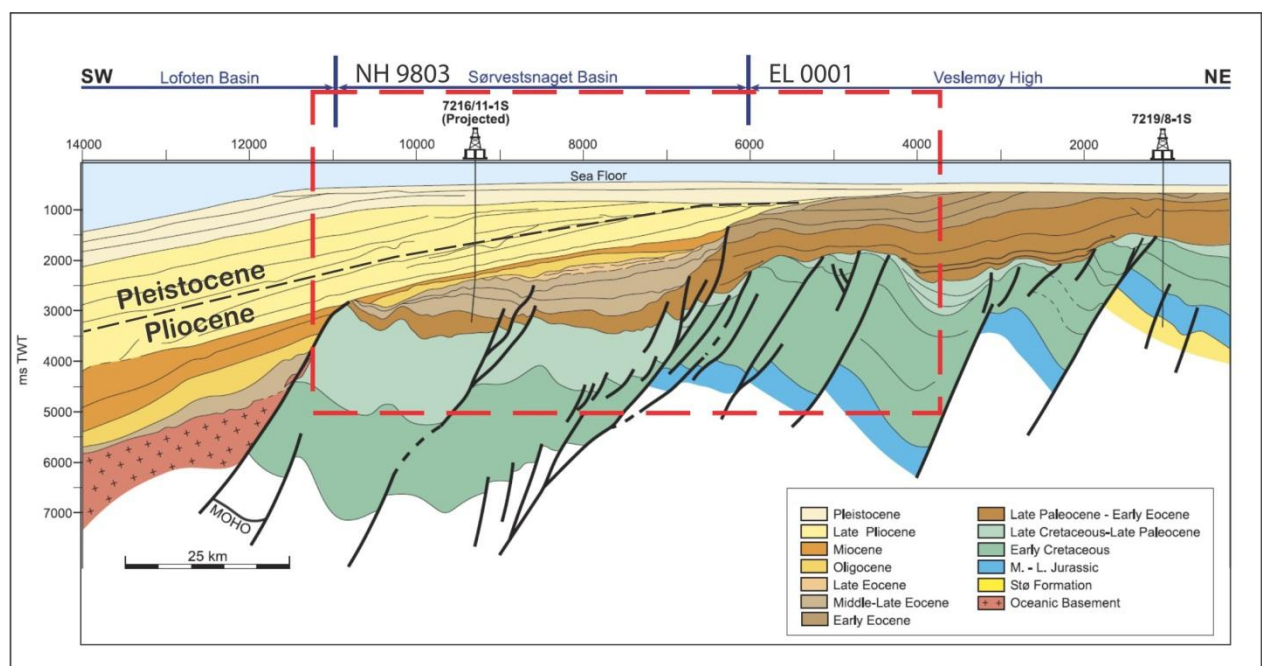


Figure 1.6 Lithostratigraphy of the western margin interpreted based on geo-seismic line NH9702_234 shown in Fig. 1.1 and boreholes 7216/11-1S and 7219/8-1S. Approximate projection of 3D surveys NH9803 & EL0001, used in this study, indicated by the red rectangle (modified from Ryseth et al. 2003). The Plio-Pleistocene boundary was updated by Andreassen et al. (2007a) and its approximate position is indicated by black dashed line.

Late Mesozoic sedimentation was characterized by significant subsidence and accumulation of the Lower Cretaceous sequence of about 1-3 km thick, extending over the Veslemøy High, Sørvestsnaget, Tromsø and Bjørnøya Basins (Dalland et al., 1988).

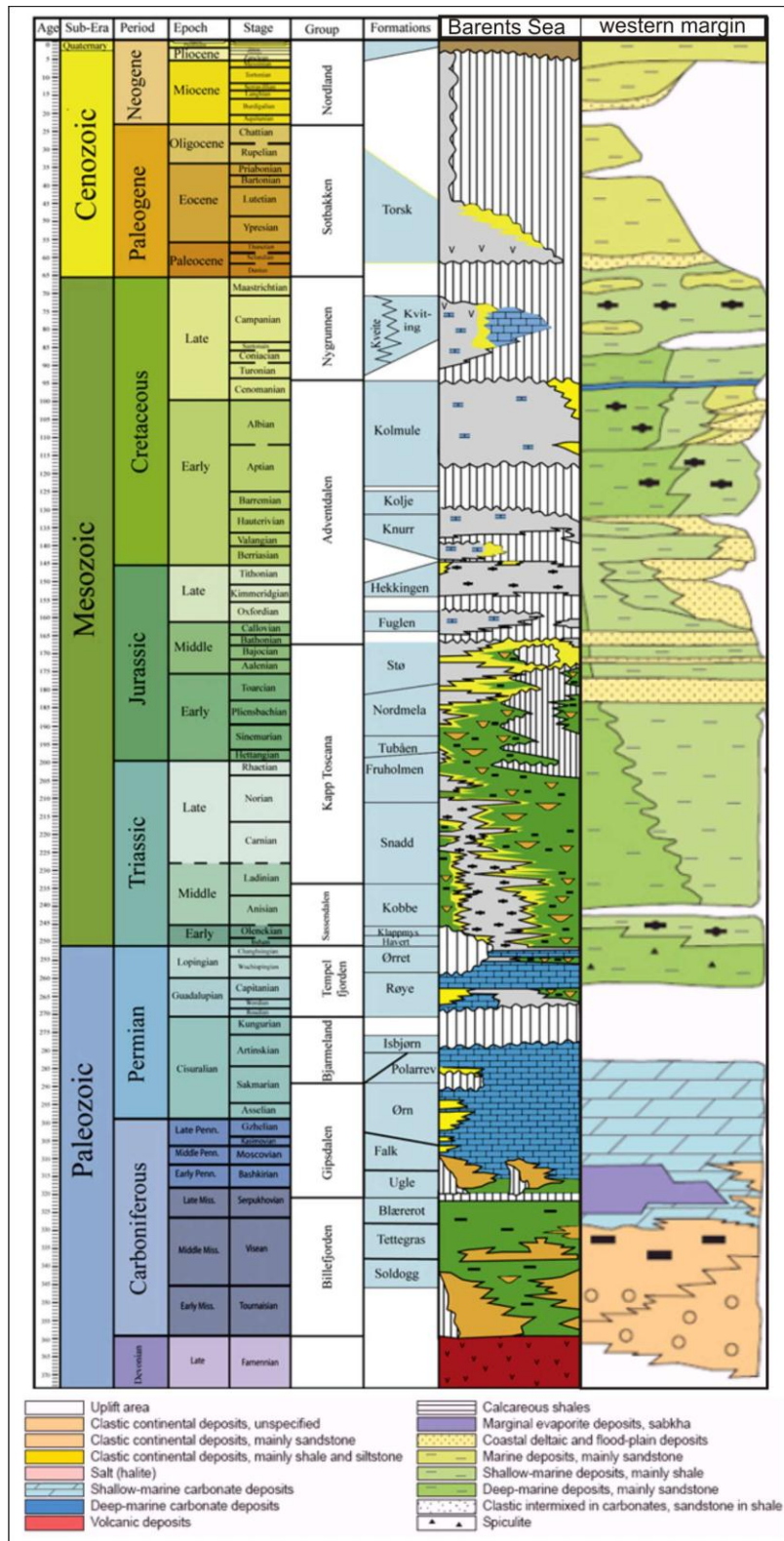


Figure 1.7 Lithostratigraphic charts for the SW Barents Sea showing in addition lithostratigraphy at the western margin. Figure modified from Smelror et al. (2009) and Glørstad-Clark et al. (2010).

SW Barents Sea basins were in distal position to the prograding from the North-East deltaic systems and dominated by fine grained marine sediments. These sediments comprise

Introduction

Kolmule and Kolje formations consisting of condensed mudrocks and organic-rich shale's of Barremian age, which might represent potential source rock (Dalland et al., 1988; Smelror et al., 2009).

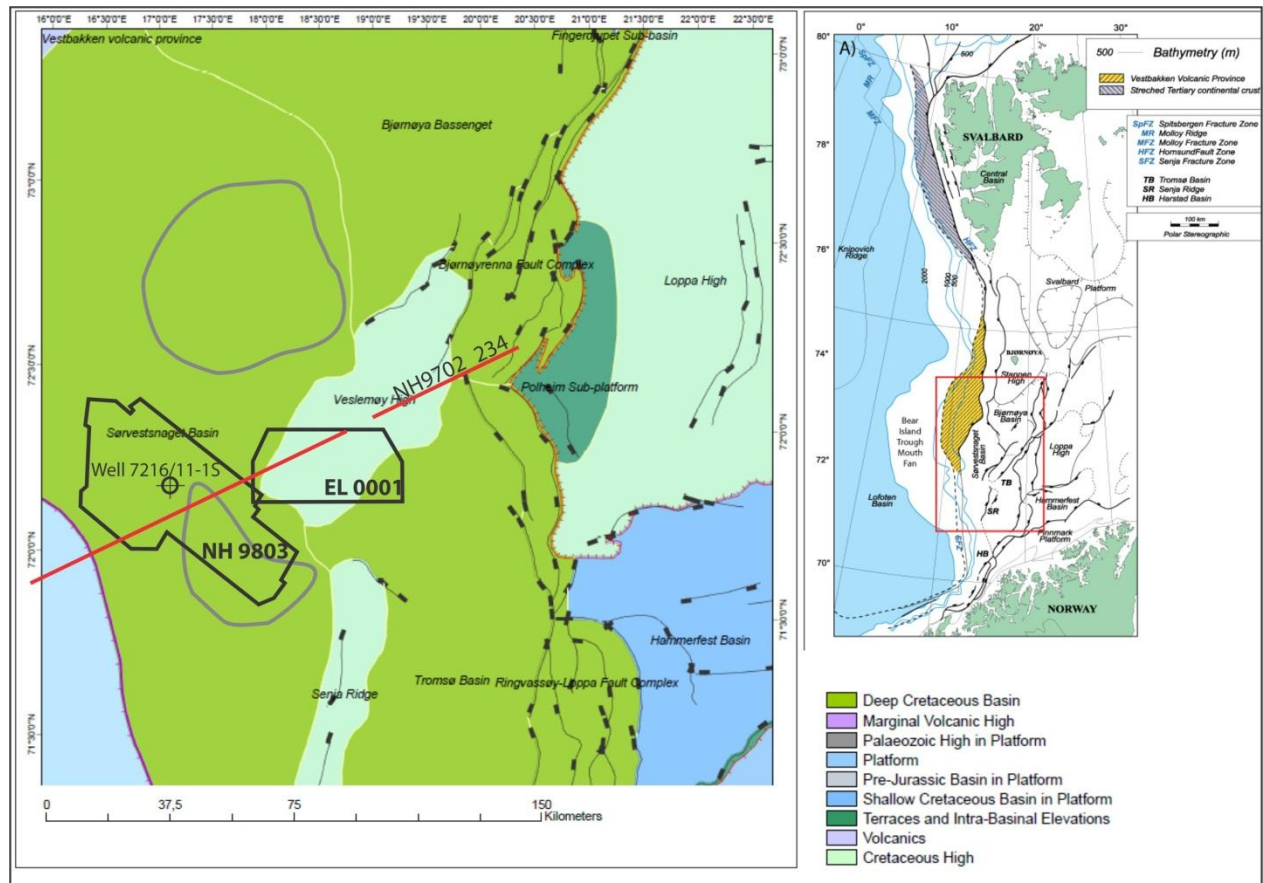


Figure 1.8 Structural map showing location of the well 7216/11-1S, 2D seismic line NH9702_234 and 3D seismic surveys NH9803 and EL0001 superimposed over main structural elements of the study area. Grey boundaries indicating depocenters within Sørvestnaget Basin, modified from Ryseth et al. (2003) and NPD (2011).

Barremian to Albian times are characterized by thick successions consisting mainly of shale, siltstone and minor sandstones, comprising the Kolmule Formation (Fig. 1.7). From the Maastrichtian to Paleocene western margin basins experienced compressional tectonic movements leading to depositional breaks and low sedimentation rates (Faleide et al., 1993; Smelror et al., 2009). Tertiary development and sedimentation is associated with break-up related movements and uplift of central Barents Sea shelf towards Eocene (Smelror et al., 2009). Vertical movement was followed by transgression leading to deposition of fine grained marine sediments over SW Barents Sea margin. As indicated from the prospecting

well 7216/11-1S, Sørvestsnaget Basin comprises rather full succession of Cenozoic sediments. Paleocene to Lower Eocene sediments inferred to consist entirely of grey to olive-colored claystones with minor siltstones indicative for low energy environment deposition of deep marine shelf (Ryseth et al., 2003). In contrast Eocene successions show periods of much more active clastic deposition related to the sediment laden gravity flows.

Middle Eocene consists of a significant sandstone unit (Fig1.9) deposited in a submarine fan setting, which was penetrated by the well 7216/11-1S at depth interval 2888- 3102 m MSL. A likely source suggested for the sandstones in Sørvestsnaget Basin is local intrabasinal supply from the uplifted Stappen High to the northeast, although a potential Fennoscandian source is not excluded (Ryseth et al., 2003).

Late Eocene is inferred to consist of grey green and dark mudrocks with stringers of limestone deposited from suspension fallout in a low-energy environment. Significant shallowing occurred towards the beginning of the Oligocene. Such shallow marine conditions persisted throughout Oligocene-Miocene times with deposition of condensed section comprised of mudrocks and limestones with minor fine-grained sandstones (2246 – 2444 m MSL in Fig.1.9).

The Late Pliocene-Pleistocene unit is lying with unconformity on older strata and encountered in the bore hole at interval 361 – 2246 m mean sea level (MSL). Prevailing lithology is comprised of grey clays and clay stones with minor interbedding sandstones. Glacimarine depositional environment is inferred to the lower parts of the Neogene wedge by several studies (Vorren et al., 1991; Sættem et al., 1994; Faleide et al., 1996; Ryseth et al., 2003) and upper part is interpreted to be deposited subglacially (Sættem et al., 1992; Andreassen et al., 2004; Andreassen et al., 2007,b). This westward progradation wedge is interpreted to be comprised of the sediments eroded from the Barents Sea shelf during the Quaternary glaciations (Vorren et al., 1988; Vorren et al., 1991).

1.5 Glacial evolution of the Barents Sea continental margin

The Barents Sea continental margin has been affected by several glaciations during the Plio-Pleistocene, with ice sheets reaching the shelf break. Glaciations of the Barents Sea shelf are manifested in deposition of the clastic glacial wedge along the margin since Late Pliocene (Sættem et al., 1994; Faleide et al., 1996). The main depositional centers of the glacial sediments were located at the trough mouth fans (TMF) (Vorren et al., 1991).

Table 1.1 Seismic sequences divided along Barents Sea – Svalbard margin and their correlation based on age constrains. Correlation between several publications is modified from Larsen et al. (2003).

Vorren et al.(1991) ¹ Richardsen et al.(1992) ² Knutsen et al.(1992) ²	Eidvin & Riis (1989) Eidvin et al.(1993)	Laberg & Vorren (1995)	Sættem et al. (1991) Sættem et al. (1992) Sættem et al. (1994)	Rafaelsen et al.(2002)	Vorren et al.(1990)	New 3D seismic stratigraphy (NH9803)	Faleide et al.(1996)	Butt et al. (2000)	Andreassen et al. 2007 Knies et al. 2009 This study		
TeE	↑	VIII	G	E					GIII		
		VII 24-12 ka	F <30 ka E <130 ka	— D	4W	H					
		VI 194-128 ka	D ₂ <200 ka	C B	3W	G	Ref.l.bH Ref.l.bG				
		V 313-258 ka	D ₁	A	2W	F					
		IV 386-359 ka	C <330 ka				Ref.l.bF				
		III -486-430 ka	B	?	1W	E					
		II -544-521 ka									
		I -622-589 ka	<0.44 Ma		0.8 Ma	Ref.l.bE	R1—0.44 Ma	R1—0.2-0.44 Ma			
		TeD	↑ Late Pliocene/ Pleistocene			D	Ref.l.bD	R2		R2—0.5 Ma	GII
						C		R3		R3—0.78 Ma	
						R4	R4—0.99 Ma				
					Ref.l.bC	R5	R5—1.0 Ma	R5—1.3-1.5 Ma			
TeC	↓ Late Pliocene/ Pleistocene					B	Ref.l.bB	R6	R6—1.6-1.7 Ma	GI	
						A		R7	R7—2.3 Ma		R7—2.3-2.5 Ma
3.0/5.5 ² Ma	Reflector 2		A ₀								
15.5 Ma	Reflector 3										

The glacial sedimentary wedge of the Barents Sea is subdivided by regionally correlatable reflectors into three stratigraphic units: GI, GII, and GIII, with GI to be lowest in the stratigraphy (Table 1.1; Fig. 1.10) (Faleide et al., 1996). Within aforementioned Plio-Pleistocene succession, seven regionally correlatable reflectors were identified, starting from

the oldest R7 and up to youngest R1 (Faleide et al., 1996; Andreassen et al., 2007,a). Age constrains for the Barents Sea – Svalbard margin are acquired from several key sources: ODP Site 986 (Butt et al., 2002; Larsen et al., 2003) location shown in Fig 1.4.2, seismic correlation to commercial wells (Faleide et al., 1996; Ryseth et al., 2003), and shallow drillings (Sættem et al., 1992; Sættem et al., 1994), although a bit uncertain due to lateral extrapolation.

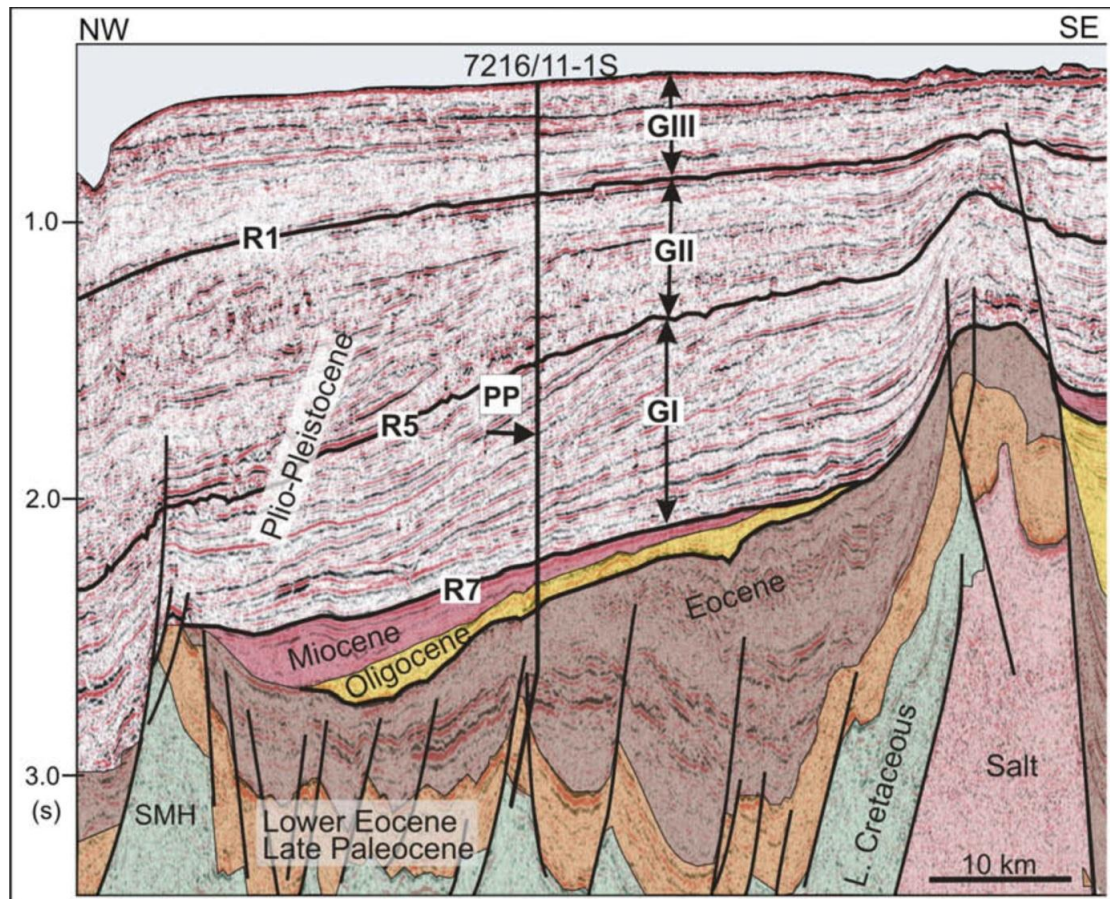


Figure 1.10 Generalized stratigraphy at the location of well 7216/11-1S shown for the inline within NH9803 3D survey across the southwestern Barents Sea margin. Seismic sequences GI, GII, GIII and main reflectors R7, R5, R1 are indicated within Plio-Pleistocene package. PP arrow marks Pliocene-Pleistocene transition boundary, from Andreassen et al. (2007,a).

Reflector R7 represents the unconformity at the base of the sedimentary clastic wedge and marks onset of glacial deposition which has been dated to 2.3 – 2.7 Ma (Knies et al., 2009). Reflector R5 was assigned the interpolated age of 1.3-1.5 Ma at the ODP Site 986 (Butt et al., 2002). Reflector R1 lies in age estimates between 440 Ka and 200 Ka obtained respectively by Sættem et al. (1992) and Elverhøi et al. (1998). Obtained age estimates for the Plio-Pleistocene package is correlated to the well 7216/11-1S located in the study area. Figure 1.10 shows regionally correlated reflectors interpreted for the glacial wedge and

underlying strata. Knies et al. (2009) has inferred three main stages of glaciations over entire Barents and Fennoscandia region, covering time span of the last 3.5 Ma.

An initial growth phase lasting from about 3.5 to 2.4 Ma (Fig. 1.11 A) was characterized by initial onset of glaciations in the Northern hemisphere. Glacial growth was confined to the sub-aerially exposed northern parts of the Barents Sea (Butt et al., 2002; Knies et al., 2009), with consequent release of the eroded sediments at the coast line. Limited extend of the glaciers is indicated by ice rafted debris (IRD) fluxes confined to the Fram Strait.

During the latest stage of this phase (around 2.7 Ma – 2.4 Ma) the ice sheets experienced significant growth, extending beyond the coast lines (Knies et al., 2009). A transitional growth phase (2.4 - 1.0 Ma) was characterized by generally wider ice extent (Fig. 1.11 B). As a response to glacial build-up on land, the glacial wedge growth began in the vicinity of the troughs between 2.4-1.5 Ma. Further development of the Svalbard ice sheet, resulted in its advance to the shelf edge at about 1.7-1.5 Ma, leading to gradual increase of glacially eroded sediment supply (Faleide et al., 1996; Andreassen et al., 2004; Knies et al., 2007; Knies et al., 2009). Gigantic submarine fan began to form at the western margin in this phase, prograding westward from the study area. It is known as Bjørnøya TMF (Laberg and Vorren, 1996) and consist of up to 4 km of glacial sediments.

The final growth phase (1.0 - 0 Ma; Fig. 1.11 C) commenced in high amplitude short term fluxes of the sediments to western margin, derived from erosion and meltwater outwash from ice sheet covering Central Barents Sea (Vorren et al., 1991). Occurrence of three major submarine slides along the margin at this phase (Laberg and Vorren, 1993) suggests repeated ice sheet advances to the shelf edge (Fig.1.11 C). The Barents Sea Ice Sheet (BSIS) is inferred to have covered the entire continental shelf several times trough out last 1.5 Ma (Andreassen et al., 2007,a; Andreassen et al., 2007,b).

Introduction

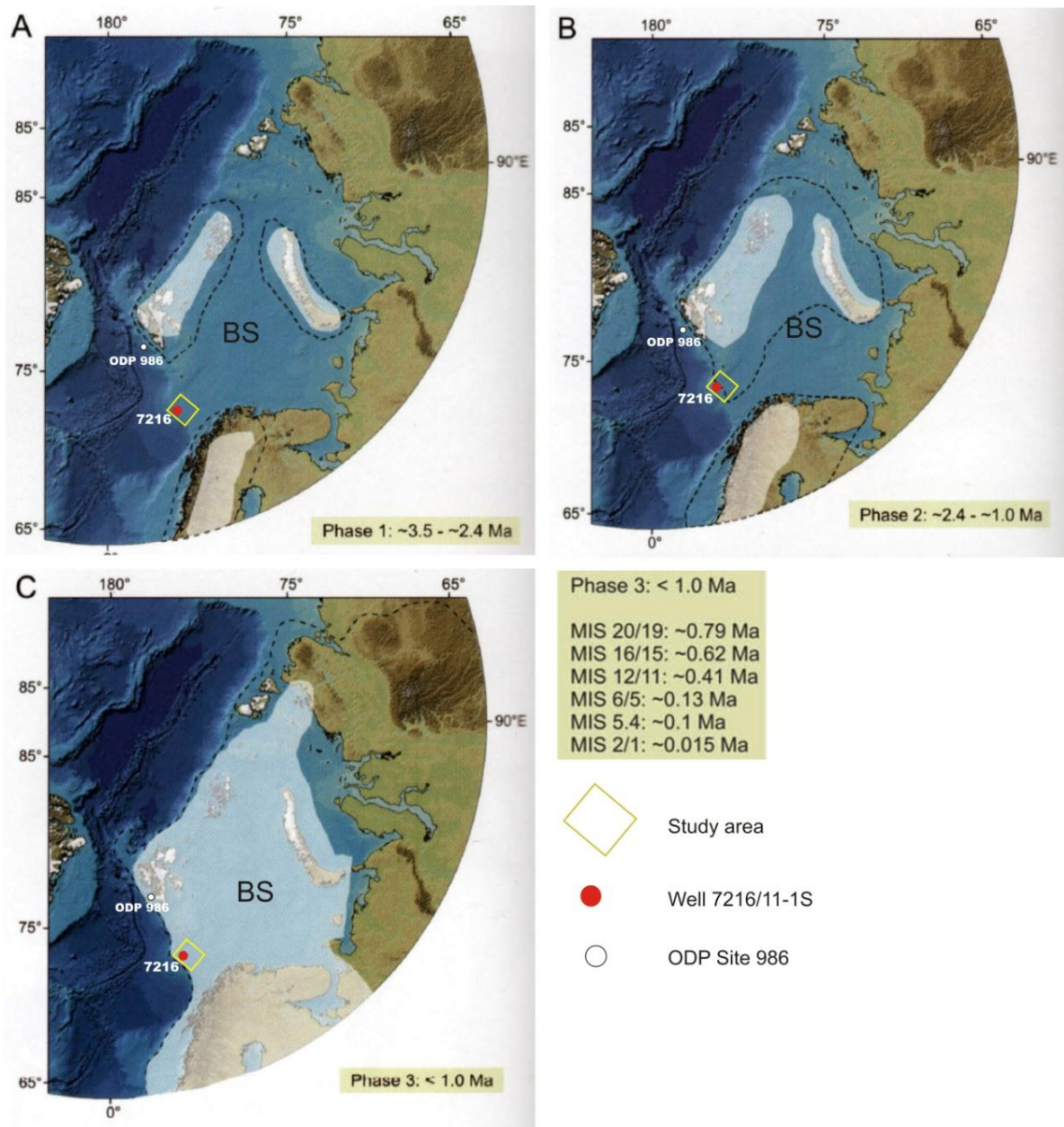


Figure 1.11 Main phases of the glacial growth in the Barents Sea during Late Pliocene-Pleistocene. Max/min lateral extension of the ice sheets indicated by stippled line and white areas respectively. Locations of the ODP Site 986 and well 7216/11-1S are indicated, yellow rectangle indicates study area shown in greater details in Fig. 1.11 D. Modified from Knies et al. (2009).

Significant rearrangement of the depositional patterns occurred at the beginning of this phase with a time span of 200 Ka, which marks transition of the Barents Sea shelf from the sub-aerial to the sub-marine environments (Butt et al. 2002).

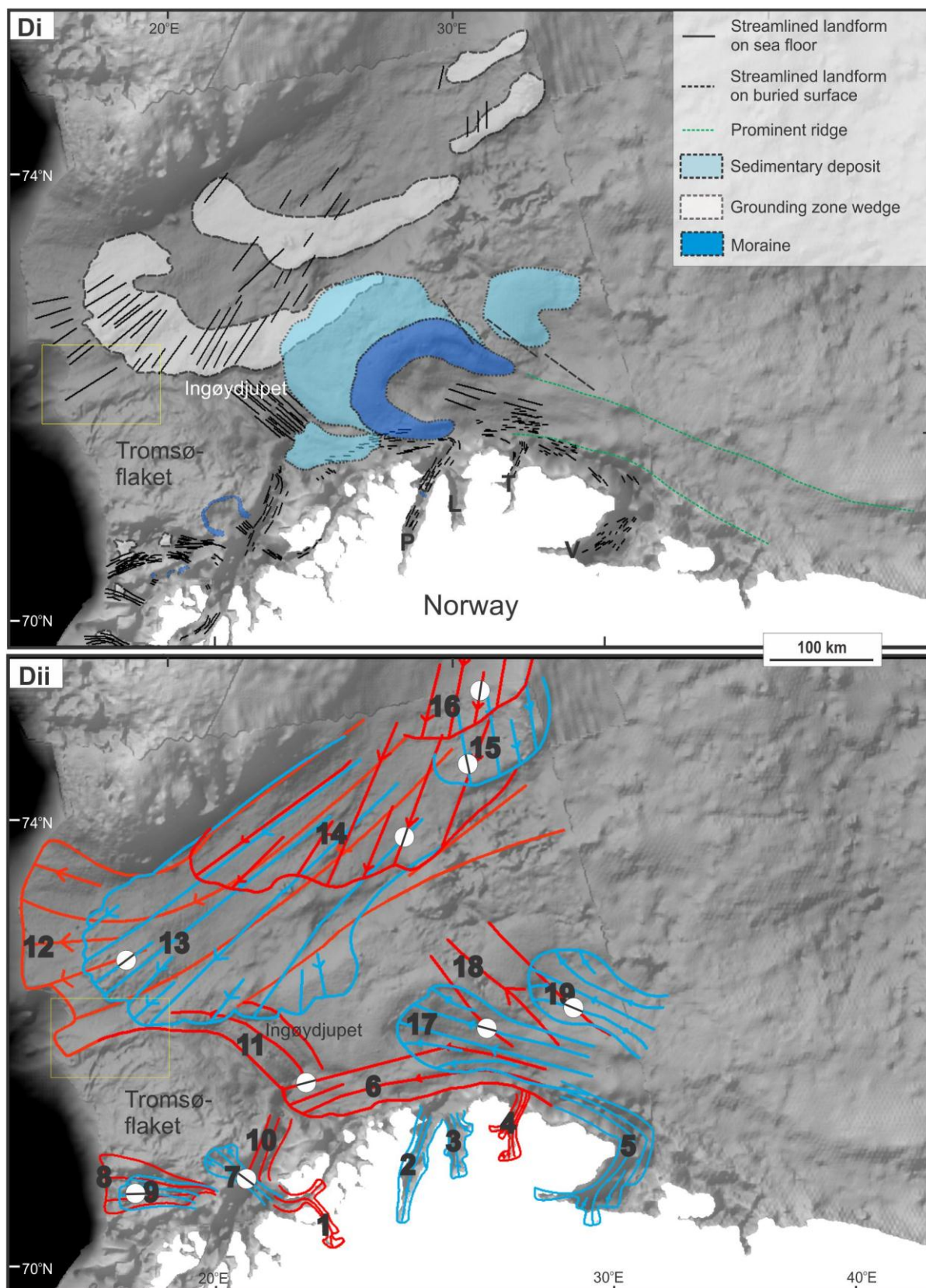


Fig. 1.11 Di) Map showing large-scale glacial landforms inferred in the southwestern Barents Sea. **Dii)** Map showing palaeo flow-sets representing different ice streaming events in the SW Barents Sea, study area is shown by the yellow box. Modified from Winsborrow et al. (2010).

Introduction

Results from 3D seismic studies within the study area indicate clearly that grounded glaciers have been reaching the shelf break here as fast flowing ice streams since the time of seismic reflector R5 (Andreassen et al. 2007b; Andreassen and Winsborrow 2009).

Different ice streams have been flowing over the study area during the deglaciation from the last glacial maximum at around 20 ka, as indicated by the glacial landforms in the SW Barents Sea (Fig. 1.11Di) and the ice stream flow sets inferred from these (Fig. 1.11Dii). During periods of maximum shelf edge glaciations the study area could have experienced ice flow with ice streams draining from the NE out Bjørnøyrenna from the Barents Sea Ice Sheet (Fig. 1.11Dii; Flow set 12), as well as ice streams draining out Ingøydjupet and bending westwards over my study area as they met the major ice stream draining out Bjørnøyrenna (Fig.1.11Dii; Flow set 11). Cold-based, relative slowly moving ice is inferred to have been located over the Tromsøflaket area during the last glacial maximum around 20 ka (Andreassen et al. 2008) and probably also during previous stages of shelf edge glaciations, and might have affected the glacial geomorphology of the study area.

Ice streams from the first retreat stage of the Bjørnøyrenna Ice Stream (Fig. 1.11Dii; Flow set 13) would also clearly have affected the study area as this stage is located just over the EL 0001 3D survey.

1.6 Glaciotectonic processes and mechanisms

This chapter gives an overview of glaciotectonic landforms and describes mechanisms and processes involved in their formation. Glaciotectonic landforms are morphological expressions of exposed or buried structures created by glacial deformation of glacial sediments or bedrock (Aber and Ber, 2007). Glaciotectonic processes are inferred to be associated with the proglacial, ice-marginal and subglacial areas of the moving glacier. Benn & Evans (2010) give the following sediment–landform classification of glaciotectonic features: 1) hill-hole pairs, 2) composite ridges and thrust-block moraines, 3) cupola hills and 4) sediment mega-blocks and rafts.

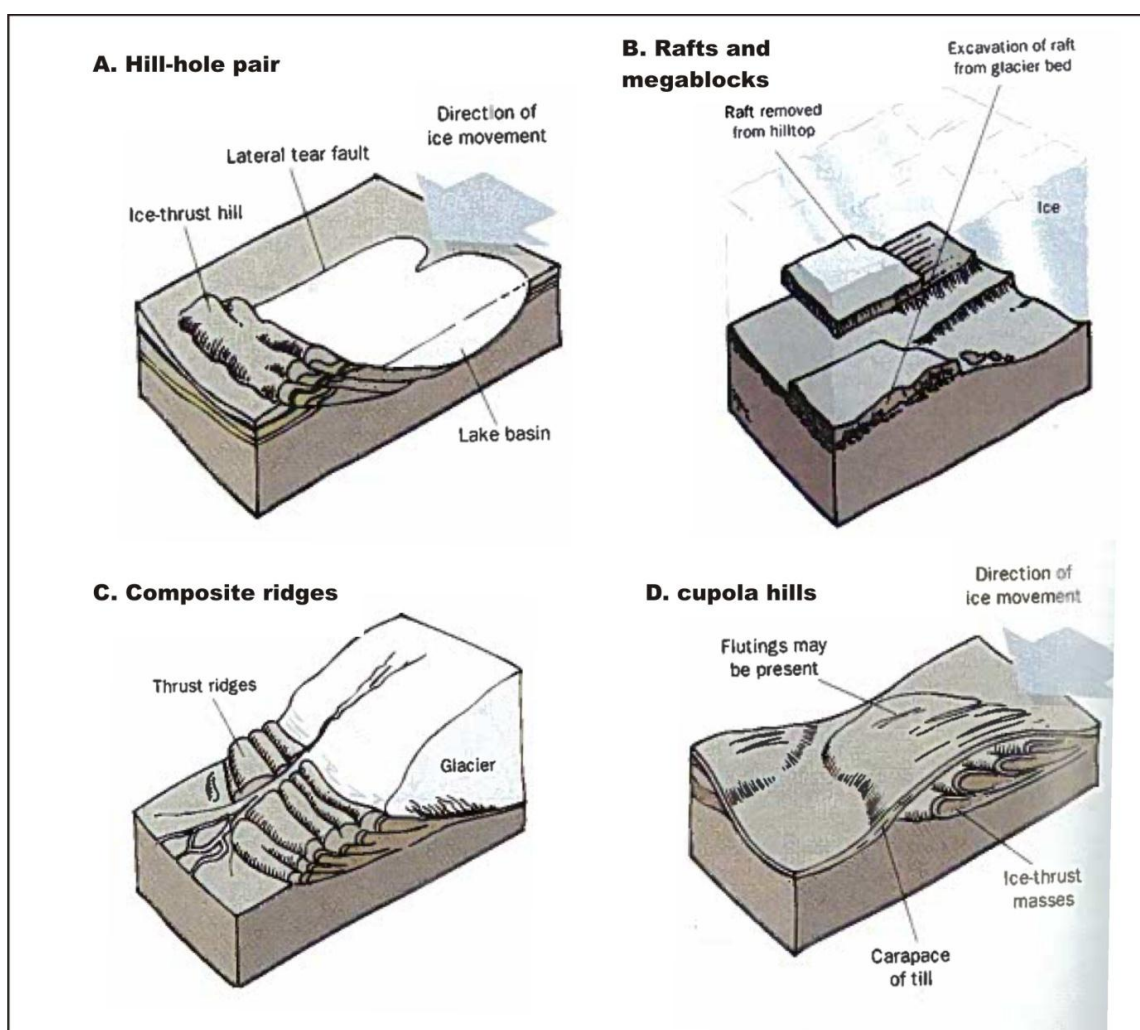


Figure 1.12 Sketches showing morphologic characteristics of main glaciotectonic landforms and their characteristics. More detailed descriptions are given in the text, from Benn & Evans, (2010).

Terms raft, megablock and floe are widely used for identifying individual masses of bedrock or sediments which have been dislocated by a glacier. Megablocks and rafts are commonly

Introduction

referred to large comparatively thin sediment bodies having more or less horizontal orientation within strata (Aber and Ber, 2007).

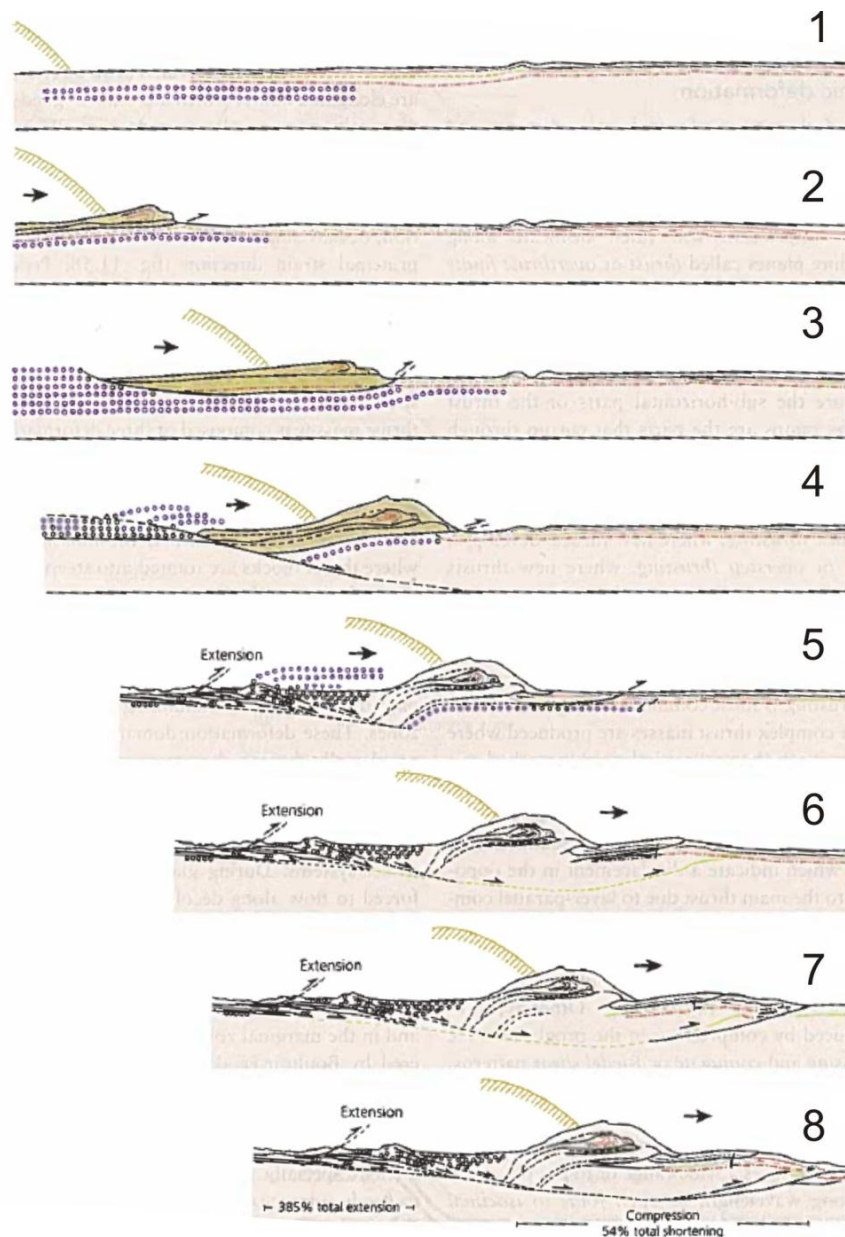


Figure 1.13 Sketches showing development stages of the glaciotectonic thrusting, exemplified on thrust moraine in front of the Eyjabakkajökull, Iceland. Black arrow indicates ice movement direction and numbers indicate 8 stages, from Benn and Evans (2010).

Proglacial glaciotectonic is defined as a large-scale deformation and displacement of proglacial and sub-marginal sediments by glacier induced stresses. The process involves brittle or ductile deformation of the material or a combination of the two. However it is indicated that frozen sediments more prone to the brittle deformation result in thrusting

along a plane of decollement (Benn & Evans, 2010). Among the factors affecting mechanisms of failure within sediments are applied stress, temperature, shear strength and pore-water pressure. Thrusting is enhanced by excess in pore-water pressure in proglacial and sub-marginal sediments. Impermeable sediments, permafrost or gas hydrates occurring at the glacier margin may enhance the pore-water pressure. This is also the case for surging glaciers which are known to produce glaciotectionic landforms at the advancing margin (Selley, 1998; Benn and Evans, 2010). The study area contains glaciotectionic features within the Pleistocene succession interpreted by Andreassen et al. (2004) as sediment megablocks and rafts, which are aligned in elongated chains within buried till units (Fig.1.14).

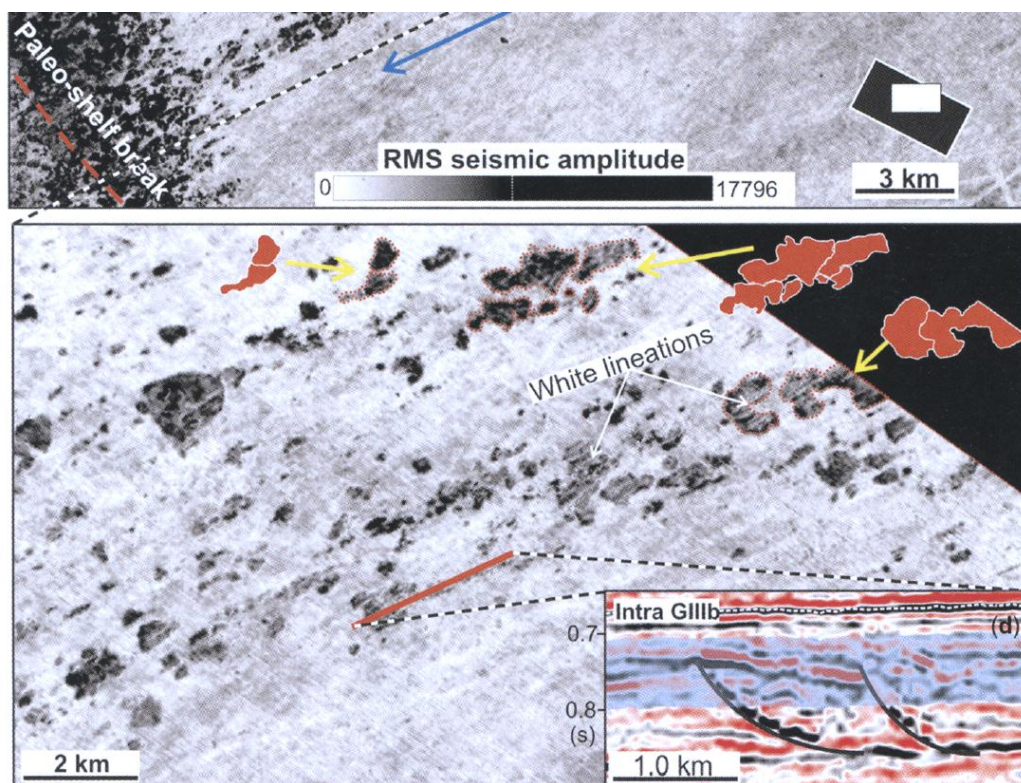


Figure 1.14 RMS amplitude map and seismic section showing interpreted mega blocks aligned parallel with ice flow direction below horizon Intra GIII in the NH9803 3D survey from Andreassen et al. (2007b).

1.7 Subsurface fluid migration, trapping and expulsion

Fluid flow is a complex and long-term process and it is an integrated part of the geological system. Geological fluid flow system includes generation, migration, accumulation and seepage from the trap of the fluids within the subsurface (Perrodon, 1983). Fluids within the sediments may be present in liquid and/or gaseous phase depending on nature of the fluid and pressure-temperature (P-T) conditions. Although solid occurrence is present as well, in the case of gas clathrate hydrates bounding gases. In most of the cases fluids are confined to the pore space of sediments from the moment of deposition and to the deep burial depth, although gradually reduced due to compaction. The liquids of interest in this study are hydrocarbon gases in free or dissolved phase. Hydrocarbon gases have been generated in the subsurface by biogenic or thermogenic decay of organic matter. Numerous geochemical surveys and shallow gas sampling have proved that methane is the most common hydrocarbon gas in marine sediments (Kvenvolden, 1998; Judd et al., 2002; Max, 2003).

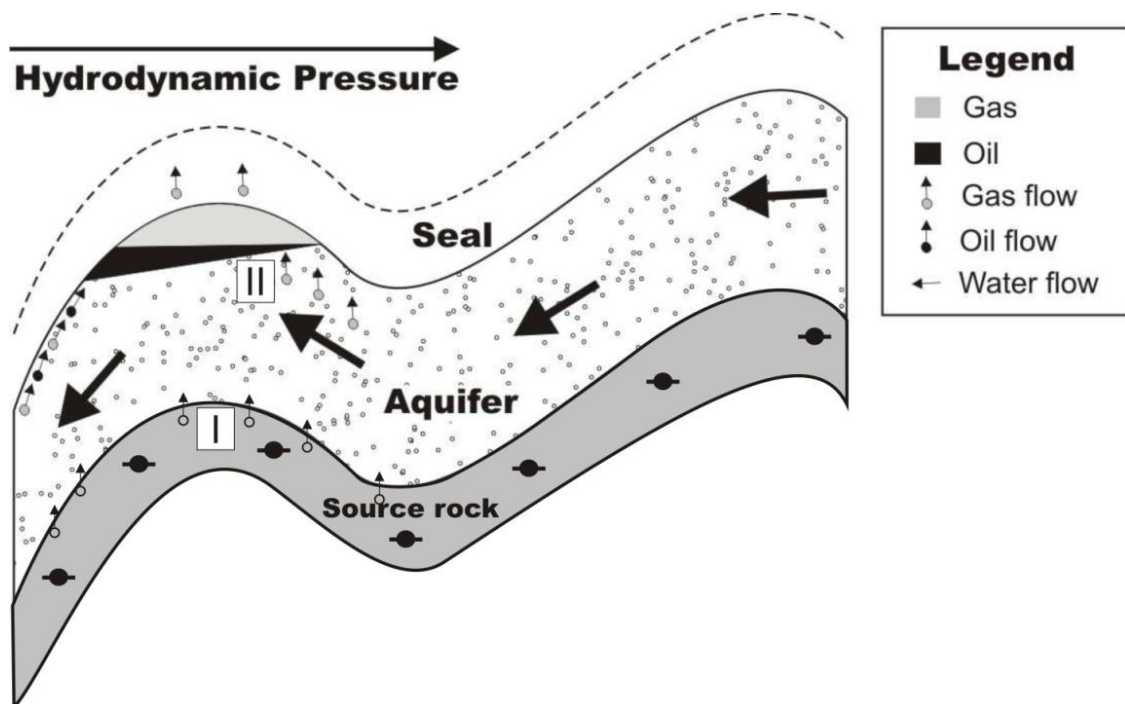


Figure 1.15 Generalized model of the fluid flow dynamics, hydrocarbons expelled from the source rock subject to primary migration (I), buoyancy controlled secondary migration occur within porous strata (II), fluid movement within aquifer is controlled by the pressure gradient. Modified from Perrodon (1983).

Two zones of gas generation are subdivided within the shallow geosphere controlled by the burial depth and geothermal gradient. The uppermost is a diagenetic zone occurring below 50° C dominated by methanogenic bacteria expelling biogenic methane as a product of organic matter decay. Above the threshold of 50° C temperature driven hydrocarbon generation become dominant with formation of thermogenic gases in the catagenesis zone (Selley, 1998; Bjørlykke, 2010). Migration of hydrocarbon fluids is subdivided in two phases (Fig.1.15). *Primary* migration is associated with hydrocarbon generation and expulsion from the source rock. *Secondary* migration occurs within porous sediments or permeable pathways towards accumulation areas in the subsurface or all the way to the seafloor, where fluid seeps may form. The main driving forces responsible for fluid migration within sedimentary basins are material buoyancy, hydrodynamics and overpressure (Selley, 1998; Judd and Hovland, 2007). Excess pore pressure is often induced by sediment compaction after rapid burial, formation of effective seal trapping fluids and/or supplies of the fluids exceeding their dissipation.

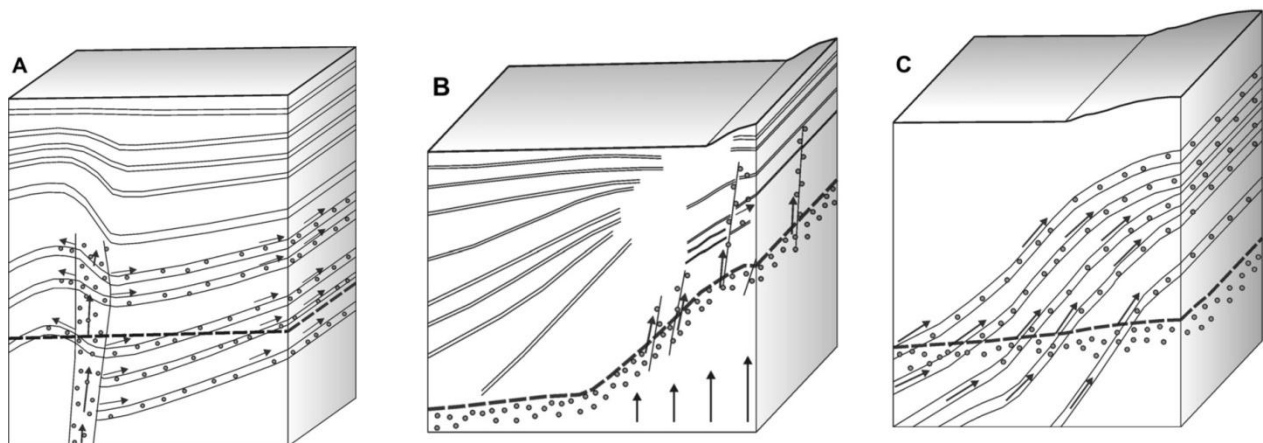


Figure 1.16 Sketches showing geological controls for migration of the gas-rich fluids in the subsurface. **A)** Focused bypass of fluids through conduit, **B)** vertical migration along the fractures and faults, **C)** flux of the fluids confined to permeable beds. Dashed line indicates position of the bottom gas hydrate stability zone. Modified from Crutchley et al. (2011).

In porous strata fluid flow is commonly controlled by diffusion and advection mechanisms and flow rates primarily rely on Darcy's law. It states that the amount of fluids migrating through the media depends on its permeability and on the pore pressure difference between the two ends of the fluid flow system (Fisher et al. 2003). In turn impermeable sediments tend to seal fluid migration, until overpressure is high enough to form a *seal*

bypass system expressed in form of fractures, faults, intrusions (sediment remobilization) or chimneys (Cartwright et al., 2007; Hustoft et al., 2009).

Faults and fractures are among the most abundant conduits for fluids migrating from deep reservoirs (Fig. 1.17) where sediments are more consolidated, towards more shallow porous sediments (Fisher et al., 2003). In the study area presence of gas in the subsurface has been inferred from reflection seismic data (Andreassen et al., 2007,a).

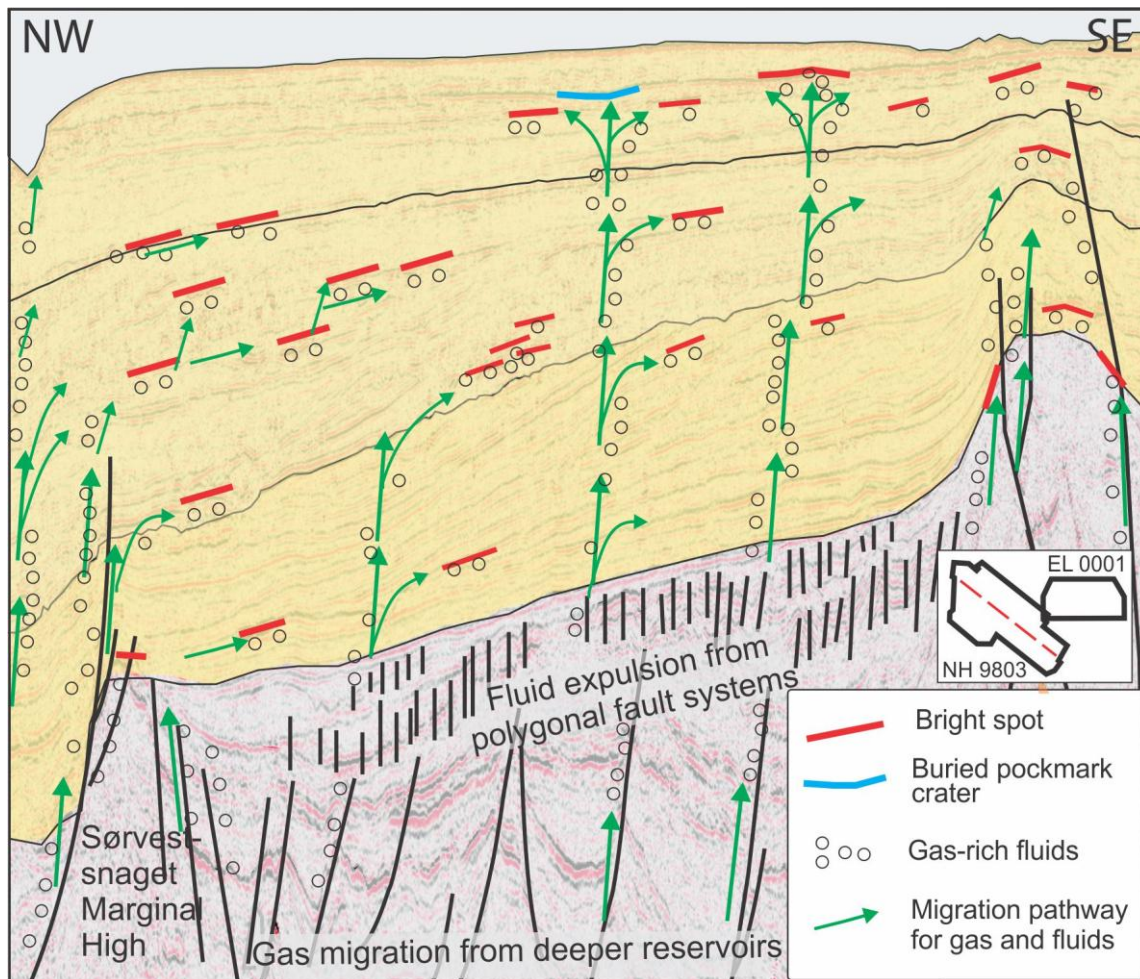


Figure 1.17 Model showing relationship between bright spots associated with gas accumulations and fluid migration pathways along the faults and within carrier beds. Location of the inline within NH9803 3D survey is indicated in black box. Modified from Andreassen et al. (2007,a).

Gas accumulations are indicated by *bright spots*, anomalously high amplitude reflections with reversed polarity compared to the seafloor reflection. The 3D seismic data used in this study show evidence of focused fluid migration along sub-vertical faults and fractured zones within Plio-Pleistocene succession (Andreassen et al., 2007,a; Pless, 2009).

Signals from fluid contacts detected by the seismic method are commonly referred to as direct hydrocarbon indicators (DHI) and include among others flat spots, bright spots, phase reversal, velocity pull down and acoustic masking (Fig. 1.18) (Sheriff, 2002). Fluid expulsion and hydrocarbon migration in the Sørvestsnaget-Veslemøy study area had likely a cyclic character associated with glacial-interglacial cycles. Glacial induced sea level changes and periods of rapid sedimentation might have cause pressure gradient differences and pulses of upward fluid migration (Andreassen et al., 2007,a).

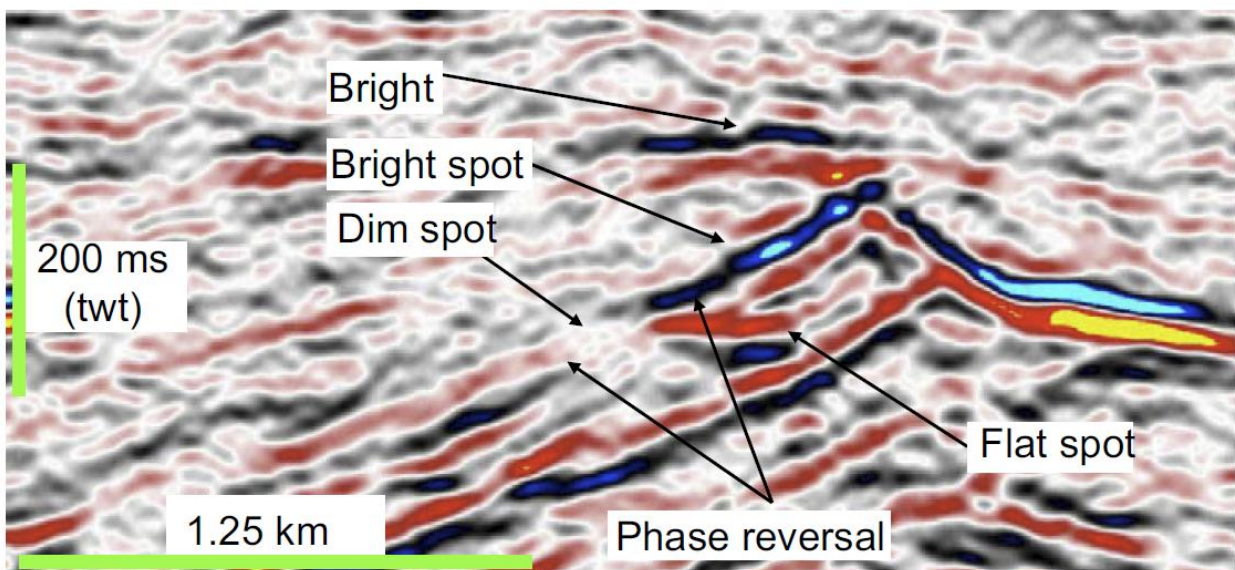


Figure 1.18 Seismic profile showing direct hydrocarbon indicators such as bright spot, dim spot, flat spot, and phase reversal which may indicate presence of hydrocarbons in subsurface. From Løseth et al. (2009).

1.8 Gas hydrate formation and stability field

Natural gas hydrate (NGH) is an ice-like crystalline solid compound (Fig. 1.19) consisting of rigid cage of water molecules, trapping gas molecules of an appropriate size in the voids (Fig. 1.20).



Figure 1.19 Photo of a natural gas hydrate massive vein, retrieved from the marine sediments in the Arctic. From <http://www.methanehydrates.org/galleries/1>, photo courtesy of IFM- GEOMAR.

The term “gas hydrates” is commonly used to describe *water-methane clathrate hydrate*, which may in addition contain mixtures of other hydrocarbon gases, and which is (methane) most abundant in the marine setting (Andreassen, 1995; Sloan Jr, 1998a; Sloan Jr, 1998c; Max, 2003). Three different structures inferred for the hydrate: structure I comprised of lower order gases, structure II is consist of higher gases and structure H is combination of both (Sloan Jr, 1998c). Formation of the natural gas hydrates (NGH) confined to the shallow geosphere and occur in the marine sediments in form of veins (Fig. 1.19), pore space infill's or/and nodules. The zone with favorable conditions for hydrate formation is referred to as a gas hydrate stability zone (GHSZ).

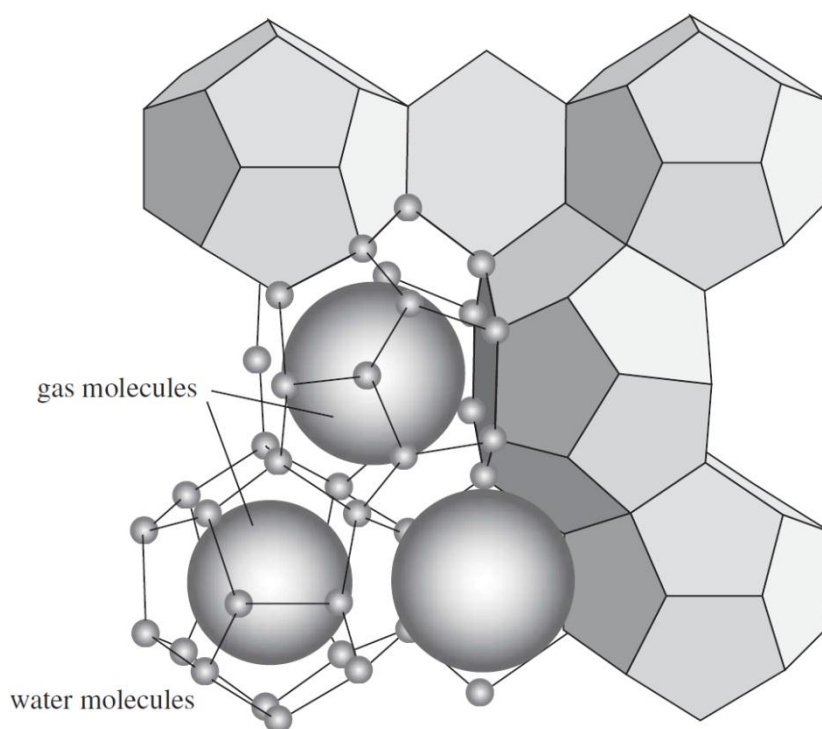


Figure 1.20 Sketch showing gas hydrate molecular structure where host water molecules create a solid cage, which is encompassing gas molecules of an appropriate size in the voids. From Maslin et al. (2010).

The following conditions are essential in order to form gas hydrates: i) temperature within hydrate phase equilibrium, ii) pressure within hydrate phase equilibrium zone, iii) gas molecules of a proper size to form hydrates, iiiii) sufficient amount of water molecules to form hydrates (Kvenvolden, 1998; Sloan Jr, 1998b). If these factors are met, gas hydrates may form within GHSZ as illustrated by means of phase diagram (Fig.1.21). Thickness of the GHSZ is determined by bottom water temperature, hydrostatic pressure and geothermal gradient, composition of the hydrate forming gas and formation water salinity (Sloan Jr, 1998c; Sloan and Koh, 2008).

The thickness of the GHSZ in the marine sediments is from tens of meters down to 1000 m (Max, 2003) and often found in water depths of over 500 m, although NGH could appear up to 300m water depth in Arctic waters where bottom water temperatures are as low as 2°C (Laberg et al., 1998).

Introduction

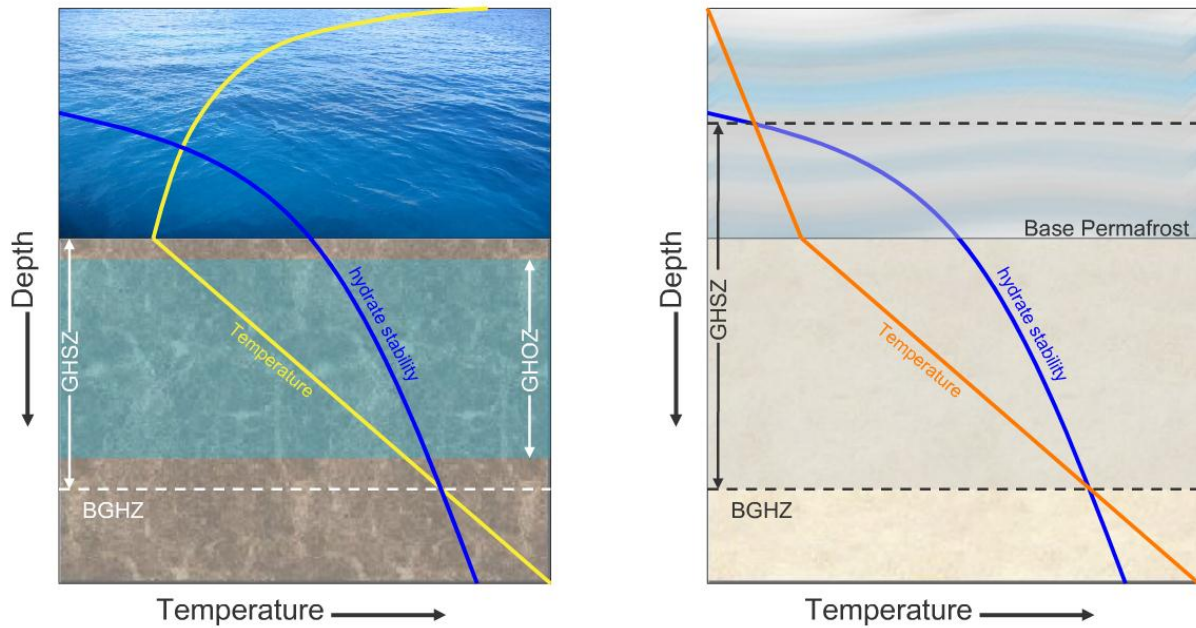


Figure 1.21 Conceptual models of the gas hydrate stability zone (GHSZ) for marine setting on left hand side, and for the onshore setting with present permafrost layer to the right. BGHZ is bottom of the GHSZ, where GHOZ is indicating gas hydrate occurrence zone, from Statoil Innovate (<http://innovate.statoil.com/challenges/Pages/GasHydrates.aspx>).

Due to the compact encaging of the gas in the NGH the volume properties are of special importance as 1 m³ of the methane gas hydrate contains about 164 m³ of gas and 0.8 m³ of water at the standard Pressure/Temperature conditions (at the surface) or around 3 m³ of gas at the burial depth (Kvenvolden, 1998). Massive methane gas hydrate is a material of a high shear strength, which is reported to be about 20-30 times stronger than the pure water ice based on laboratory experiments (Durham et al., 2003).

The bottom of the gas hydrates stability zone (BGHSZ)(Fig. 1.21) is a highly dynamic boundary which can move vertically in response to continued sedimentation, seafloor warming, temperature gradient changes, sea level fluctuations or, as in case of the Barents Sea shelf area, to glaciations and interstadials responsible for hydrostatic pressure changes (Andreassen, 1995; Max, 2003; Fichler et al., 2005; Max and Johnson, 2011). Upward movement of the BGHSZ will cause dissociation of the gas hydrate if present. Consequently if released gas is trapped under the top seal, for example glacial tills or remaining permafrost, it may produce overpressure which will have a potential to drive pore water (Max and Johnson, 2011). If the overpressure will overcome hydrostatic pressure venting of

the fluids to the seafloor may take place or natural blowout of gas could occur (Lammers et al., 1995; Fichler et al., 2005; Max and Johnson, 2011). Based on the GHSZ modeling performed by Chand et al. (2012) for the SW Barents Sea the study area is outside of methane hydrate stability field at the present day conditions (Fig 1.22 A). Although it is indicated that during last glacial maximum (LGM) hydrate stability zone thickness in the SW Barents Sea was up to 600 m (Chand et al., 2012) and reached around 200 m in the study area (Fig 2.22 B).

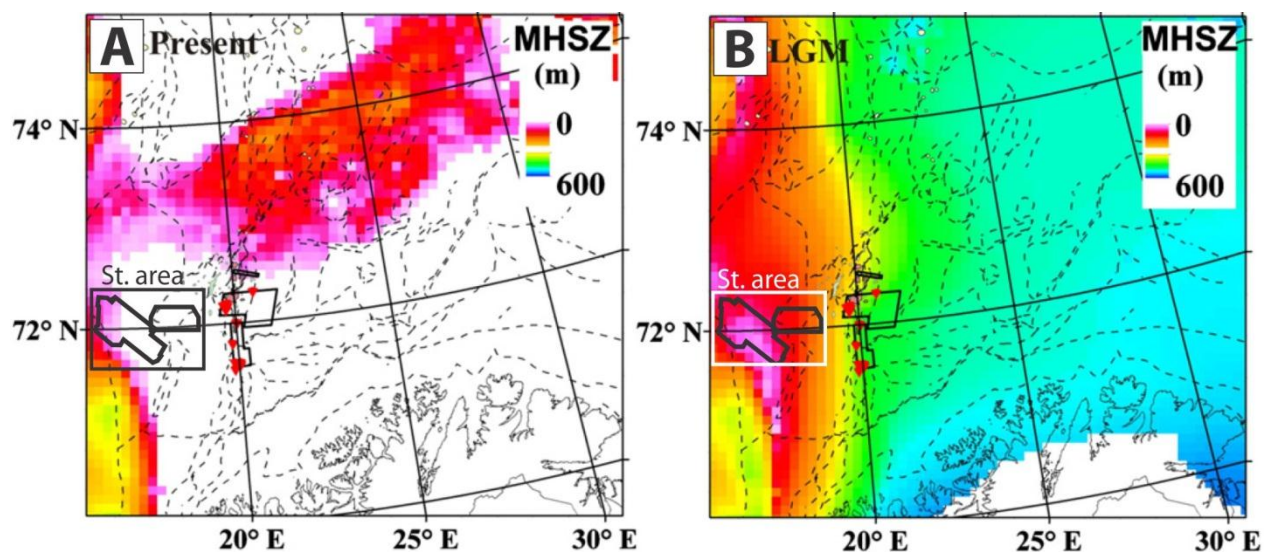


Figure 1.22 Maps showing the methane hydrate stability zone thickness in the SW Barents Sea area during present day conditions A and last glacial maximum in B. The study area of this thesis and location of 3D seismic surveys is indicated at the western limit of the map. Modified from Chand et al. (2012).

The occurrence of the hydrate is inferred by the presence of the bottom simulating reflection (BSR) around 40 km east of the study area (Andreassen, 1995; Laberg and Andreassen, 1996; Laberg et al., 1998). Here presence of the hydrate is interpreted to be associated with the higher hydrocarbons fluxes from the underlying reservoirs where hydrate accumulations are found in the vicinity of the large faults (Laberg and Andreassen, 1996; Chand et al., 2008).

Moreover it is indicated that BGHSZ could be elevated above the faults associated with high fluid fluxes locally increasing subsurface temperatures and leading to pull ups of the BSR (Max et al., 2006).

2 Data and methods

2.1 Seismic datasets

This study is based on the two industry semi-regional 3D seismic surveys NH9803 and EL0001, the regional 2D seismic survey NH9702 and the industry borehole 7216/11-1S applied for lithological control (Fig. 2.1). In addition a bathymetry chart is used compiled from the 2D seismic grid of SW Barents Sea available from the University of Tromsø database. This chapter covers technical aspects of the data and describes methods used for visualization and interpretation.

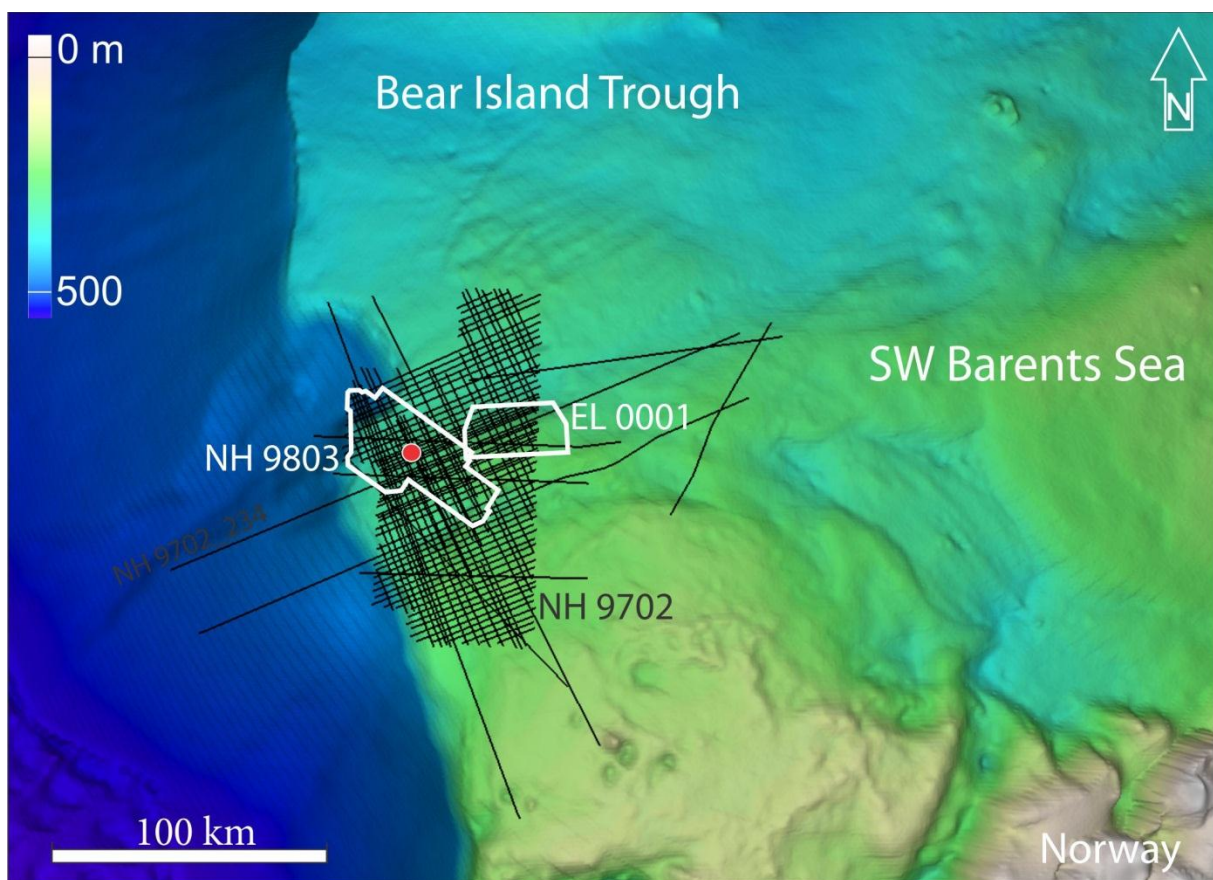


Figure 2.1 Shaded bathymetry map (vertical exaggeration 50 times, illumination from the SW) showing location of the seismic data sets used in this study. The white polygons indicate location of the 3D seismic surveys, black lines show grid of the 2D seismic survey NH9702 and red dot indicates location of the well 7216/11-1S.

2.1.1 Two-dimensional (2D) Seismic survey

The regional 2D seismic dataset NH9702 was used here in order to extend seismic interpretation of the 3D surveys farther east and evaluate deep-seating faults. The 2D survey consists of 101 long offset lines with line spacing of 1-2 km, and was acquired by the consortia of companies under Norsk Hydro ASA operatorship in 1997-1998. The long lines across SW Barents Sea continental slope and shelf allow investigating the glacial wedge in full scale in order to correlate reflectors.

2.1.2 Three-dimensional (3D) seismic surveys

Main input into this study is based on two 3D surveys NH9803 and EL0001 acquired and processed for the Norsk-Hydro ASA in 2000 and Total in 2001 respectively.

The Sørvestsnaget NH9803 survey covers an area of approximately 2000 km² and has following acquisition parameters. Source was represented by two G-air guns, with a volume of 3090 cubic inches and pressure of 2500 p.s.i. towed at 6 m depth with 50 meters array separation. Recording cables were 4050m long with 280 m near offset, towed at 8 meters depth and 150 m line separation. There were 324 groups with 8 hydrophones in each having 12.5 m group interval and 2 ms sampling interval.

Table 2.1 Geographical coordinates for the 3D seismic surveys NH9803 and EL0001.

Survey name	Latitude	Longitude
Sørvestsnaget	72°04'49.8" N	15°24'25.0" E
NH9803, 3D	72°20'34.9" N	16°02'22.7" E
	71°38'33.4" N	17°16'29.1" E
	71°53'56.5" N	17°55'05.5" E
Veslemøy High	72°11'56.7" N	18°39'22.6" E
EL0001, 3D	72°11'56.3" N	17°20'31.6" E
	72°00'06.6" N	17°20'58.2" E
	72°00'06.5" N	18°38'58.0" E

The Veslemøy EL0001 survey covers an area of 990 km² and overlaps Sørvestsnaget survey at its. A line spacing of 12.5 m was used with sampling interval of 4 milliseconds (ms) and recording time 8000 ms. Geographic coordinates for these surveys are given in table 2-1.

Seismic Resolution

Vertical resolution is measure to which degree two vertical boundaries with different acoustic impedance can be separately distinguished on the recorded seismic trace. Vertical resolution is a function of seismic interval velocity and signal frequency and it is measured in wave length (λ). Theoretical vertical resolution is inferred to be $\lambda/4$ and it is equal to velocity divided by four times frequency:

$$\text{Vertical resolution: } \lambda/4 = v/4f$$

Where: λ (m) is the dominant wavelength, v (m/s) is interval velocity and f (Hz) is signal frequency.

Seismic wave velocity tend to increase with depth due to compaction of sediments, on the other hand frequency is decreasing because higher frequencies are absorbed and attenuated with depth causing lower frequency component in deeper parts of the section. These factors are leading to a generally lower vertical resolution with increasing depth (Brown, 2004).

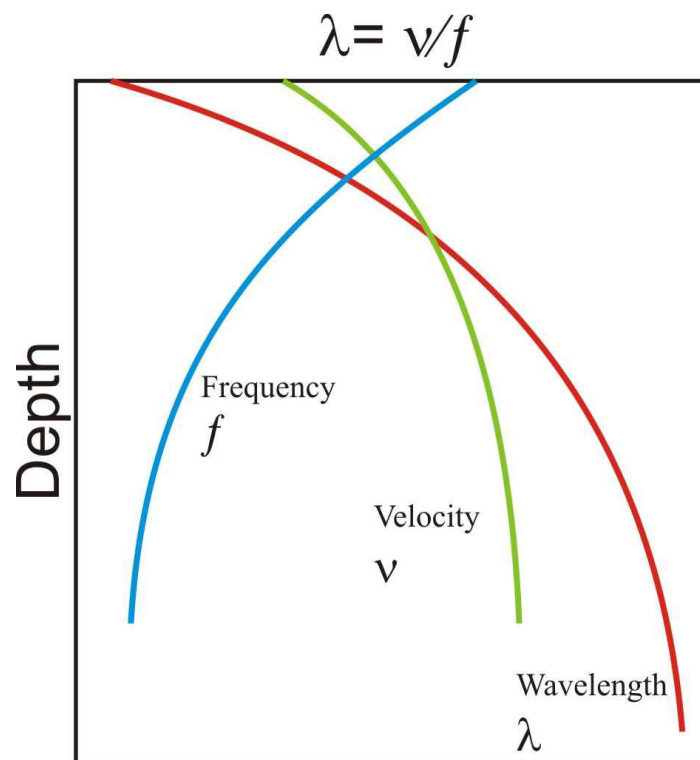


Figure 2.2 Diagram showing generalized relationship between frequency, velocity and wavelength with the increasing depth. From Brown (1999).

Seismic velocities for the glacial package in western margin was indicated by (Fiedler and Faleide, 1996), as for the deeper parts of the area the seismic velocity is inferred to exceed 3000 m/s (Ryseth et al., 2003). The dominant frequency content of the shallow part of the dataset is 25-30 Hz and it is about 15 Hz for the deeper part (Nilsen, 2006; Pless, 2009).

Vertical resolution of the 3D surveys can be calculated as follows:

$$\text{Average vertical resolution of GI: } \lambda/4 = V/4f = 1970 \text{ ms}^{-1} / 4 \times 30\text{Hz} = 16 \text{ m}$$

$$\text{Average vertical resolution of GII: } \lambda/4 = V/4f = 2150 \text{ ms}^{-1} / 4 \times 25\text{Hz} = 20 \text{ m}$$

$$\text{Average vertical resolution of GIII: } \lambda/4 = V/4f = 2600 \text{ ms}^{-1} / 4 \times 25\text{Hz} = 26 \text{ m}$$

$$\text{Average vertical resolution of deeper parts: } \lambda/4 = V/4f = 3000 \text{ ms}^{-1} / 4 \times 15\text{Hz} = 50 \text{ m}$$

Vertical resolution of the 2D survey NH9702

Vertical resolution of the 2D survey is equal to $\lambda/4$ and calculated for the upper part of the subsea-bed sediments assuming sound velocity of 2000 m/s and the frequency values around 50 Hz (Andreassen et al., 2008).

$$\text{Average vertical resolution of GI-III units: } \lambda/4 = V/4f = 2000 \text{ ms}^{-1} / 4 \times 50\text{Hz} = 10 \text{ m}$$

Horizontal resolution

The horizontal resolution indicates the minimum distance between two features that can be identified or separated from one another laterally. Seismic horizontal resolution has dramatically improved with evolved 3D seismic technology and ability to apply migration process to the data. The initial horizontal resolution for the reflection seismic method defined by the Fresnel zone which defined as an area covered by the wave front within $\frac{1}{4} \lambda$. Migration technique improves resolution by focusing energy spread over the Fresnel zone to a smaller area along the seismic line, creating an ellipse perpendicular to the 2D line direction (Brown, 1999 2004).

For the more advanced 3D migration, allowing three dimensional collapse of Fresnel zone, this focused area will represent a small circle generated by intersecting lines of the survey thus. Thus 3D seismic migration result in horizontal resolution comparable with the vertical and gives detailed 3D stratigraphic imaging, suitable for interpretation of complex geological

structures. Idealized migration will lead to an area collapse equal to $\frac{1}{4}$ of original Fresnel zone, although it is not always a case and on practice it is generally around half a size of unmigrated Fresnel zone (Brown, 1999). Due to physical constrains horizontal resolution will decrease with depth, increased velocity and reduced frequency (Badley, 1985).

Idealized horizontal resolution for the 3D surveys can be calculated as follows:

Average horizontal resolution of package GI: $\lambda/4 = v/4f = 1970 \text{ ms}^{-1} / 4 \times 30\text{Hz} = 16 \text{ m}$

Average horizontal resolution of package GII: $\lambda/4 = v/4f = 2160 \text{ ms}^{-1} / 4 \times 25\text{Hz} = 21 \text{ m}$

Average horizontal resolution of package GIII: $\lambda/4 = v/4f = 2400 \text{ ms}^{-1} / 4 \times 25\text{Hz} = 24 \text{ m}$

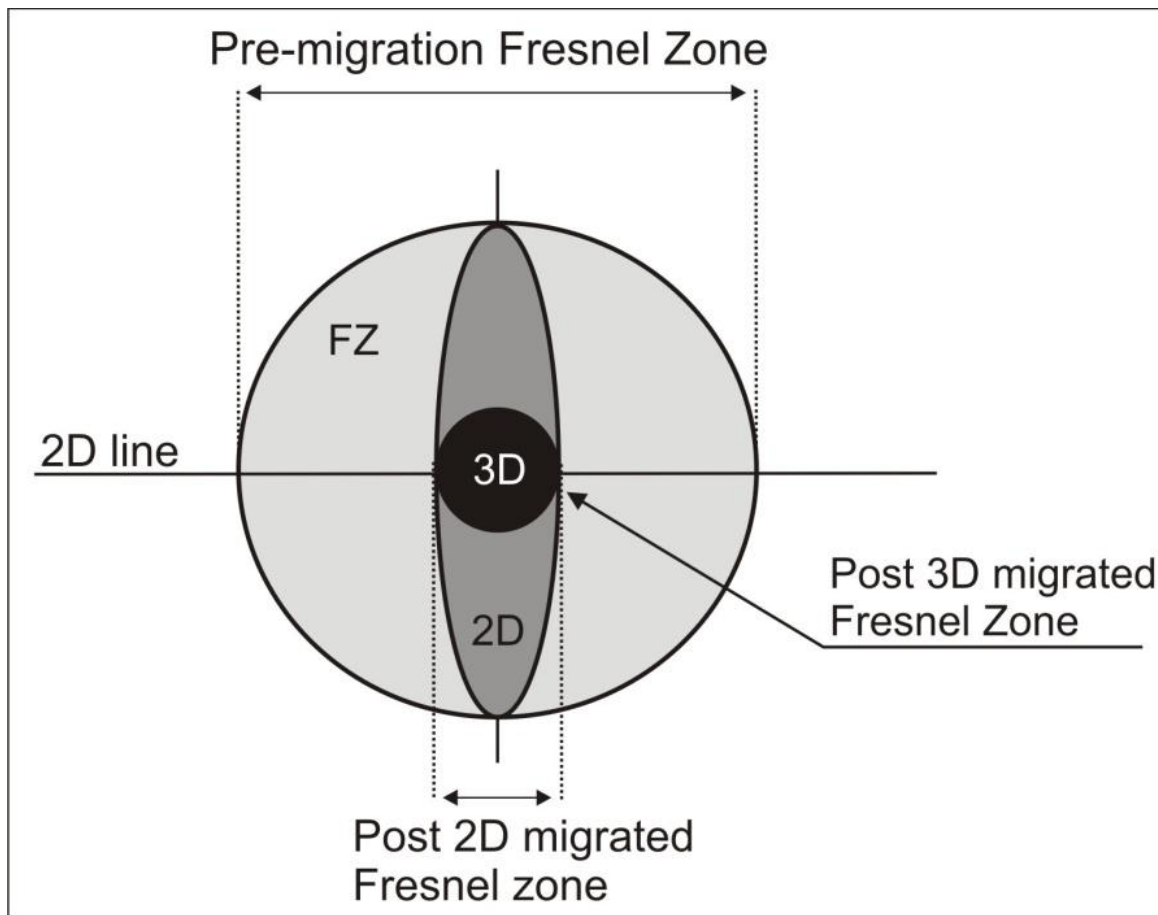


Figure 2.3 Sketch showing size of the original Fresnel Zone and collapsed zones after 2D and 3D migrations, modified from Brown (2004).

Horizontal resolution of the 2D seismic survey is indicated to be around 60-100 m (Andreassen et al., 2008) within the line and spatial resolution of the NH9702 dataset is dependent on the line spacing, which is about 1-2 km.

2.2 Artifacts

Artifacts are unnatural effects or features appearing within datasets which were created by the data acquisition technique or by the consecutive processing. The interpreter should consider a number of artifacts arising from the seismic method in order to distinguish them from real features or events (Bulat, 2005).

One of the typical artifacts for the 3D surveys is an acquisition footprint generated during data collection and manifested by elongated parallel ridges aligned with the inline direction (Fig. 2.4). Formation of these artifacts may be explained by the difference in towing depth for the streamers or uneven acquisition geometry between lines. Such artifacts can be easily identified and “ignored” while interpreting real data.

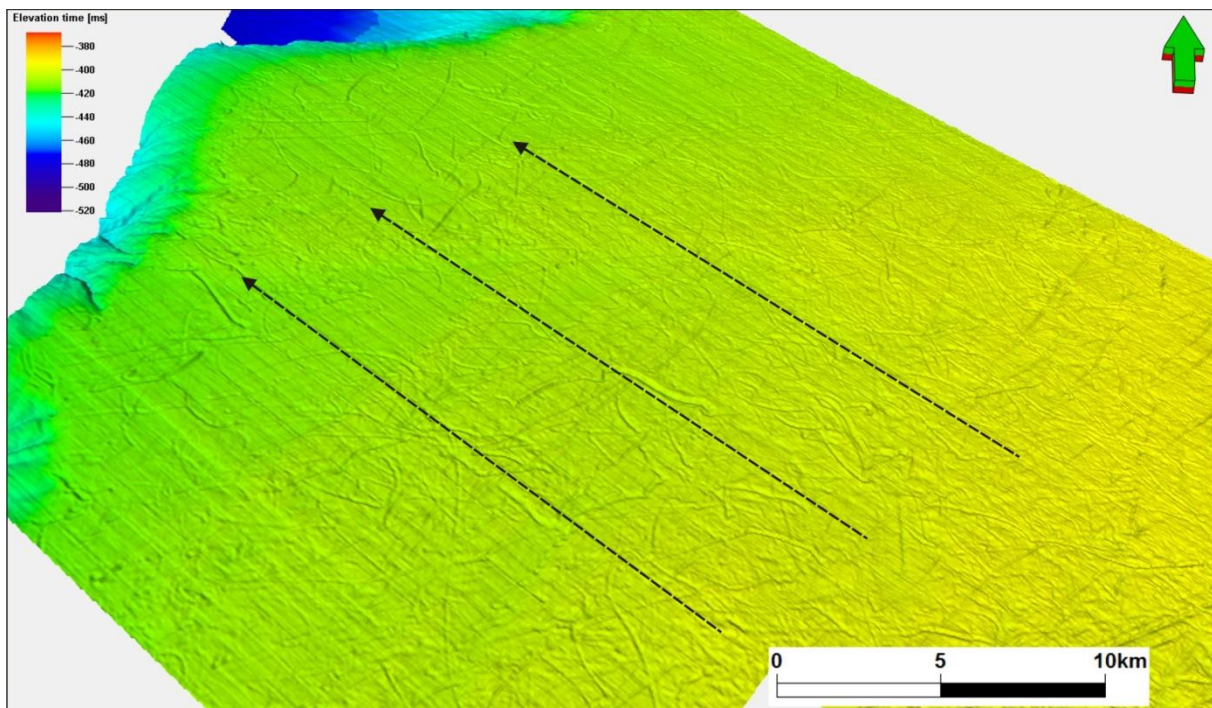


Figure 2.4 Shaded seabed horizon of the NH9803 3D seismic dataset showing acquisition footprints visible on its surface. Black arrows indicate the artifact ridges aligned with direction of the inlines.

The seismic survey E10001 also poses subtle acquisition footprints, as well as artifacts related to the processing of the dataset. These artifacts most likely related to the error with static corrections and resulted in four SW-NE trending lines along which some of the seismic traces have been moved down for a distance of 40-90 ms (Fig. 2.5).

Aforementioned artifacts appear both on the seismic cross sections and on the interpreted horizons (Fig. 2.5) and can be disregarded as the real features, due to their striking linearity

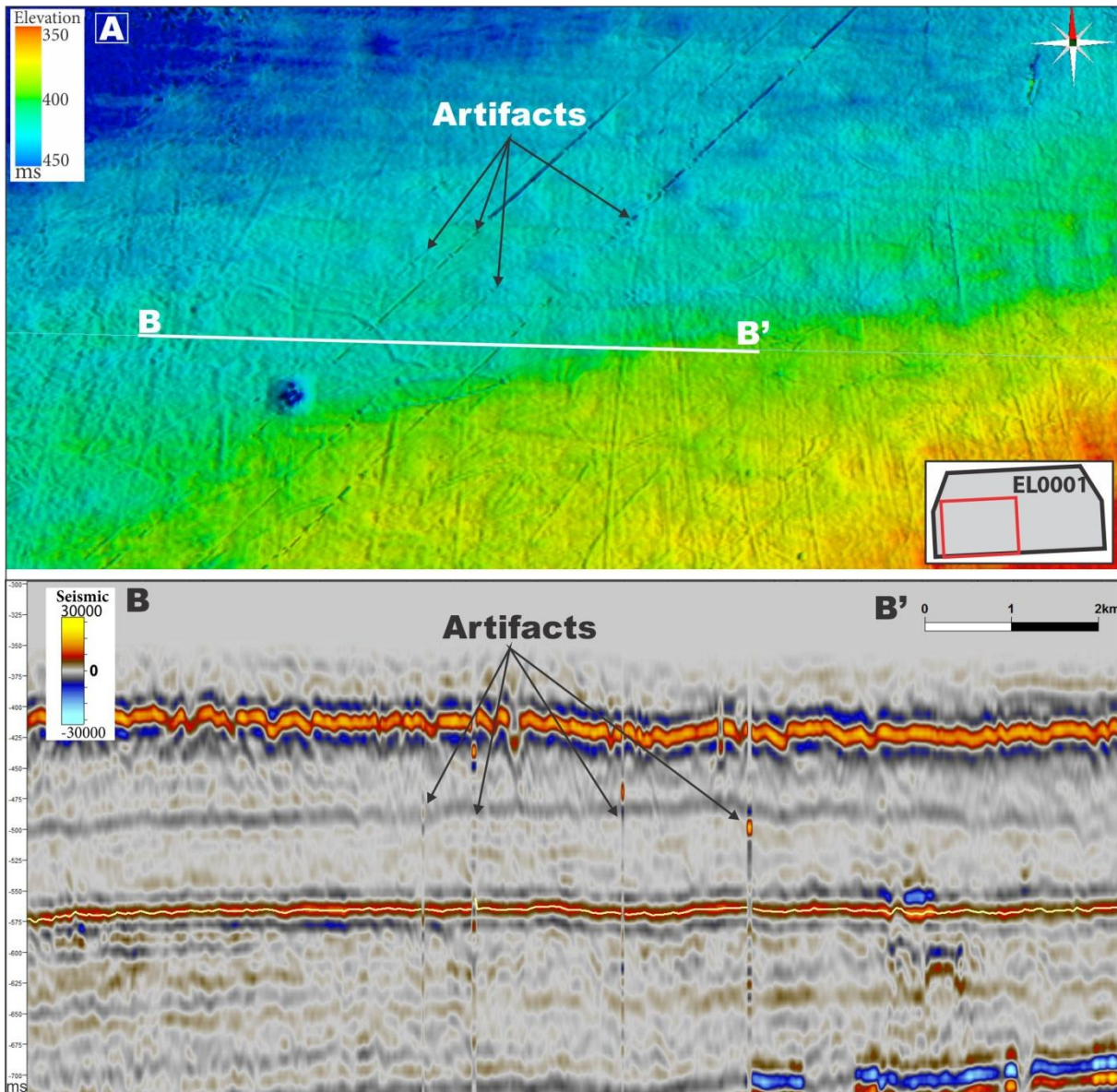


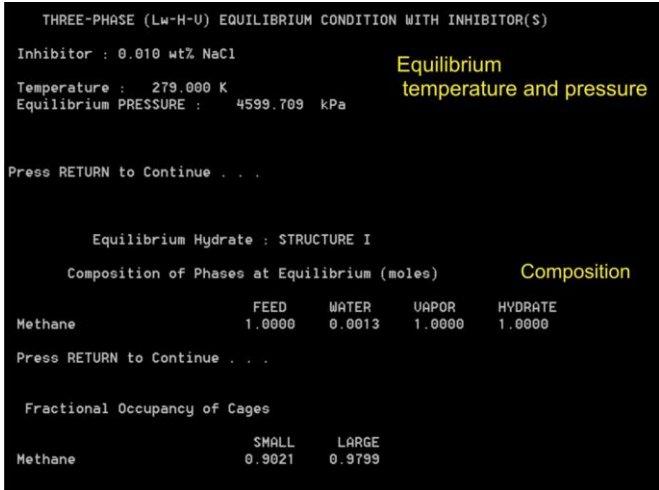
Figure 2.5 A) Shaded time map of the buried horizon showing processing artifacts indicated in the E10001 seismic survey, location within the survey shown in lower right corner. **B)** Seismic section showing location of the surface from A (indicated with yellow line) and processing artifacts with down shift of the reflections.

2.3 Interpretation tools

The Schlumberger Petrel 2011.1 seismic-to-simulation software was used as a main interpretation and visualization tool in this thesis, run on a 64-bit mobile workstation. Petrel 2011 provides the interpreter with a range of horizon interpretation tools, seismic attribute calculations applicable to horizons or to seismic volumes, and ability to visualize features in 3D, improving the understanding of their spatial distribution. The CorelDraw X5 software was used for creating and adjusting the figures.

Modeling of the gas hydrate stability field

The equilibrium conditions of gas hydrates and the thickness of the gas hydrate stability zone (GHSZ) was modeled using the CSMHYD software from Sloan Jr (1998b). This software calculates pressure/temperature conditions for the phase boundary between free gas and gas hydrate for different hydrate structures (I, II and H). The software allows changing or adjusting gas composition, thermal gradient, and pressure, as well as, formation water salinity. The CSMHYD modeling results were used to estimate changes in the gas hydrate stability zone between shelf edge glaciations and ice free interstadials, as well as for evaluating gas composition. Temperature at depth is assumed to follow present day geothermal gradient which can be obtained from exploration wells.



THREE-PHASE (Lw-H-U) EQUILIBRIUM CONDITION WITH INHIBITOR(S)

Inhibitor : 0.010 wt% NaCl

Temperature : 279.000 K

Equilibrium PRESSURE : 4599.709 kPa

Equilibrium temperature and pressure

Press RETURN to Continue . . .

Equilibrium Hydrate : STRUCTURE I

Composition of Phases at Equilibrium (moles)

	FEED	WATER	UAPOR	HYDRATE
Methane	1.0000	0.0013	1.0000	1.0000

Composition

Press RETURN to Continue . . .

Fractional Occupancy of Cages

	SMALL	LARGE
Methane	0.9021	0.9799

Figure 2.6 Table showing the interface of the modeling software CSMHYD by Sloan Jr (1998b) for the gas hydrate phase stability calculations (<http://hydrates.mines.edu/CHR/Software.html>).

2.4 Volumetric 3D Seismic attributes

Volumetric attributes can be applied on the entire dataset or user predefined volume allowing the interpreter to enhance visualization and improve recognition of the geological features in the subsurface.

Structural smoothing

Structural smoothing is a useful attribute performing smoothing of the data by applying of the Gaussian weighted averaging filter. It improves signal to noise ratio allowing to enhance structural interpretation and continuity of the seismic reflectors. The Structural smooth attribute is used as an input for the Variance, Chaos and Ant-tracking attributes workflows, and in order to establish structural framework (Schlumberger, 2010).

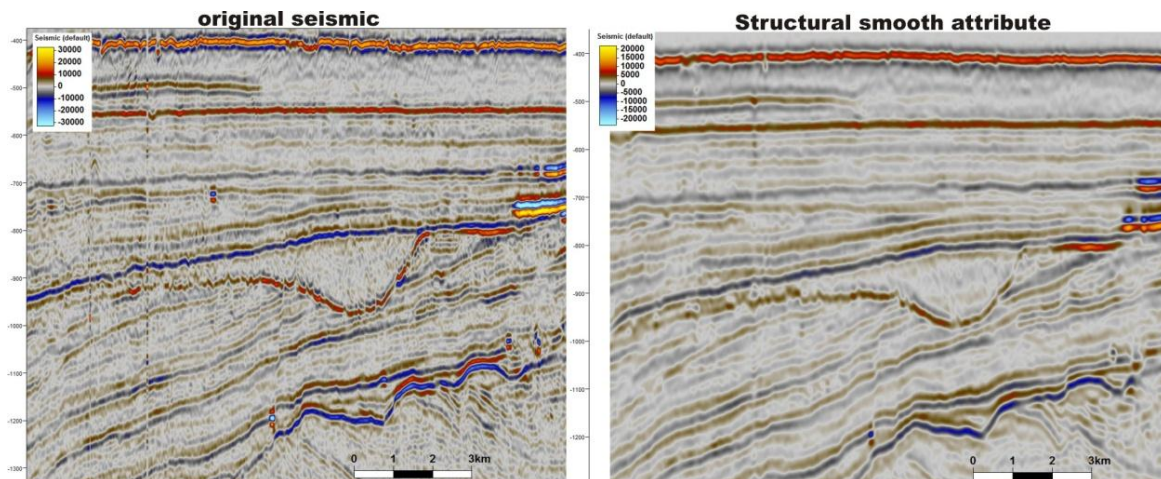


Figure 2.7 Two seismic profiles of the same inline of the E10001 survey showing comparison of the original seismic (left) and Petrel structural smooth attribute (right) in the interpretation window.

Chaos seismic attribute

The Chaos seismic attribute is mapping the “chaos” of the local seismic signal based on statistical analysis of dip to azimuth estimate applied to the seismic volume. This attribute is useful for identifying and enhancing faults, fractures and discontinuities, as well as helps to distinguish channel infill’s, gas chimneys and salt diapirs (Schlumberger, 2010).

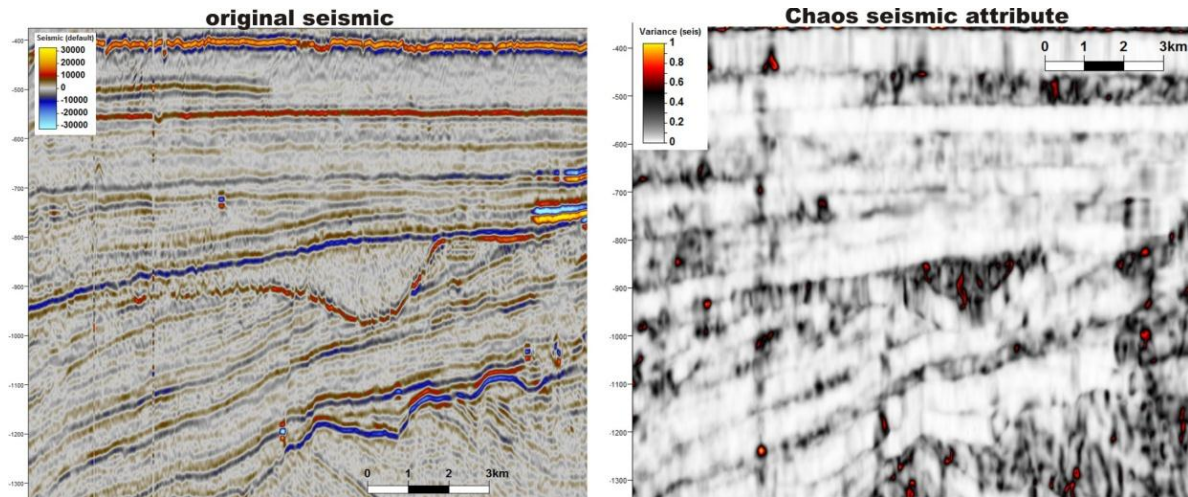


Figure 2.8 Two seismic profiles showing comparison of the original seismic (left) and Petrel Chaos seismic attribute (to the right), displayed in interpretation window.

Variance attribute

The Variance volumetric attribute is an edge detection method, which basically estimates local variance in the seismic signal (Schlumberger, 2010). Parameters and the size of the filter can be defined for each orientation by the inline-crossline range parameters and vertical smoothing can be applied in range of 0-200 milliseconds.

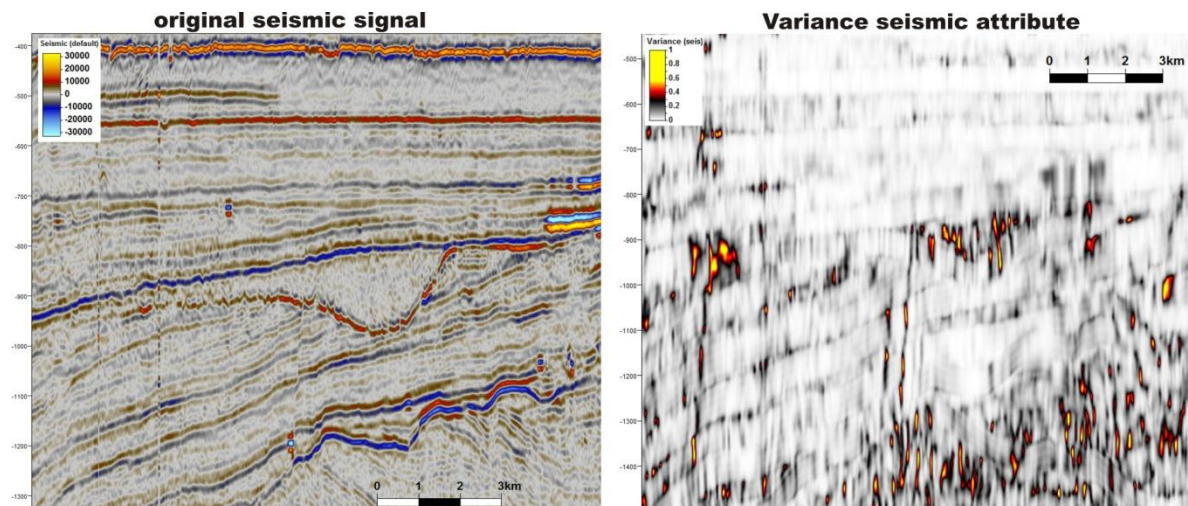


Figure 2.9 Two seismic profiles of the same line, showing comparison of the original seismic (left) and profile with applied Variance attribute on the right side.

Ant-tracing seismic attribute

Ant-tracking filter is another advanced algorithm in Petrel 2011, which helps to identify and separate faults and fractures, as well as vertical acoustic pipes by the algorithm imitating the ant's behavior in nature. It is possible to adjust certain parameters such as Stereonet, in order to search for discontinuities in preferred orientation. This attribute is useful for automatic fault extraction and enables fast detection of the structural framework (Schlumberger, 2010).

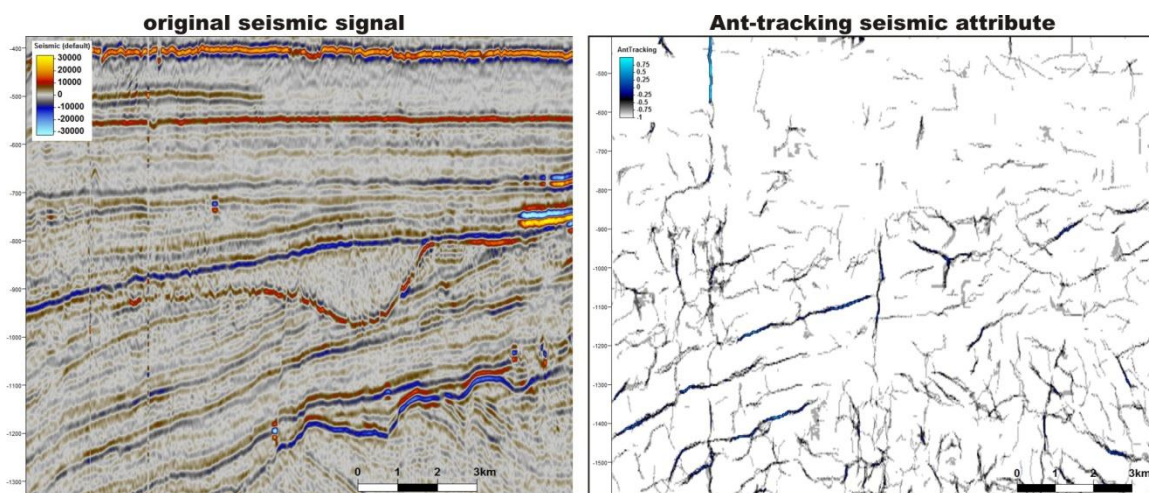


Figure 2.10 Two panels showing original seismic line of the EL0001 3D survey and profile from Ant-tracking cube applied for the cropped volume.

2.4.5 RMS Amplitude attribute

Root Mean Square (RMS) Amplitude is defined as the root of the sum of the squared amplitudes, divided by the number of samples (Schlumberger, 2010). *RMS Amplitude* is very useful for mapping the geological features which are isolated from the background by amplitude response such as gas accumulations, isolated sediment blocks etc. Since the mapping is performed to isolate features laterally *RMS Amplitude* is applied as a surface attribute, where user can define certain volume for calculations, but the resultant output is surface.

Volume render in Petrel

3D visualization using the volume render attribute in Petrel gives an excellent opportunity for studying internal structures and spatial relationship of high-amplitude segments

observed on seismic. The opacity function makes low amplitude values transparent and allows displaying three-dimensional views of the high-amplitude anomalies.

2.5 Well Data

Well dataset is represented by the exploration borehole 7216/11-1S, acquired by NorskHydro and drilled in the central part of the 3D seismic survey NH9803 within Sørvestsnaget Basin (Fig. 2.12, Fig 2.1). Well penetrated to a 4215 m MSL (3709 m TVD due to deviated well path) and encountered sediments down to the Early Paleocene Danian age with constructed lithological log based on drill cuttings (Ryseth et al., 2003). Well data is used for lithological correlation and for the information on geothermal gradient for the GHSZ modeling. Location of the well within 3D survey NH9803 is shown in Figure 2.12.

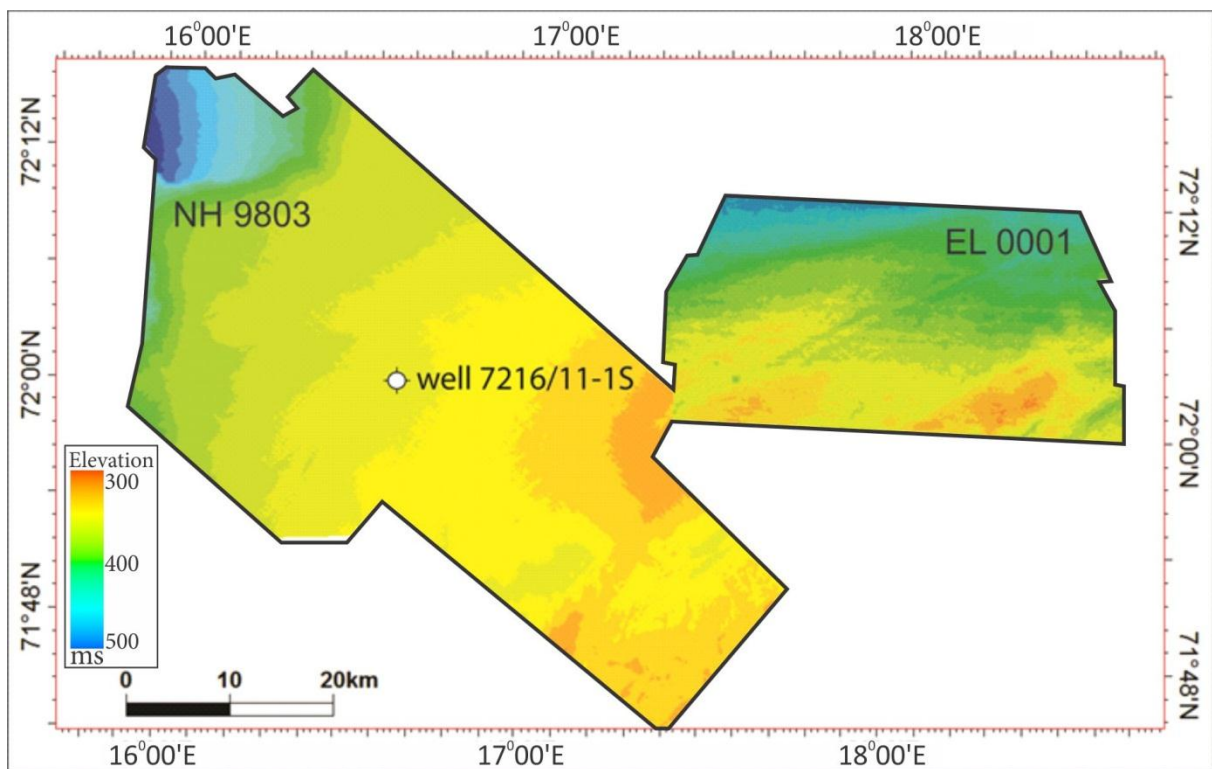


Figure 2.12 Map view of the 3D seismic surveys NH9803 and EL0001 seafloor showing location of the exploration bore hole 7216/11-1S indicated with the white circle.

3 Results

This study has the focus on studying a potential relationship between glacial erosion and fluid flow. For this purpose key seismic horizons have been interpreted, and the relationship with glacial erosional features and indications of fluid flow has been mapped and evaluated. Thorough description and interpretation of the features observed on the 3D seismic surveys is presented in the following chapter with focus on 3D visualization. In addition modeling of the gas hydrate stability field and changes in this field between glacials and interglacials has been modeled to evaluate in gas hydrates may have been involved in formation of the observed glacial erosional features.

3.1 Geomorphological features on the 3D seismic data

The study area is located close to the present day continental margin (Fig. 3.1) and on a formally glaciated shelf (Vorren et al., 1988; Andreassen et al., 2004) The Seabed is gently dipping in a W-NW direction with a significant down step observed (Fig. 3.1) on the northern tip of the survey NH9803, revealing the back wall of a slide scar.

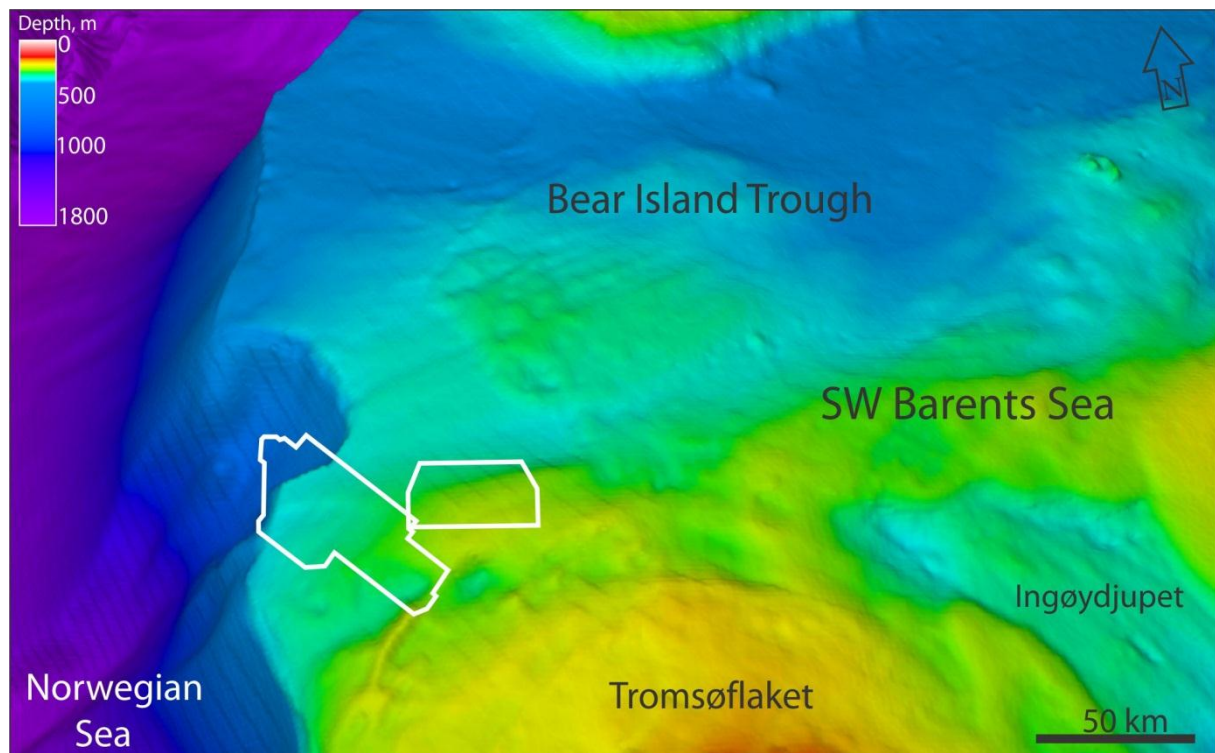


Figure 3.1 Perspective view of the shaded bathymetry map showing large scale landforms on the seabed of the SW Barents Sea (vertical exaggeration 50 times). The boundaries of the 3D surveys are indicated by the white polygons.

Several prominent geomorphic features are observed on the interpreted horizons of the NH9803 and EL0001 3D surveys. Most types of observed geomorphic features are better imaged on the seabed horizon due to the higher resolution and better preservation. Therefore, the general description of the different morphologic features given here is using examples from the seafloor horizon.

3.1.1 Elongated curved furrows

Description of elongated curved furrows

Surfaces of the interpreted seabed horizons are dominated by curvilinear furrows with different orientation and size. The length of the features is from 200 m up to 10 km with exceptional furrows reaching to 44 km and crossing both 3D surveys. Depth of the furrows, assuming sound velocity in the water of 1470 m/s, ranges between 3 and 17 m and they are generally 100 to 250 m wide with some furrows up to 450 m. Examples of elongated curved furrows are shown in Fig. 3.2. It is several generations of them observed on the horizons which are overprinting each other and many poses elevated levees on the sides.

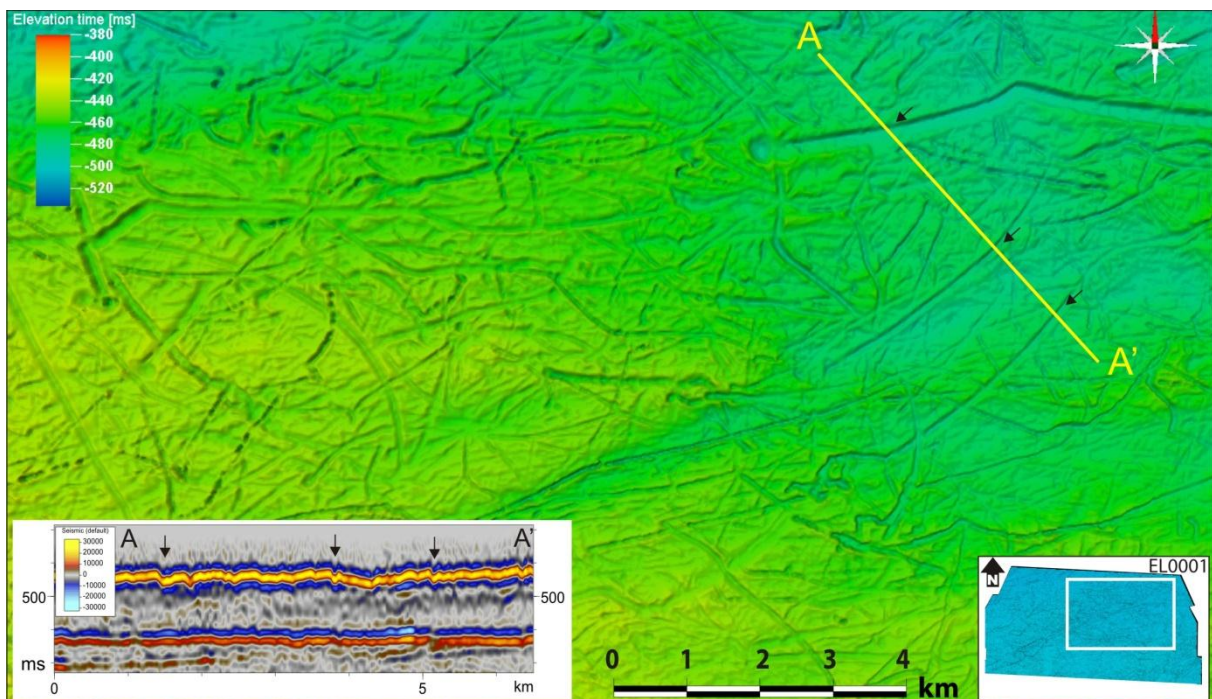


Figure 3.2 Shaded time map of the seafloor horizon within the EL00013D survey showing irregularly spaced curvilinear furrows exposed on the surface. Extent of the figure within 3D survey is indicated in right corner. Seismic profile A-A' shows vertical extent of the furrows indicated by black arrows.

Interpretation of elongated curved furrows

Curvilinear furrows observed on the seafloor horizon and on some horizons below seabed are interpreted to be a scours or plough marks produced by the icebergs scratching the seafloor (Stoker and Long, 1984). Appearance of the iceberg plough marks is characteristic for the glacial marine environments (Rafaelsen et al., 2002; Andreassen et al., 2007,b) , where calved icebergs could travel for long distances, driven by wind and currents, and plough the unconsolidated shelf sediments at shallower than the iceberg keel depth's (Stoker and Long, 1984).

3.1.2 Parallel linear ridges and troughs

Description of the parallel linear ridges and troughs

Almost every interpreted horizon above R5 poses on its surface parallel elongated ridges and troughs. On the seafloor reflector these linear features are distinguished from the artifacts due to their orientation and continuation.

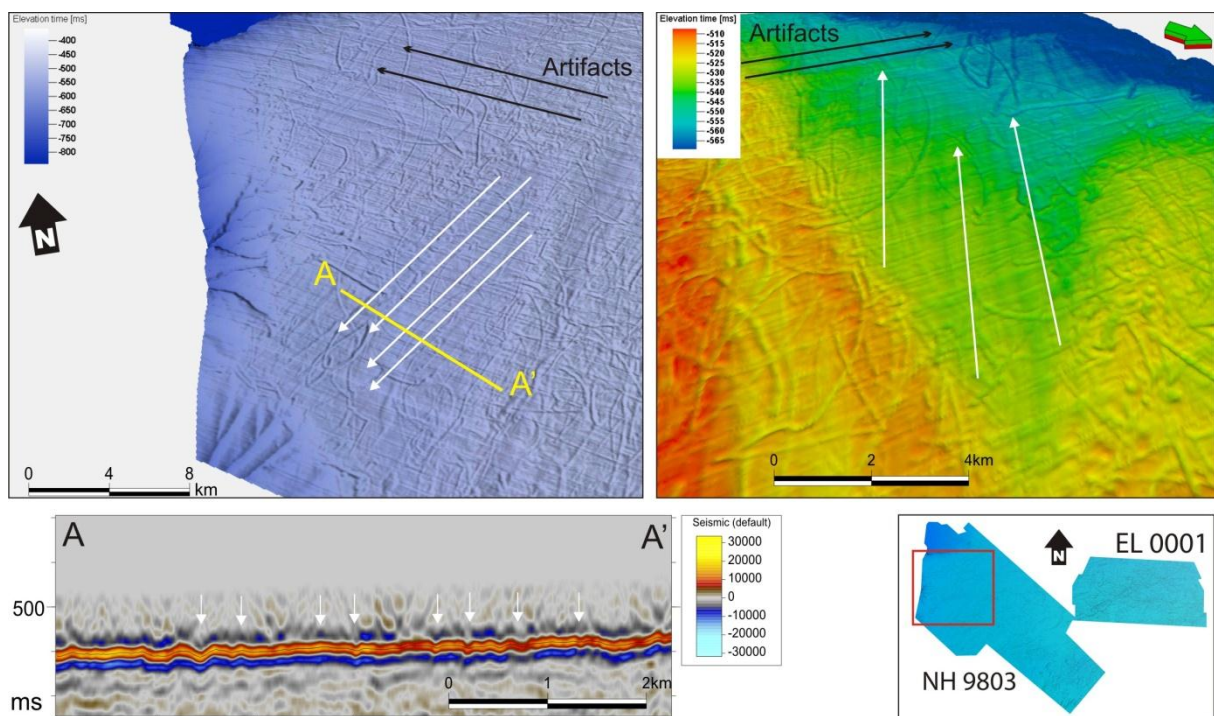


Figure 3.3 Shaded time maps showing features interpreted to be the Mega-Scale Glacial Lineation's (MSGSLs) observed on the seafloor horizon of Sørvestsnaget 3D survey (maps location indicated in lower right corner, note view from the northeast in the right figure). White arrows indicate MSGSLs , black arrows show acquisition footprint artifacts.

Both surveys seabed horizons incorporate groups of parallel linear features with different orientation, but having SW-NE trend. Observed lineation's range in length from several kilometers up to 28 km and generally 150 to 250 m wide, the height difference between ridges and troughs is about 10 m, assuming that sound velocity in the water is 1470 m/s. It is hard to say either this features has an erosional or depositional nature.

Interpretation of the parallel linear ridges and troughs

Based on their morphological criteria (Stokes and Clark, 1999) and geological history of the study area (Faleide et al., 1996; Rafaelsen et al., 2002; Andreassen et al., 2004) parallel linear features can be interpreted as mega-scale glacial lineations (MSGs), formed under fast flowing ice (Stokes and Clark, 2002). MSGs are bundles of glacial flutes interpreted to be formed by the deformation of sediments at the base of a fast flowing ice streams (Tulaczyk et al., 2001; Clark et al., 2003), draining the Barents Sea Ice Sheet (Andreassen et al., 2008), and known to be a common features on glaciated margins (Cofaigh et al., 2003). Existence of a former ice streams in the study area is inferred from the different data sources by several previous works (Solheim et al., 1990; Vorren and Laberg, 1997; Rafaelsen et al., 2002; Andreassen et al., 2004; Andreassen et al., 2007,b). Importance of the MSGs is in their indicative role for the ice stream direction and subglacial processes preserved in geological record and resolvable by the 3D seismic method.

3.1.3 Sub circular depressions

Description of the circular depressions

Interpreted seafloor horizons are revealing circular and sub circular depressions of different dimensions scattered over the areal extent of the Sørvestsnaget and Veslemøy 3D surveys. Group of three largest circular depressions observed in the west end of the EL0001 Veslemøy survey (Fig 3.4 A). These depressions vary in diameter from 500 m up to 1.2 km and from 5 m to 25 m deep assuming sound velocity of 1470 m/s. Depressions poses elevated rims around central deep and heavily affected by the ploughmarks (Fig 3.4 D).

Results

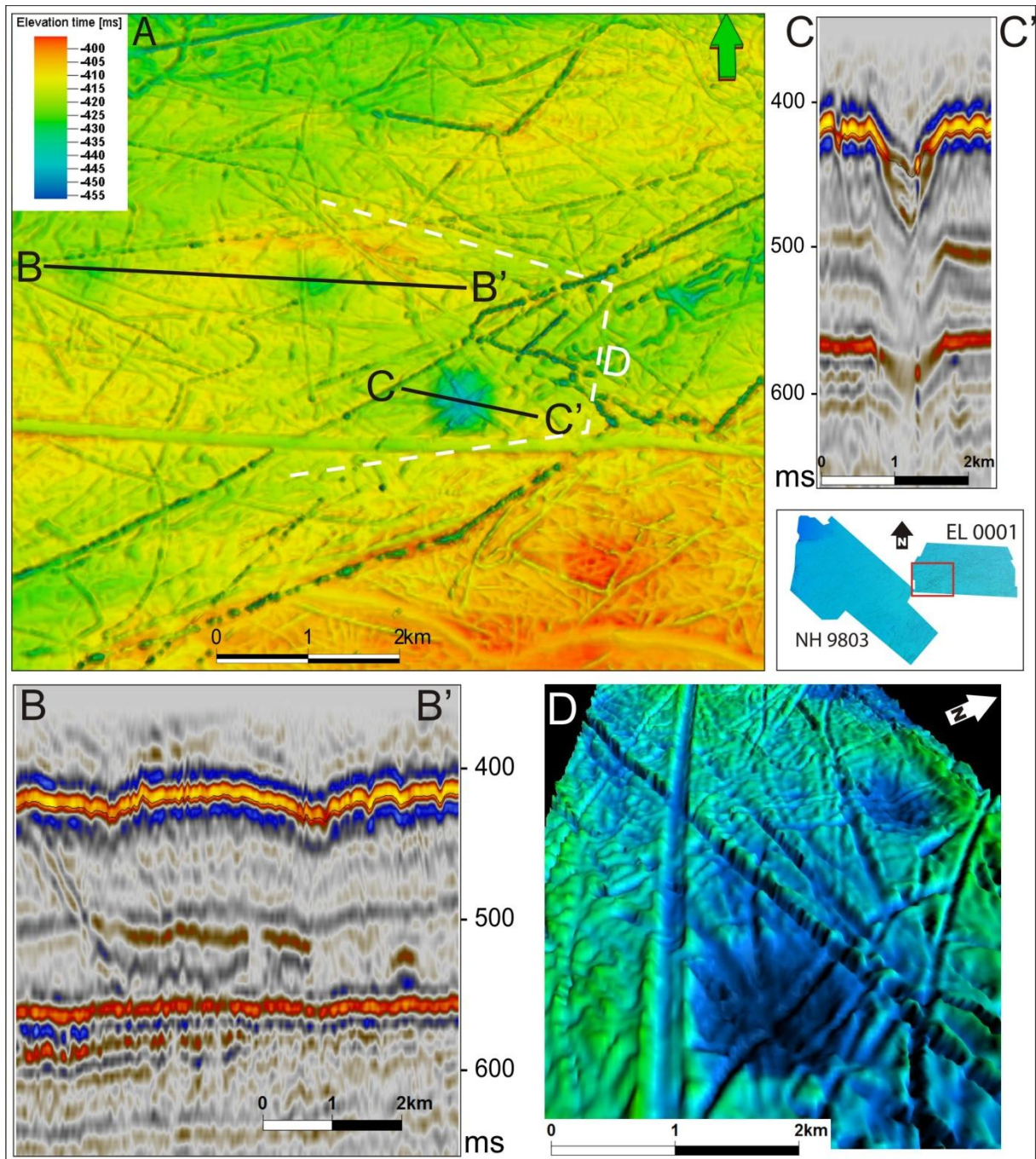


Figure 3.4 **A)** shows time map of the seafloor horizon of the Veslemøy 3D survey, with exposed circular depressions interpreted to be pockmarks. **B** and **C** showing seismic profiles across pockmarks indicated in **A**. **D)** Illuminated perspective view of the seabed showing elevated rims around pockmarks and heavy iceberg scouring reaching bottom of the depressions (View angle indicated in **A** by white dashed line).

Interpretation of the circular depressions

Circular depressions can be produced by a range of geological processes among others are volcanism, glaciotectionic, meteorite impact or grounded icebergs (Fichler et al., 2005). Although aforementioned genesis's are not excluded, likely interpretation of these depressions is a giant pockmarks formed by the expulsion of fluids and gas from the seabed leading to removal of sediments (Hovland, 1981; Hovland and Judd, 1988; Judd and Hovland, 1992; Lammers et al., 1995).

Interpretation is based on the typical for the pockmarks shape of depressions and their subsurface expression (Hovland et al., 2002) characterized by vertical stack of palaeo-pockmarks (Fig. 3.4 C). Although, inferred stack of pockmarks could be due to pull-down effect whoever it is interpreted that they are real features based on slightly different shape on the profile and in map view as well as truncated reflection on its flanks. The Iceberg plough marks overprinting the giant pockmarks interior are indicating that the second is older and have been formed and became inactive prior the scouring took place.

3.2 Interpreted seismic horizons

The two 3D seismic surveys, the NH9803 Sørvestsnaget and the EL0001 Veslemøy High, are the main datasets used in this study. These seismic surveys reveal tens of continuous reflections which are possible to interpret throughout the surveys. The focus of this thesis was the relationship between glacial erosional features and indications of fluid flow. In order to have an overview of relevant features, most of the reflections have been interpreted, but only key horizons that reveal features relevant for the topic of this thesis were chosen for more detailed studies and are presented here. Figure 3.5 shows these key horizons on a composite seismic profile across the two 3D surveys.

Results

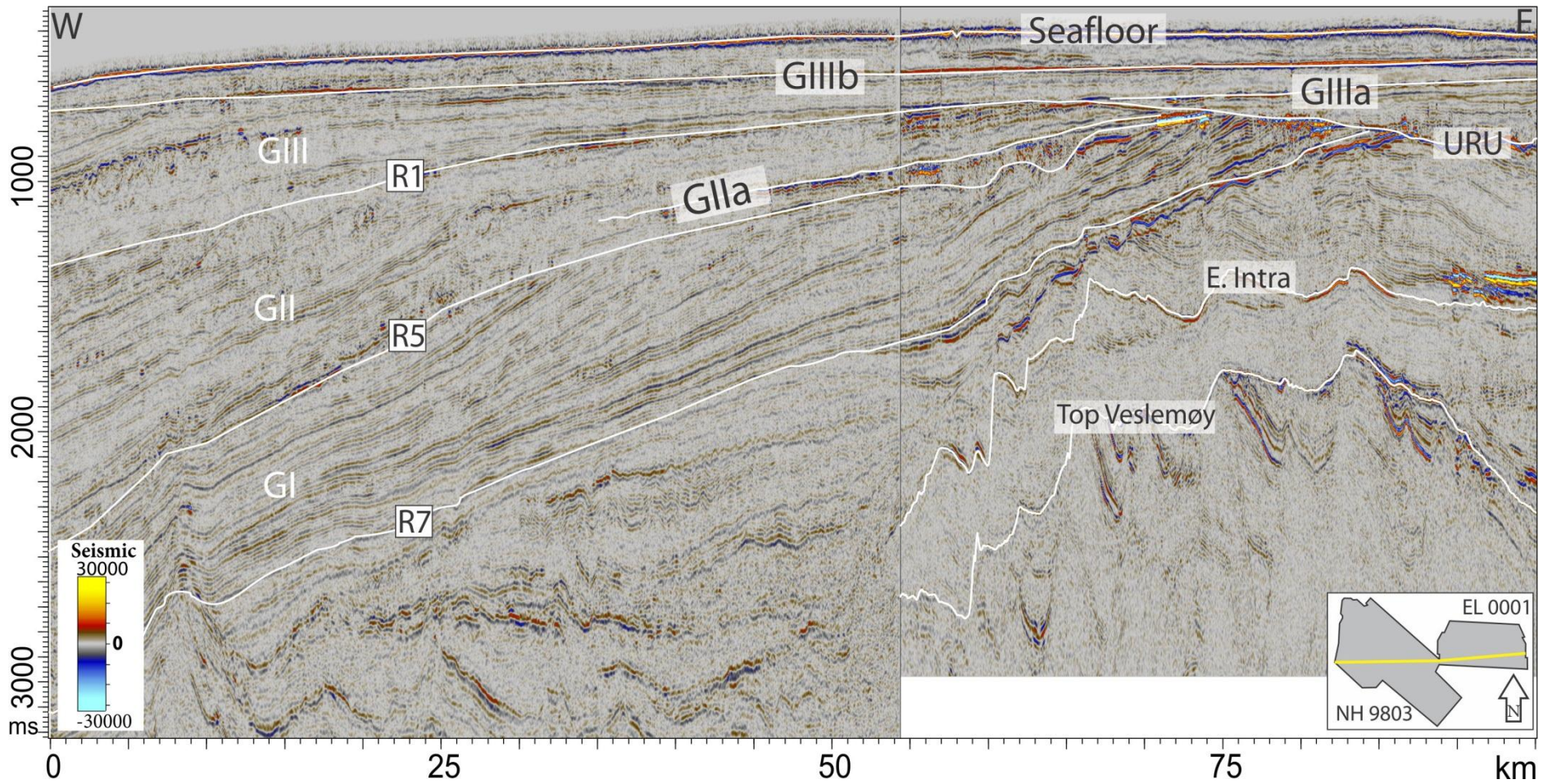


Figure 3.5 Composite seismic profile showing location of the key horizons interpreted in this study. The GI-GIII are indicating the Plio-Pleistocene glacial packages, and location of the profile within the surveys is shown by yellow line in the lower right corner. R1, R5 and R7 are regionally correlatable reflectors.

3.2.1 Seafloor horizon

Location of the datasets in vicinity of the present day continental margin and on a formally glaciated shelf (Vorren et al., 1988; Andreassen et al., 2004) are resulting in a associated seafloor morphology resolved by resolution of the 3D seismic surveys.

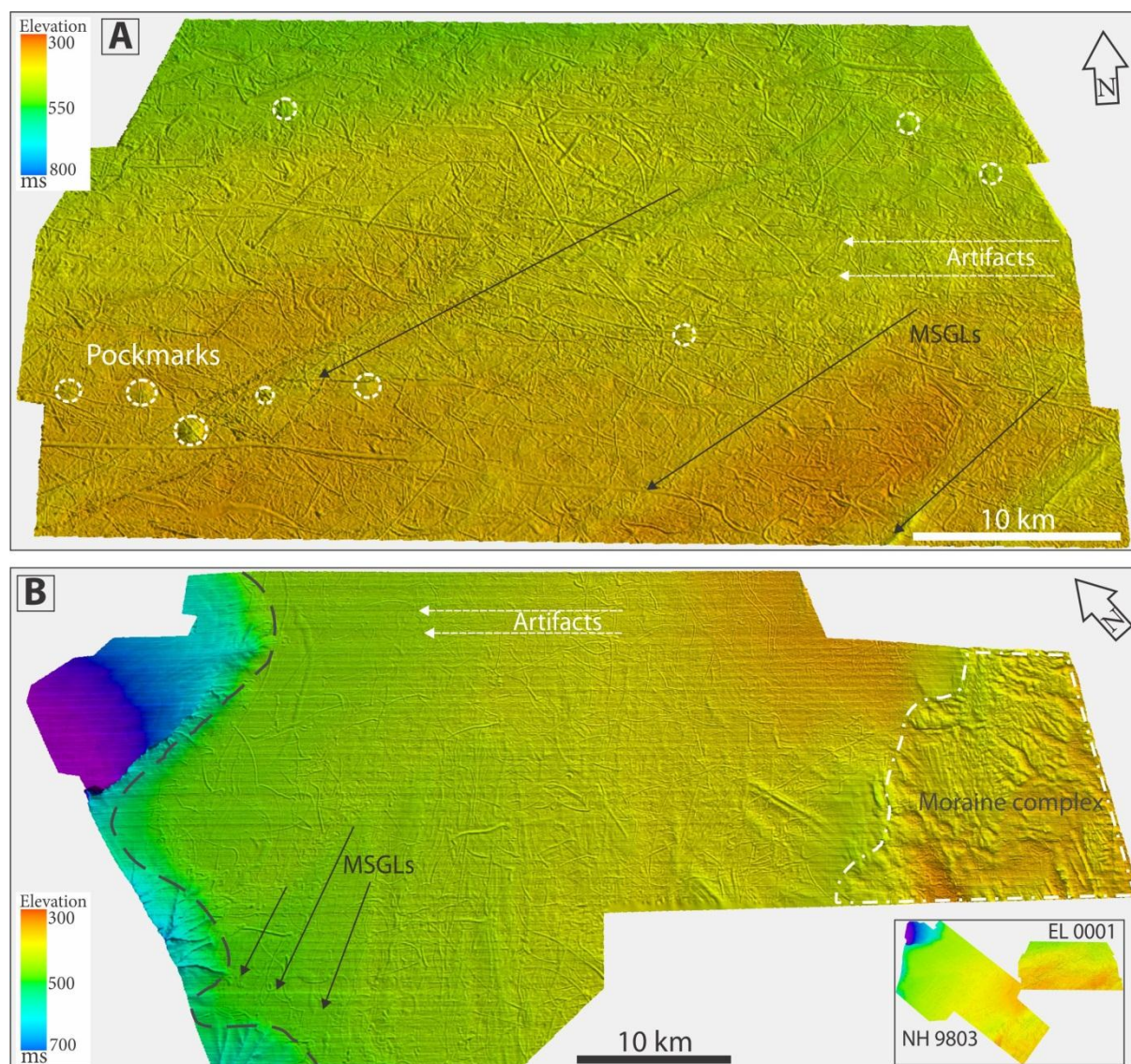


Figure 3.6 Shaded relief time maps of the interpreted seafloor horizons of the two 3D seismic surveys showing geomorphologic features. **A)** Interpreted seafloor horizon of the EL0001 seismic survey showing heavily ploughed by icebergs surface overprinting older features. The black arrows indicate orientation of mega-scale glacial lineations and dashed circles show interpreted pockmarks. **B)** The time map of the NH9803 survey seafloor horizon showing abundant iceberg plough marks, MSGLs and interpreted moraine complex at the SE limit of the survey. The black dashed line in the NW part of the survey is outlining head wall of the submarine slide scar.

Results

The seafloor is gently dipping towards west-north-west with a significant down-step observed on the northern tip of the survey NH9803 (Fig. 3.6). This down step represents parts of the headwall of the Late Pleistocene slide scar that took place on the continental slope of SW Barents Sea about 200 ka (Laberg and Vorren, 1993). The seafloor horizons of both surveys show subtle mega-scale glacial lineations over-printed by the iceberg ploughmarks. A group of giant pockmarks of up to 1 km in diameter is observed in the south-western part of the Veslemøy survey. It seems that iceberg ploughmarks are disturbing the flanks of the pockmarks, indicating the fluid flow forming the pockmarks took place after the ploughing of icebergs. There is a certain decrease in the amount of the iceberg ploughmarks with depth towards western part of the study area and they are absent in the slide scar area. In the southeastern part of the survey NH9803 seabed show large scale irregularities (Fig. 3.6 B) expressed as curved ridges of different orientation. These ridges are interpreted as a terminal moraine complex deposited during last glacial maximum by slowly-moving ice centered over the Tromsøflaket bank area south of the study area (Andreassen et al., 2008). Mega-scale glacial lineations indicated on the seafloor horizon are interpreted to be formed under the fast-flowing ice stream. Based on MSGLs orientation similar to the flow sets 12 and 13 (Fig. 1. 11Dii), it is suggested that they were formed by the former ice stream draining Bear Island Trough (Bjørnøyrenna) during last advance of the Barents Sea Ice Sheet to the shelf break (Winsborrow et al., 2010).

3.2.2 Pleistocene horizon GIII b

The GIII b horizon is interpreted within upper part of the Pleistocene succession GIII and it represents strong reflection of normal polarity, compared to the seafloor. This horizon can be followed throughout both 3D surveys and it has slight dip in north-west direction.

The GIII b horizon appears within upper part of the Pleistocene succession GIII (Fig. 3.7) and it represents strong reflection of normal polarity, compared to the seafloor reflection (Fig. 3.8B). This horizon can be followed throughout both 3D surveys and it slightly dipping towards north-west (Figs. 3.7A and 3.7C).

There are several elongated curved furrows observed on the horizon, which are interpreted as the buried iceberg ploughmarks (Fig. 3.8A). These are most likely to be formed during a former Pleistocene deglaciation phase in the marine environments. The surface of the

interpreted GIIIb horizon shows two sets of MSGs (Fig. 3.7) with different orientation. The first set of the MSGs of south-west direction are expressed as low-relief (4 m assuming sound velocity of 1600 m/s) and very long straight lineations of up to 90 km long (Fig.3.7 A white arrows). This set of mega-scale lineations can be traced throughout both of the 3D surveys and extends beyond the eastern limit of the EL0001 seismic survey. The second set of the MSGs shows approximately north-south direction and made of curved lineations of about 250m wide and up to 20 km long (Fig. 3.7 B black arrows). These lineations appear to be a combination of ridges and furrows on the cross-section and exhibit relief of up to 14 m and the second set of MSGs is overprinting the first set described earlier.

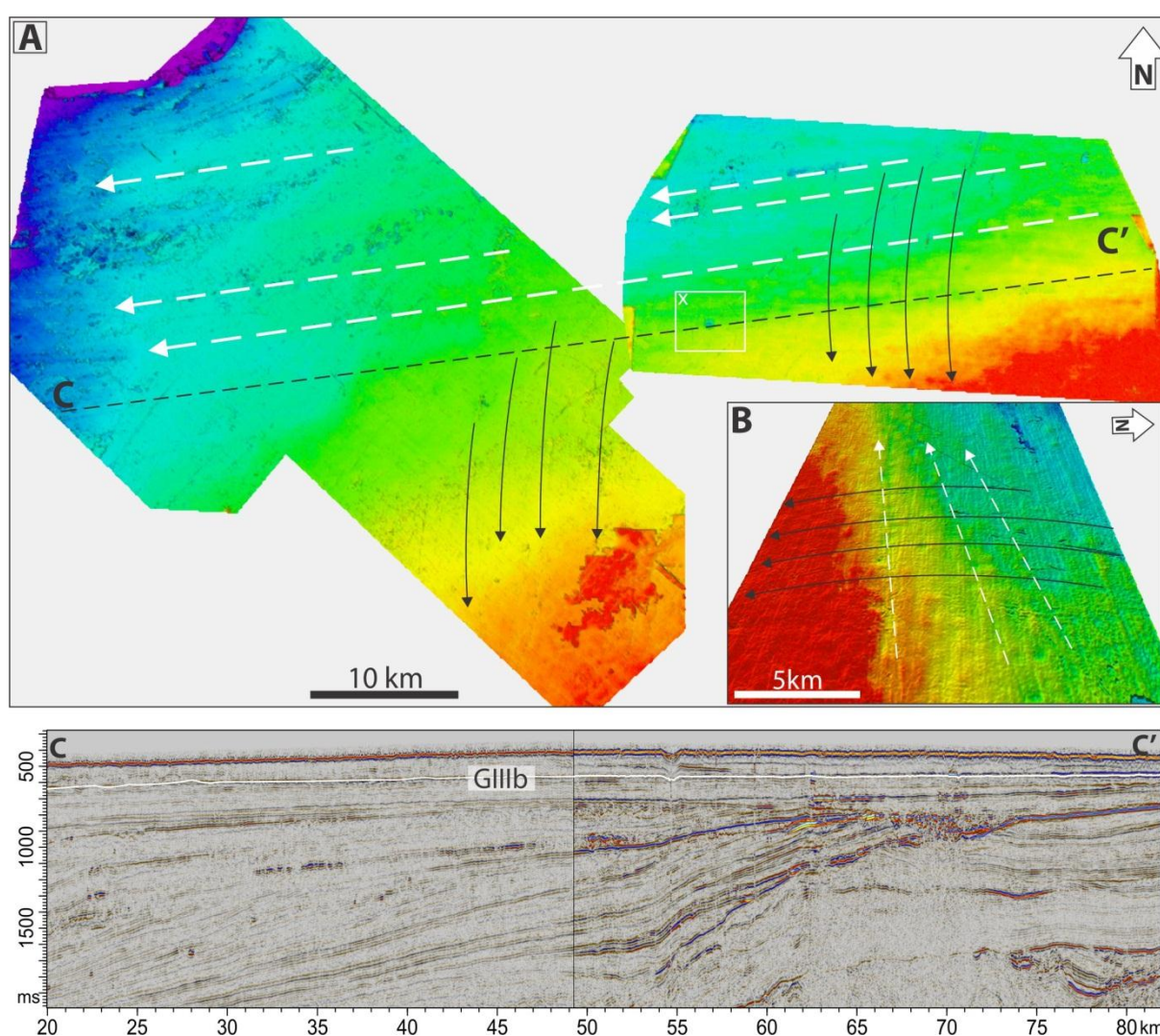


Figure 3.7 A) Shaded relief time-structural map of the horizon GIII b interpreted within Sørvestsnaget and Veslemøy 3D surveys. Two different sets of mega-scale glacial lineations shown by white and black arrows and black circles show location of the depressions. **B)** Perspective view from the east on

Results

the EL0001 seismic survey showing two sets of the MSGs indicated by black and white dashed arrows. **C)** Arbitrary seismic profile showing location of the interpreted horizon GIII b.

These two sets of mega-scale glacial lineations are interpreted to be formed by the fast-flowing ice streams draining former Barents Sea and Fennoscandian Ice sheets. The first set of the lineation has similar orientation with palaeo flow set 11 (Fig 1.11 Dii) (Winsborrow et al., 2010) is interpreted to be formed by the palaeo Ingøydjupet Ice Stream draining Fennoscandian Ice Sheet. The second set of the MSGs is showing curved pattern and interpreted to be formed by the palaeo Bjørnøyrenna Ice Stream (Fig. 3.1).

Several circular depressions are observed at the south-western part of the EL0001 seismic survey (Fig.3.7 A, white box X). One particular depression is about 1.1 km in diameter and up to 25 m deep (assuming sound velocity of 1600 m/s) and show truncation of the underlying reflection at its western flank (Fig. 3.8). This depressions are interpreted as giant palaeo pockmarks formed by the expulsion of fluids and gas from the deeper sources (Hovland and Judd, 1988; Solheim and Elverhøi, 1993).

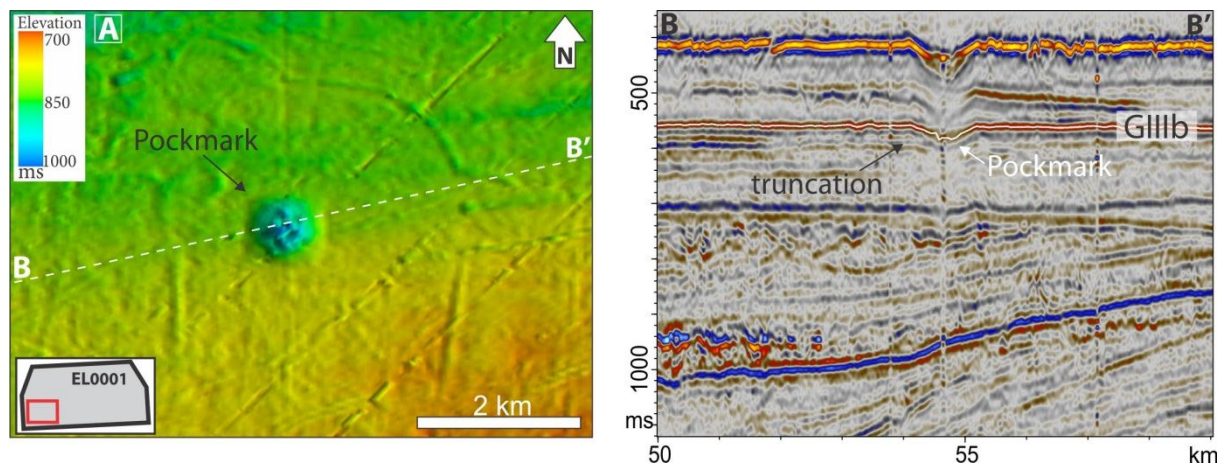


Figure 3.8 A) Shaded relief time map of the horizon GIII b showing well-developed palaeo pockmark at the south-western part of the Veslemøy 3D survey. Numerous curve-linear furrows visible on the surface are interpreted as the palaeo iceberg plough marks. **B)** Arbitrary seismic profile across the palaeo pockmark shows location of the GIII b horizon. Note vertical stack of palaeo pockmark under the giant pockmark expressed on the seafloor.

At the north-eastern part of the NH9803 3D survey a zone of are expressed as thrust and dislocated segments of high-amplitude (Fig 3.9 B). These chains of high-amplitude seismic anomalies are interpreted as dislocated sediment blocks or zones with extensive thrusting of

sediments. These ones are aligned in chains of SW-NE orientation and likely indicating a palaeo ice flow from the north-east, the same orientation as inferred from MSGs in the area. The MSGs of this orientation are inferred to be formed by fast-flowing ice streams draining out Bjørnøyrenna from the NE and so are also the chains of thrustsediments.

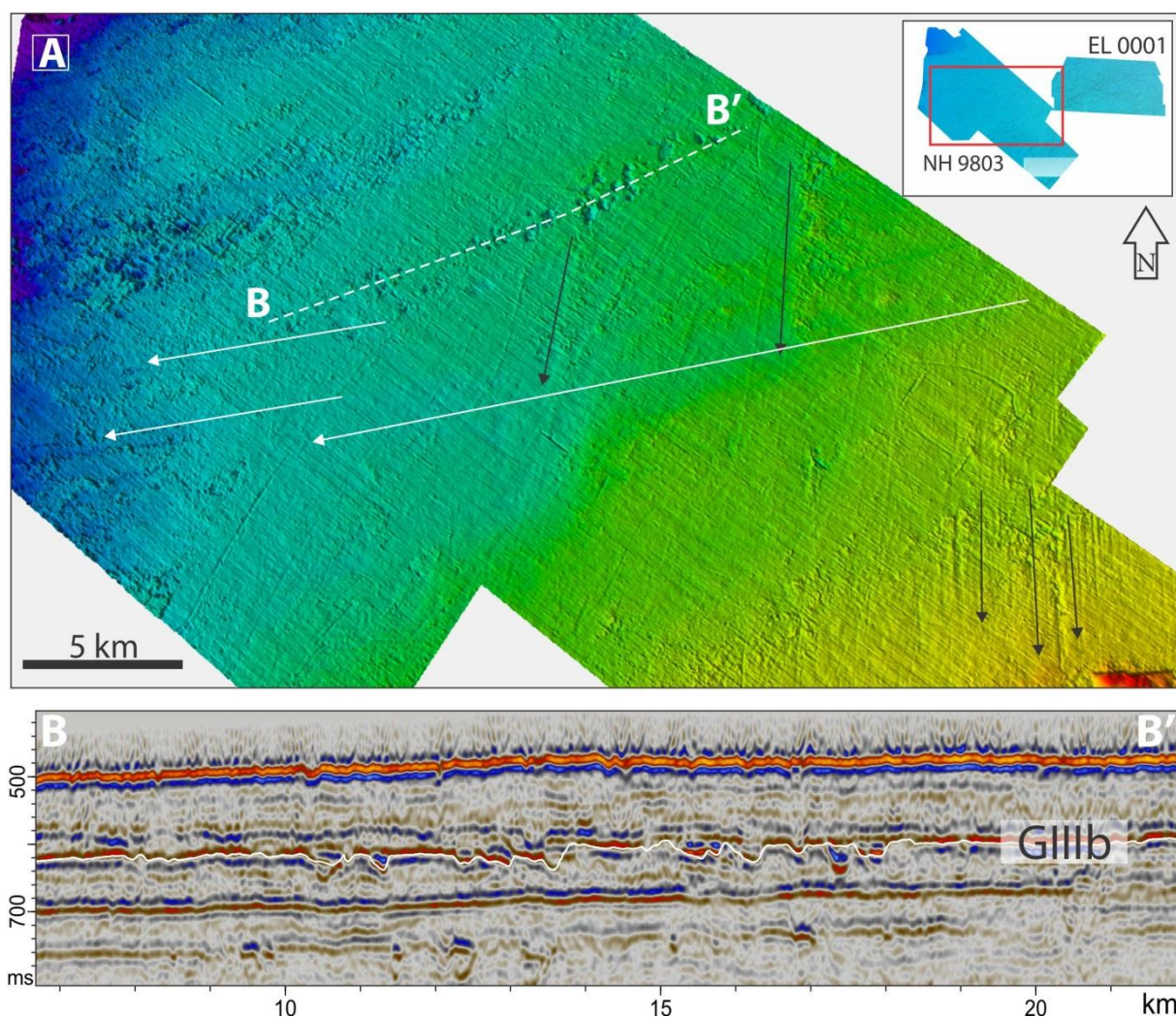


Figure 3.9 A) Shaded relief time map showing central part of the horizon GIII b in the NH9803 seismic survey, where distinctive zone of depressions is observed. Arrows indicate palaeo ice flow direction inferred from MSGs. **B)** Seismic profile showing vertical distribution of the observed amplitude anomalies associated with the upthrusting and imbrication of the segments.

3.2.3 Horizon Upper Regional Unconformity (URU)

Horizon upper regional unconformity (URU) is interpreted within eastern part of the study area where it is expressed as strong reflection (Fig. 3.10). Farther to the west this horizon is splits into reflection of different ages and genesis making it impossible to trace. At the eastern part of the EL0001 seismic survey URU represents the lower boundary of the Pleistocene succession GIII where it is overlying older Tertiary sediments (Ryseth et al., 2003), farther west URU shows parallel linear furrows on the eastern part of the EL0001 seismic survey (Figs 3.10A and 3.10B). These lineations are up to 15 km long and have a north-west orientation. On seismic profiles they appear as a combination of ridges and troughs about 5 m in relief (Fig 3.10C). At the south-eastern limit of the 3D area four large-scale troughs of NW-SE trend are observed (Fig 3.10). These troughs are up to 11 km long and 3 km wide, and as they are extending beyond the limits of the Veslemøy 3D survey, these are minimum estimates of their size. These troughs are appearing to be aligned parallel with the strike of the subcropping bedrock (Fig3.10 C), and most likely reflect subglacial erosion along weaker layers. Numerous sub-circular depressions on the URU are about 400 m in diameter and up to 20 m deep (assuming sound velocity of 1700 m/s). Based on their distinct shape and zones of acoustic masking under them (here you should refer to a fig showing this) these depressions are interpreted to be pockmarks. Many of these pockmarks are found within the large-scale erosional troughs and aligned with their long axes (Fig. 3.10B). There are no iceberg ploughmarks is observed on URU within extent of the EL0001 seismic survey. The eastern part of URU shows clear glacial erosional nature evident from the mega-scale glacial lineations indicative for the fast-flowing grounded ice. The MSGs appear also within the western part of the troughs (Figs 3.10 A and 3.10 B), indicating that ice streaming took place after formation of the erosional troughs. The WSW-ENE orientation of the MSGs suggest, from comparison with ice stream flow sets on the sea floor (Fig. 1.11Dii) that these were most likely formed by ice streaming out Ingøydjupet from the Fennoscandian Ice Sheet.

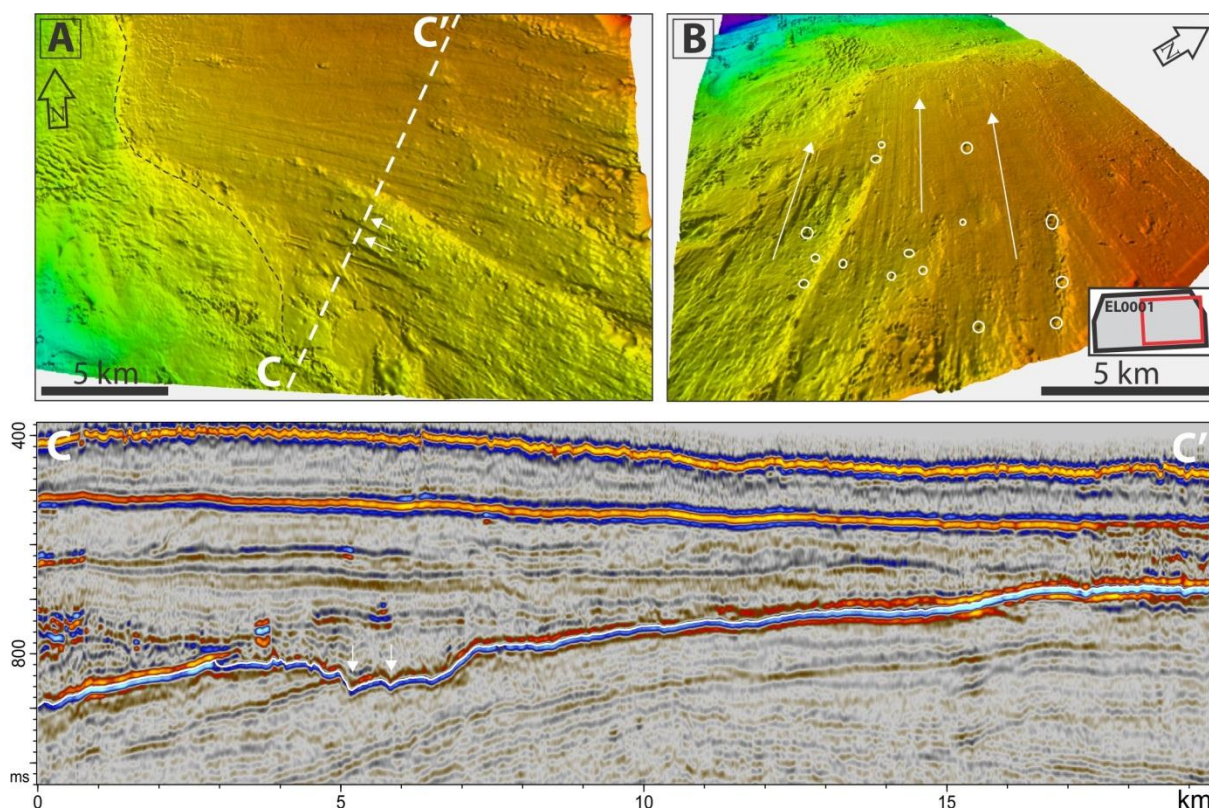


Figure 3.10 **A)** Shaded relief time map of the horizon R1 (URU) in the eastern part of the EL0001 seismic survey. Figure show well-developed MSGLS on the surface and erosional depressions at the south-eastern part of the figure. **B)** Perspective view of the horizon (URU) showing interpreted ice flow direction (white arrows) and distribution of the interpreted pockmarks indicated by the white circles. Note concentration of the pockmarks coinciding with the erosional depressions.

Farther to the west the lower boundary of the glacial package GIII is marked by the reflector R1 (Fig. 3.5) which separates it from the underlying Plio-Pleistocene packages GI and GII (Fig 3.5).

3.2.4 Horizon Intra GII a

Horizon GII a is interpreted at intersection of the two datasets and extends in the south-western part of the Veslemøy 3D seismic survey and at the north-eastern limit of the NH9803 seismic survey (Fig. 3.11). The eastern extent of the reflection is truncated by overlying erosional unconformity and western extent has a transition into a chaotic seismic facies making it impossible to interpret. This horizon is located in the lower part of the GII Plio-Pleistocene succession and right above zone of high-amplitude anomalies.

Results

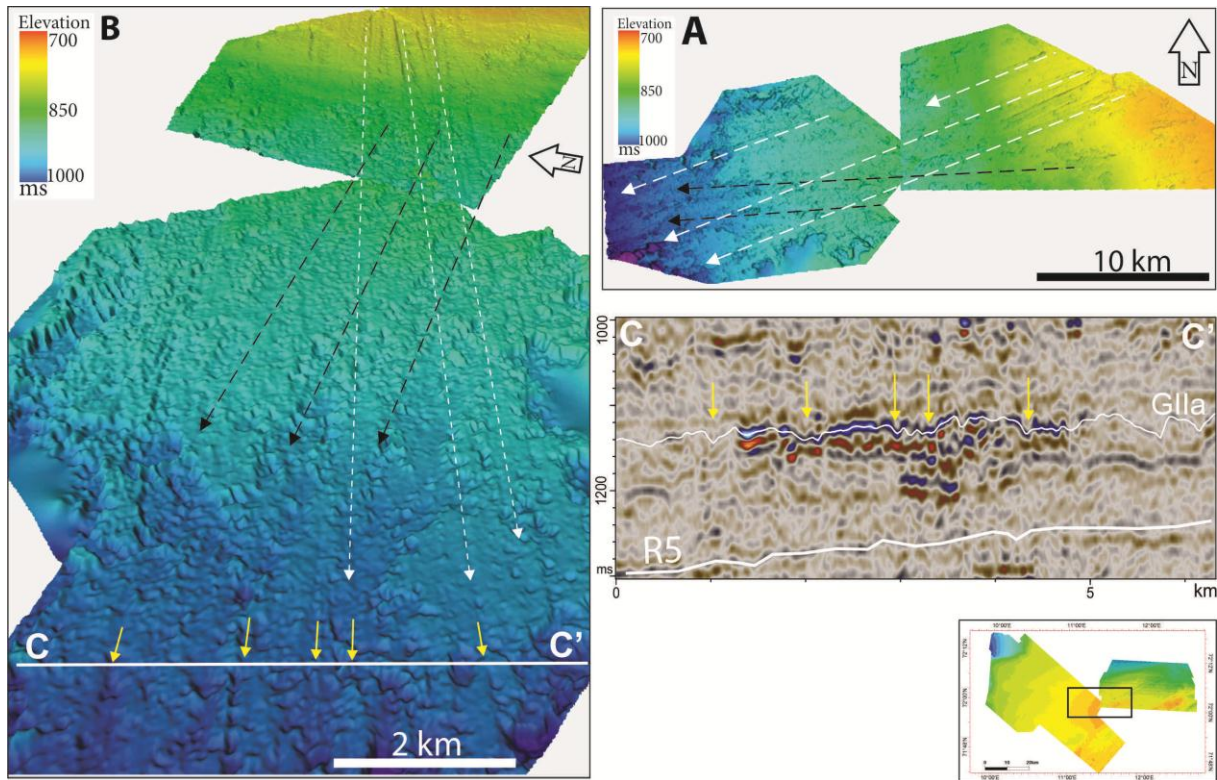


Figure 3.11 **A)** Illuminated time-structure map of the horizon GII a located at the intersection of the NH9803 and EL001 seismic surveys and showing two sets of the MSGLs indicated by dashed arrows. Location of the horizon shown in the lower right corner **B)** Perspective view of the horizon GII a from the west showing palaeo ice-flow direction inferred from the MSGLs and location of the seismic profile. **C)** Seismic profile showing location of the horizon GII a and high-amplitude anomalies right below horizon. Yellow arrows indicate interpreted MSGLs visible on time map and seismic profile.

Horizon GII a is exhibiting parallel linear furrows in two directions of western and south-western orientation (Fig. 3.11 B) and expressed as a negative relief features. They are up to 27 km long and reach up to 25 m deep at the eastern part. These linear furrows are interpreted as mega-scale lineations, indicating formation by fast-flowing ice streams. This horizon has been chosen due to its distinct geomorphologic features, such as MSGLs, and location right above high-amplitude anomalies, which allows investigating the relationship between those two.

3.2.5 Horizon R5

Horizon R5 is the regionally correlatable reflector extending through entire NH9803 seismic survey and passing into the south-western part of the EL0001 3D survey (Fig. 3.5). Farther to the east it is truncated by overlying younger unconformity of the R1 (URU) horizon (Fig. 3.5). On the seismic profile R5 shows its unconformable nature, truncating underlying westward dipping internal reflections of the GI unit and it represents the boundary between the sediment packages GI and GII. The R5 horizon has several distinct morphological features on its surface.

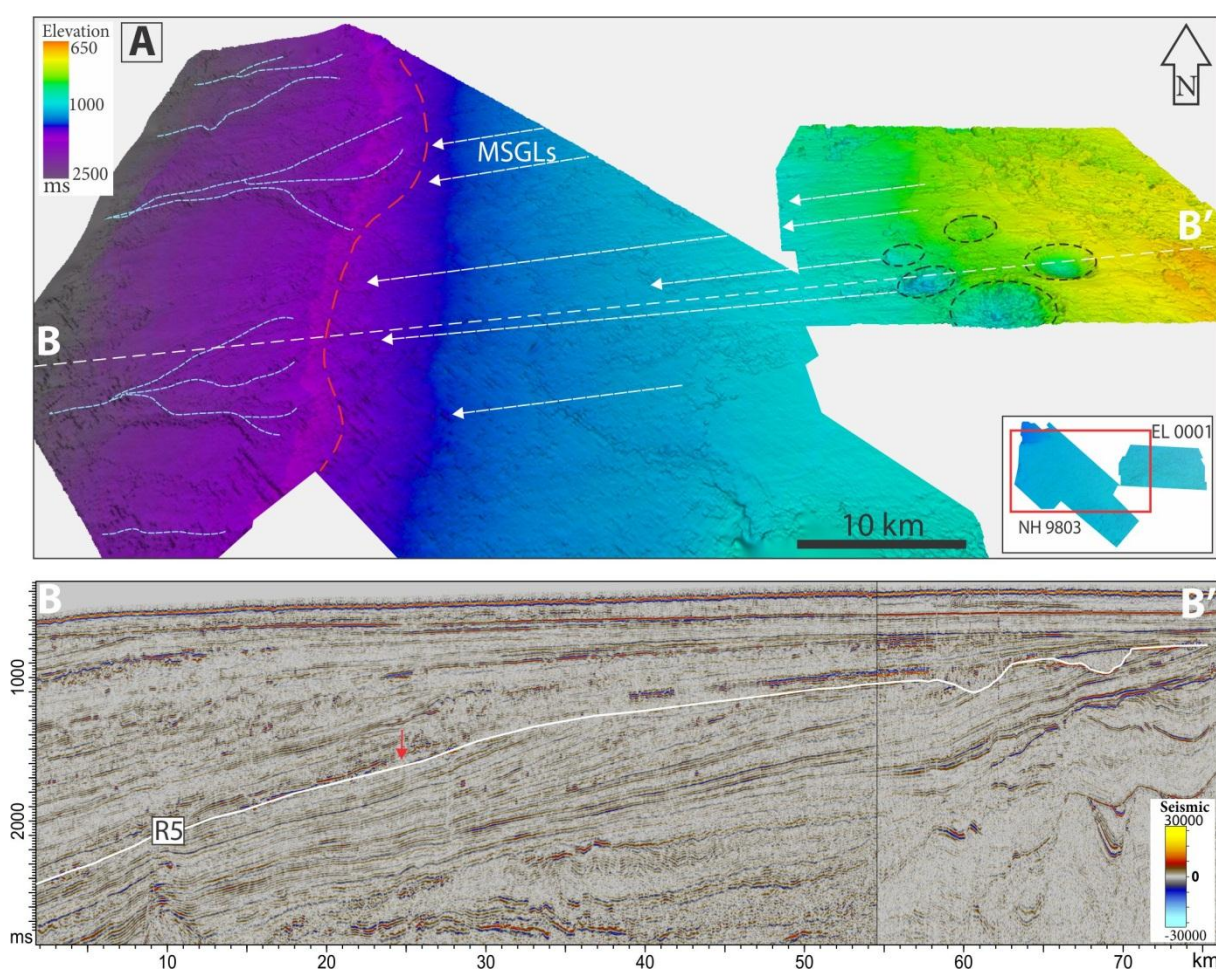


Figure 3.12 A) Perspective view of the time map showing horizon R5 and interpreted geomorphologic features. White arrows indicate mega-scale glacial lineations, red dashed line marks palaeo shelf break and maximum extent of the grounded ice. Blue dashed lines show interpreted submarine channels on palaeo slope and black circles indicate location of the depressions. B) Random seismic profile across two datasets, showing location of the R5 horizon and interpreted palaeo shelf edge indicated by red arrow. Vertical line indicates intersection of NH9803 and EL0001 3D seismic surveys.

Results

The structural time map of R5 shows sub-parallel elongated lineations of WWS-EEN orientation, which are up to 30 km long and 400 m wide and all of them terminate at the narrow zone of the N-S orientation (Fig.3.12A). To the west of this narrow zone, the R5 horizon starts to dip more steeply westward and is eroded by curved elongated furrows, which are merging downslope. In the eastern part of R5 within the Veslemøy EL0001 3D survey a group of large slightly elongated sub-circular depressions is observed (Fig. 12A). These depressions are from 1.7 km up to 5.2 km in diameter and reach up to 270 m deep (assuming sound velocity of 2000 m/s)

The parallel elongated lineations on the palaeo shelf part of R5 are interpreted as the mega-scale glacial lineations, formed at the base of the fast-flowing ice streams, whereas the curved furrows are inferred to be submarine palaeo slope channels. The narrow zone is interpreted as palaeo shelf break marking maximum extend of the grounded ice. The east-west orientation of the MSGs is suggesting that they were formed by the palaeo Ice stream draining Fennoscandian Ice sheet.

The R5 surface is a key horizon of this study and it has been used for visualization of morphologic features and generation of the RMS amplitude maps. Interpretation of the distinct geomorphological features observed on the horizon allows evaluation of the processes related to the glacial erosion and deposition. More detailed description and visualization of the features observed on the R5 horizon is provided in the chapter 3.3, dedicated to visualization and interpretation of the large depressions, which are interpreted to be glaciotectionic features. The MSGs are imaged in more detail in this chapter.

3.2.6 Horizon Eocene intra

The interpreted intra Eocene strong reflection within the Tertiary sediments is expressed as a normal polarity signal on the seismic profile. The time map of this horizon shows an undulating character which mimics structure of the underlying Veslemøy High (Fig. 3.13 B). In the western part of the EL0001 3D seismic survey this horizon shows significant faulting with down-throw of up to 350 m assuming sound velocity of 2000 m/s.

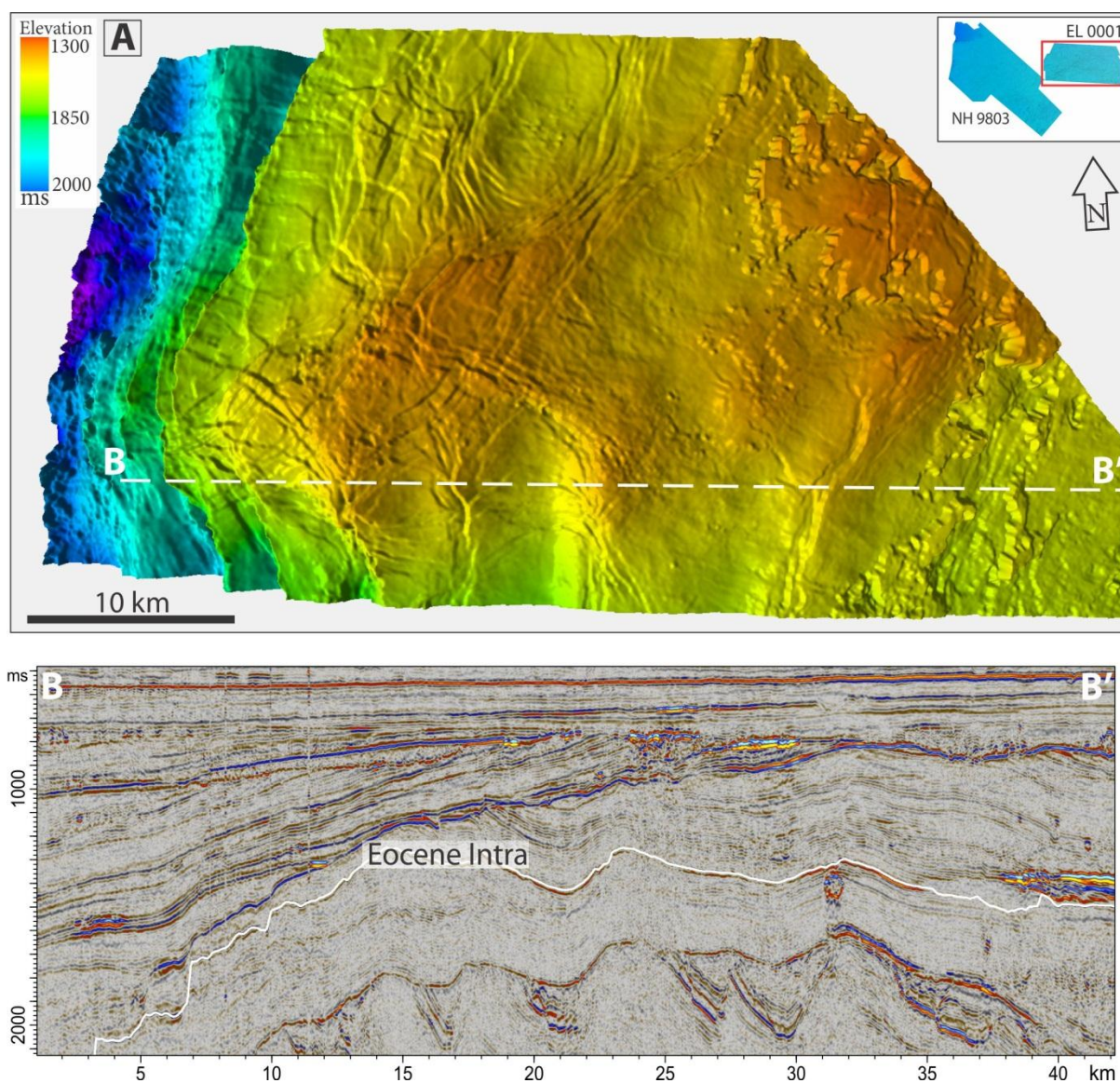


Figure 3.13 A) Illuminated relief time map of the Eocene Intra horizon within Veslemøy seismic survey showing large-scale folding and a network of subtle faults, as well as well-developed normal faulting towards Sørvestsnaget Basin at the western part of the survey. **B)** Seismic profile of the Inline 610 showing location of the horizon Eocene Intra and its conformable nature with the underlying Veslemøy High.

The surface of the *Eocene Intra* horizon displays a complex pattern of the discontinuities revealing two main orientations: one is in NNE-SSW direction and the second is in the NW-SE (Fig. 3.13A). These discontinuities show good correlation with the apex of anticlines of this surface and form intersecting patterns in central part of the survey.

The discontinuities on the Intra Eocene horizon are interpreted to be a network of faults related to tectonic deformation of the Tertiary succession associated with compressional

movements. This horizon is used as an input for RMS amplitude attribute to map high-amplitude anomalies and evaluate vertical fluid migration path ways associated with the fracture flow.

3.2.7 Horizon Top Veslemøy High

The Top Veslemøy horizon (Fig 3.14) is the lowermost horizon interpreted in this study and located within EL0001 3D seismic survey. This horizon appears on the seismic as a high-amplitude reflection of normal polarity likely indicating sediments with the higher density/velocity properties below it (Fig. 3.14). The western part of the horizon shows significant down-stepping associated with extensive listric-faulting, evidenced from seismic profiles. The truncation of underlying strata reveals the erosional nature of this horizon. The Top Veslemøy reflection has high continuity and reveals a low angle undulating surface of the High with fault assisted bulges and depressions (Fig. 3.14A).

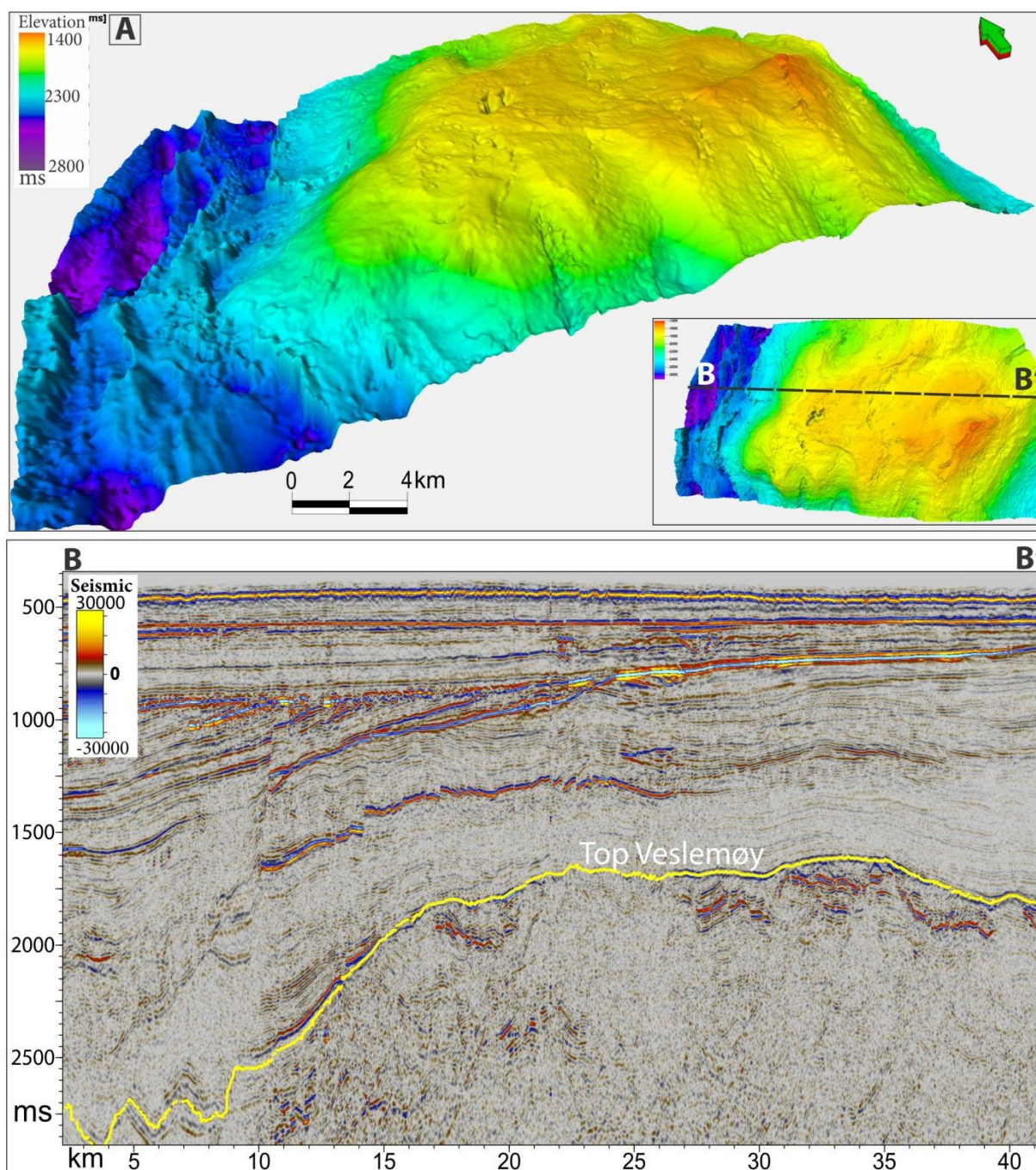


Figure 3.14 **A)** Tree-dimensional perspective view of the interpreted horizon Top Veslemøy High showing well developed fault complex of NNE-SSW direction bounding western limit of structural high. **B)** Seismic profile across the Veslemøy High shows location of the interpreted horizon and listric deep-sited faults with significant down-throw in the western side of the line.

A group of parallel ridges and troughs are observed on the SE end of the horizon (Fig.3.15). These grooves have N-S orientation and are followed for up to 7 km and are around 3 to 7m high. The observed ridges, although they might resemble mega-scale glacial

Results

lineations, are interpreted represent sub-cropping sediment layers and vertical fault displacements (Fig 3.15).

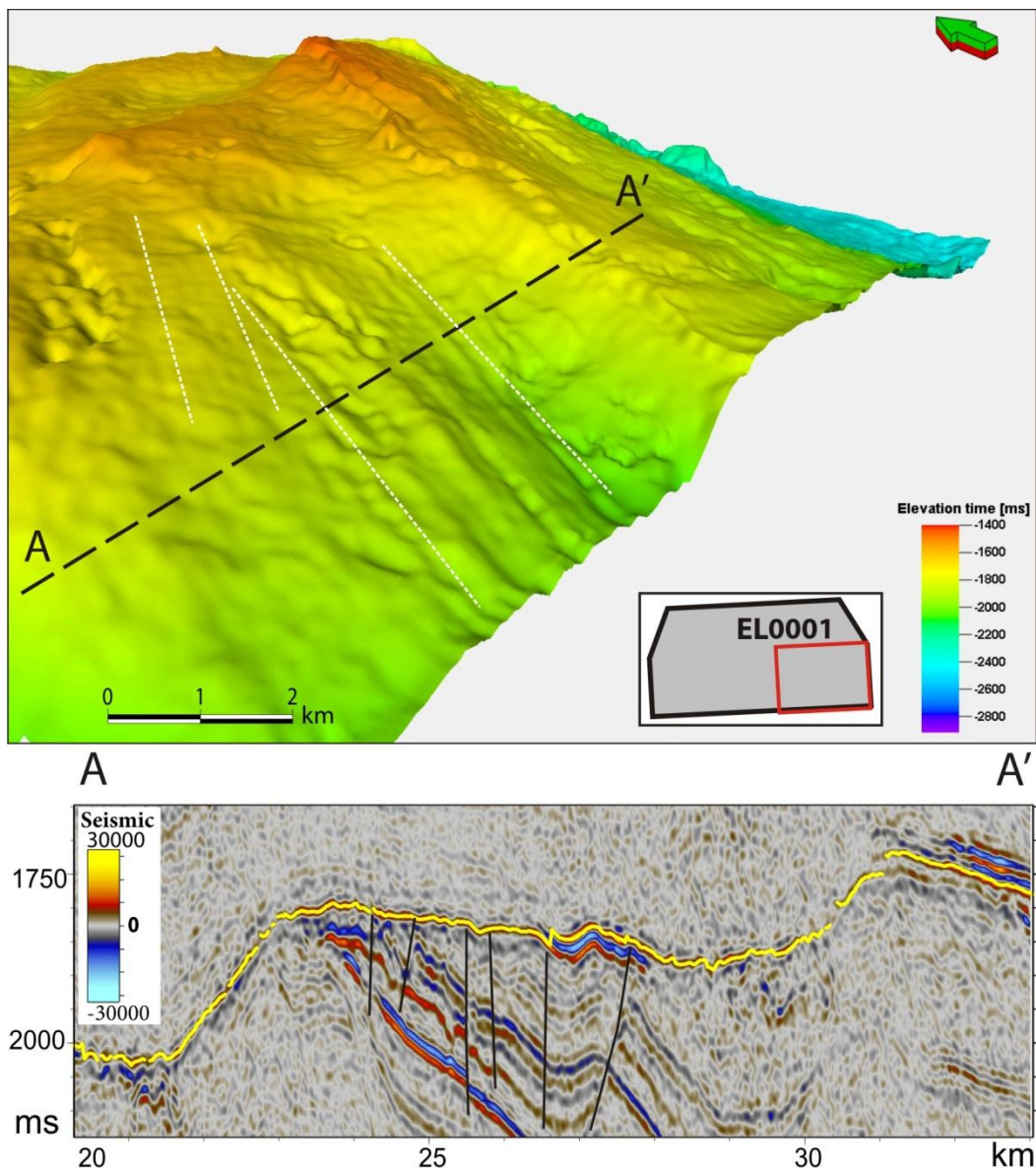


Figure 3.15 Illuminated perspective view of the Top Veslemøy time surface showing parallel ridges outlined by white dashed lines. Seismic profile below show location of the surface in yellow, where black lines indicate interpreted faults.

3.3 Buried glaciotectionic features

3.3.1 Sediment blocks and rafts

Description of high-amplitude seismic anomalies

Seismic profiles crossing the glaciogenic packages GII and GIII reveal high-amplitude seismic anomalies scattered within the westward dipping GII and GIII units in both 3D surveys used in this study (Fig. 3.16). The amplitude anomalies have normal polarity compared to seafloor reflection (Fig. 3.16), indicating higher density/velocity of these features than the sediments in which they are embedded. The high-amplitude anomalies are from 20 m to 80 m thick (assuming sound velocity of 2000 m/s) and groups of stacked anomalies can be as wide as 12 km on the seismic profiles (Fig. 3.16) although commonly single features are about 0.5-1.5 km wide. (Fig 3.17) The advanced 3D-interpretation techniques and high lateral resolution of the 3D surveys give a range of volumetric attributes that are well suited for mapping the distribution of these high-amplitude seismic anomalies. Several attributes and shaded time maps are used in order to outline boundaries of the anomalies and image them.

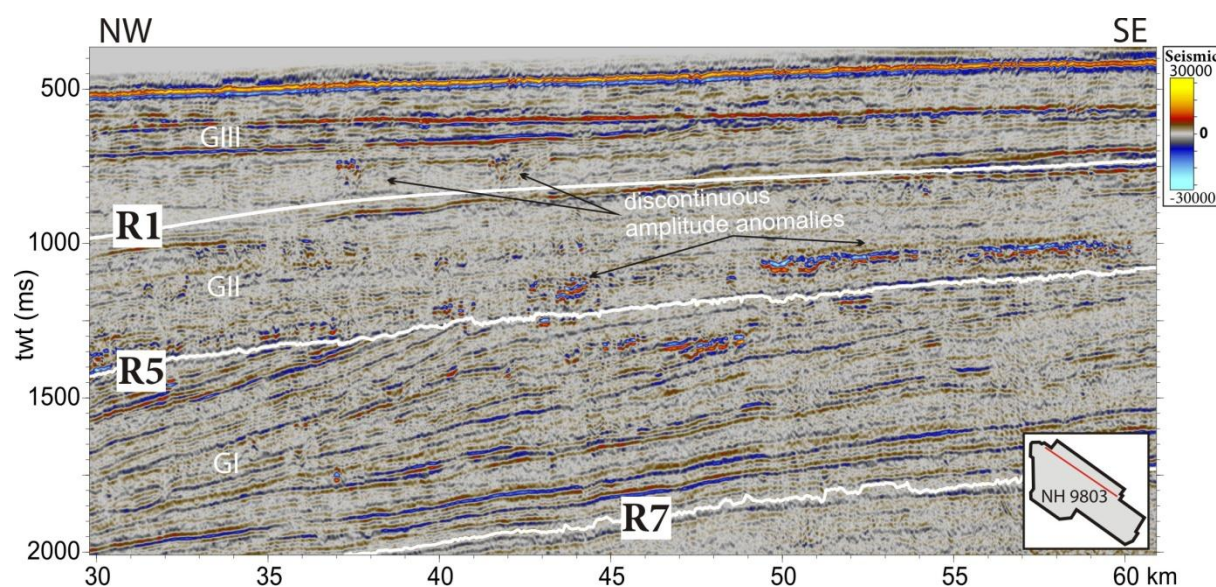


Figure 3.16 Seismic profile of inline 2293 within Sørvestsnaget NH9803 3D survey showing high-amplitude anomalies with normal polarity within the glaciogenic sequences GII and GIII. Regionally correlated reflectors R7-R1 are indicated and location of the cross-section is indicated by red line.

Lateral distribution of the high-amplitude seismic anomalies above the R5 reflection (Fig3.16) is well imaged using the volume based RMS amplitude attribute (Fig. 3.17).

Results

This RMS map, calculated for a window of 100 ms above horizon R5 indicates that amplitude anomalies above R5 in some areas are aligned in a sort of chains of W-E direction, in other areas they are just located in large hummocks. The lengths of the of high-amplitude seismic anomalies are up to 50 km long and it seems that they continue farther to the east out of the seismic survey. This observation is also confirmed by the presence of similar elongated chains of anomalies within western part of the EL0001 Veslemøy High 3D survey at the same stratigraphic level and the same orientation (Fig. 3.19 B). High concentrations of high-amplitude seismic anomalies exhibiting chaotic pattern occur in the central part of the NH98003 Sørvestsnaget 3D survey comprising an about 5 km wide zone of North-South direction, located at the continental shelf break of the underlying R5 reflection (Fig 3.18).

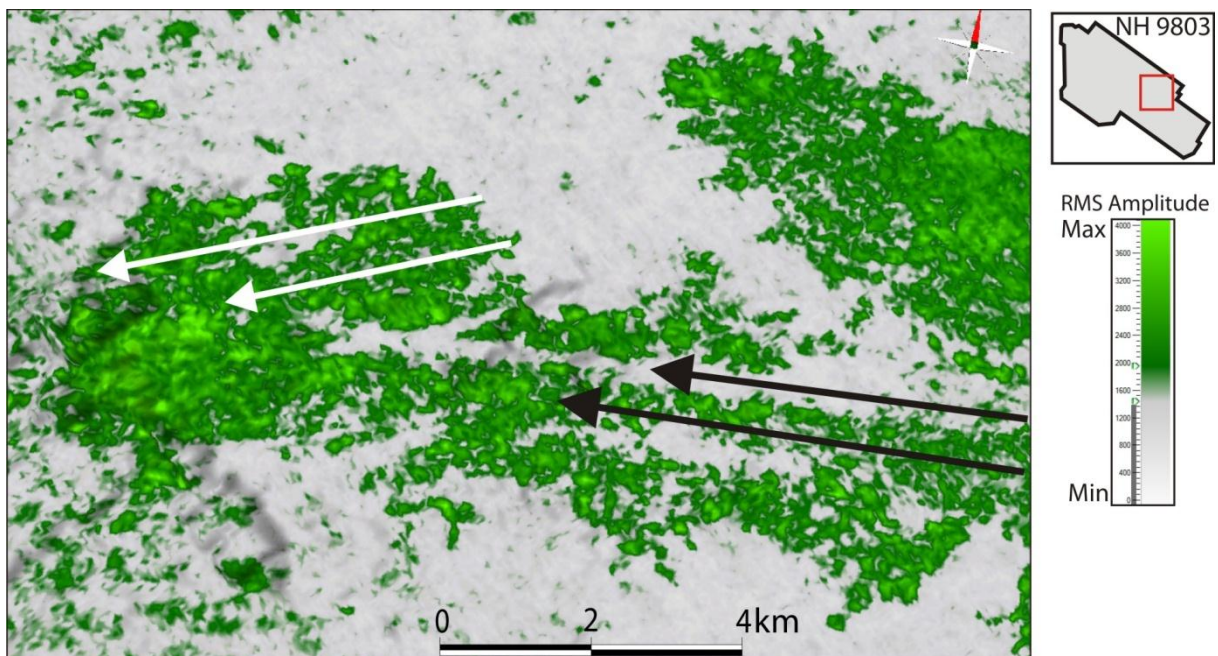


Figure 3.17 RMS amplitude map of the 100 ms window above R5 horizon showing spatial distribution of high-amplitude anomalies aligned in chains. Arrows indicate two different generations of the lineations with inferred palaeo ice flow directions.

Interpretation of the high-amplitude anomalies

The zone of high-amplitude anomalies subdivides the Sørvestsnaget survey into an eastern continental shelf part with many anomalies located in chains. And at western part with generally higher amplitude values, where the high-amplitude anomalies are unevenly distributed (Fig.3.18), or localized in some of the mapped continental slope channels of the R5 horizon. Also, the high-amplitude anomalies in the western part of the NH9803 survey

are parallel to mega-scale glacial lineations (MSGs) present on the shaded relief map of the horizons above and below the anomalies, described earlier in this chapter (Figs. 3.11 & 3.12). Group of high-amplitude anomalies with areal extent of about 89 km² is documented near the base of glacial package GII above the regionally correlatable reflector R5 (Fig 3.19).

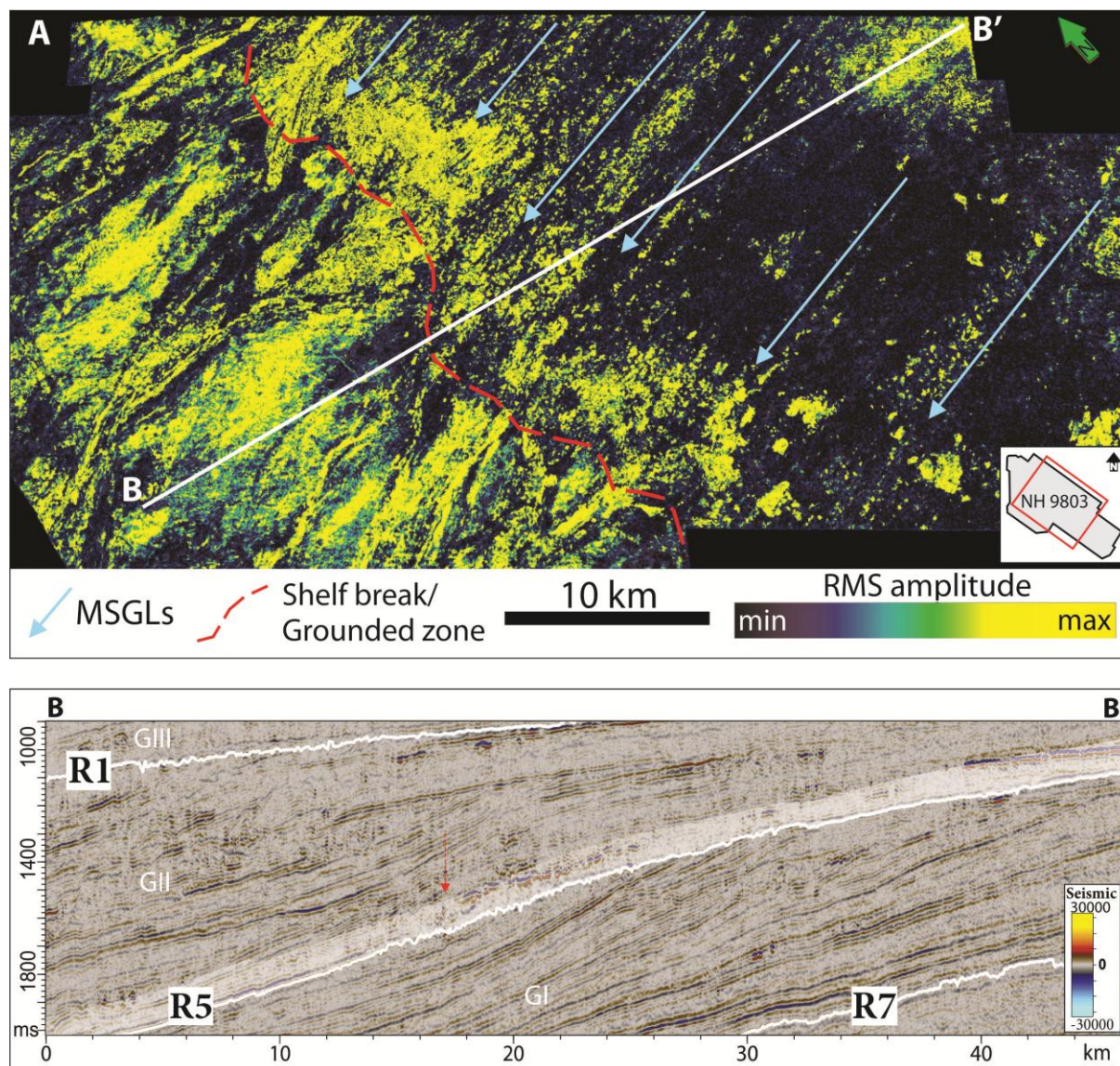


Figure 3.18 A) Root-mean-square (RMS) amplitude map of the 100 ms window above horizon R5, showing distribution of high-amplitude anomalies within the NH9803 3D survey. Blue arrows indicate interpreted direction of interpreted mega-scale lineations, and the red dashed line shows approximate position of the interpreted palaeo shelf break. **B)** Seismic profile showing groups of high-amplitude seismic anomalies above horizon R5 indicated. Shaded area indicates extent of the RMS amplitude window in A and red arrow marks interpreted position of the ice grounding line at the R5 continental shelf break.

Results

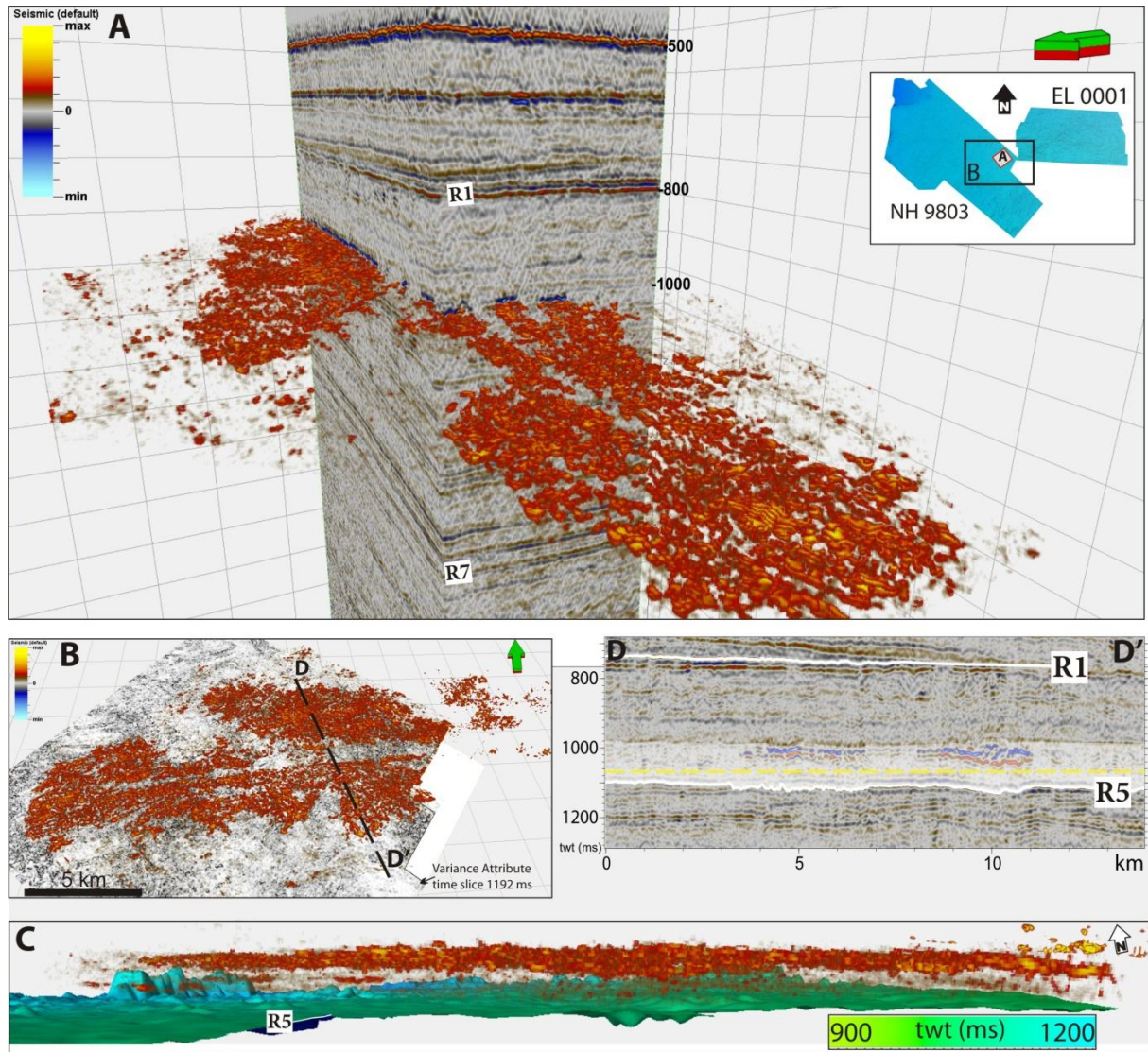


Figure 3.19 A) Image showing 3D perspective view of the interpreted sediment blocks and rafts visualized by volume render attribute (extent shown in D), combined with the cropped seismic volume of the Sørvestsnaget survey. Location of the area is indicated in the upper right corner. **B)** Perspective view of the high-amplitude seismic anomalies from (A), showing extent of the inferred sediment blocks and rafts in the EL0001 Veslemøy survey at the eastern end of the figure. **C)** Perspective view of the inferred sediment blocks in relation to the R5 surface, revealing their limited vertical extent confined to the base of the GII unit. **D)** Seismic profile across the blocks and rafts (location shown in B). Light shaded area defines the volume used for opacity attribute in A, B, C, and the yellow dashed line indicates location of the Variance time slice in B.

Based on their distinct morphology and glacial setting where they occur, in addition to their internal structure, the discontinuous high-amplitude seismic anomalies are interpreted to be long chains and zones of sediment mega-blocks and rafts. The group of mega blocks

and rafts within lower part of the glacial package GII interpreted as an accumulation glaciotectonically dislocated sediments.

The chains of sediment blocks and rafts are interpreted to be eroded, transported and re-deposited by the ice streams within former Barents Sea Ice Sheet (BSIS).

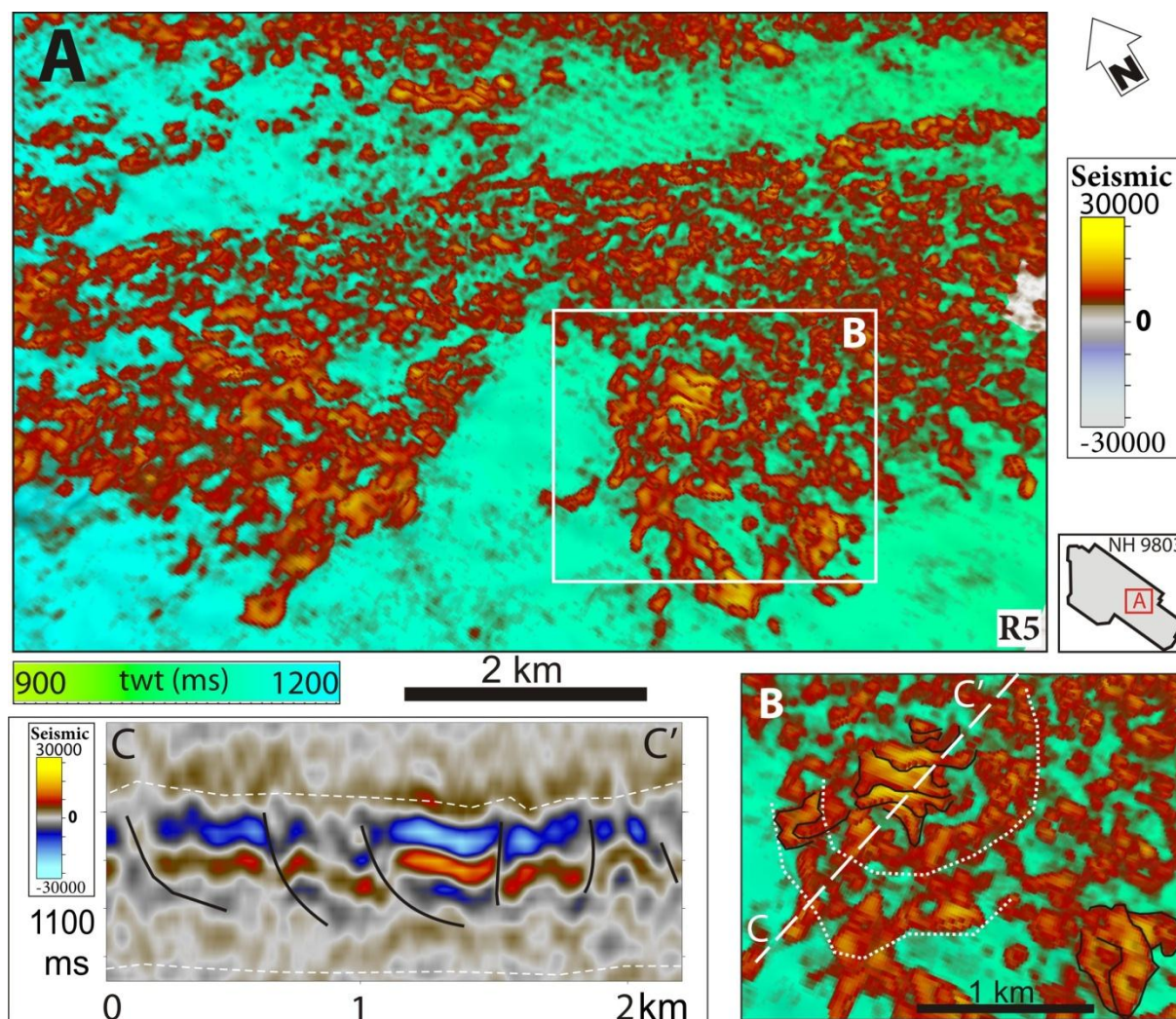


Figure 3.20 **A)** Perspective view of the Volumetric attribute showing high-amplitude anomalies interpreted to be sediment blocks, visualized by the volume render attribute draped over R5 time map. Larger blocks consist of separate segments similar to break up structures. **B)** Image revealing details of sediment block's internal structure from A, interpreted as imbrication or pull-apart structures within some of the largest blocks. **C)** Arbitrary seismic profile across the group of blocks and rafts identified in B, showing imbrications pattern and upthrusting or disintegration along the fault planes indicated by black lines in C and white dotted lines in B.

Results

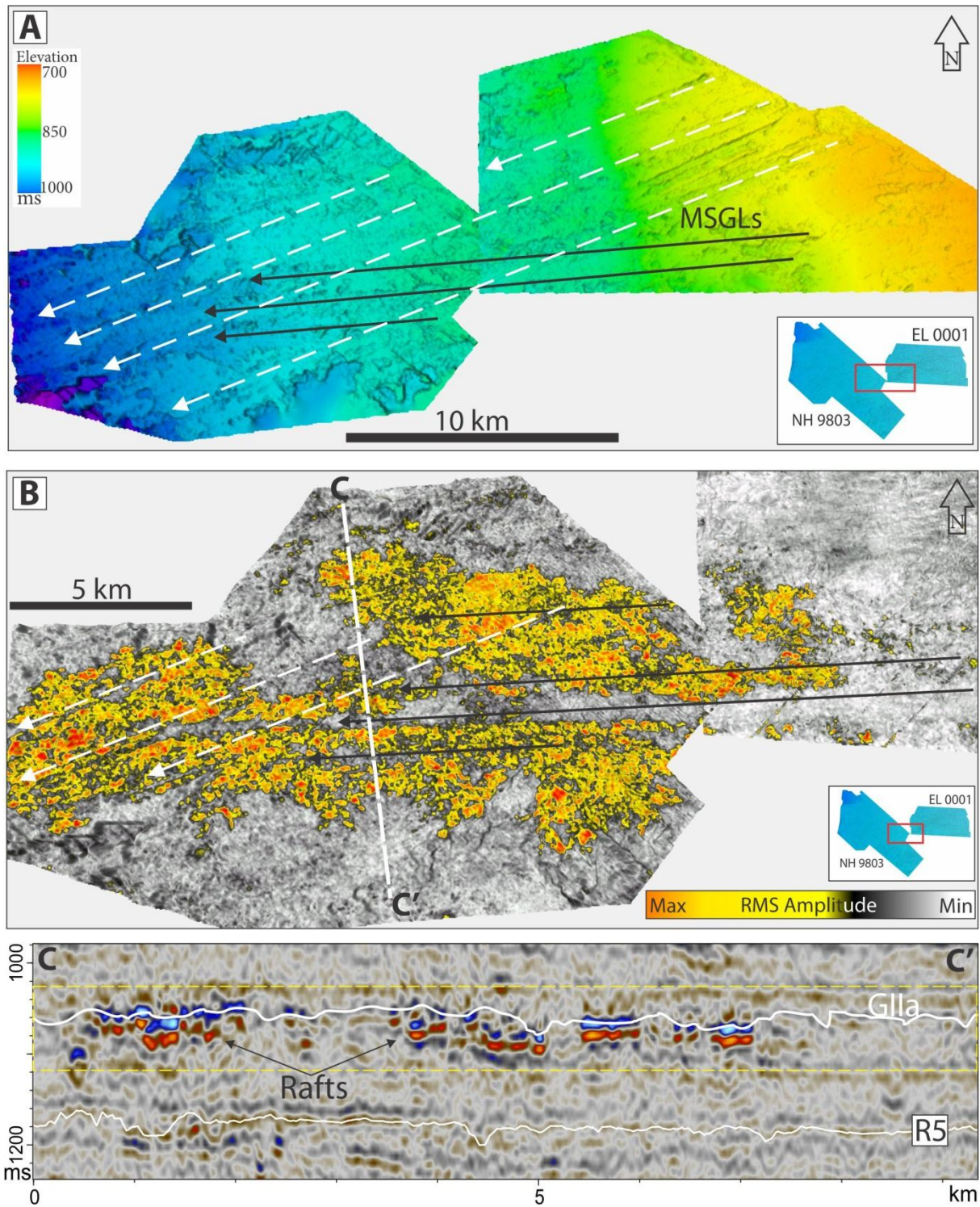


Figure 3.21 A) Illuminated time map of the Glla horizon showing two sets of mega-scale glacial lineations indicated by arrows of the south-west and western orientation. B) RMS amplitude map of Glla horizon displaying the lateral distribution of sediment blocks and their relation to the MSGLs indicated by black and white arrows. C) Arbitrary seismic profile showing location of the horizon Glla and extent of the RMS amplitude volume of 100 ms indicated by a yellow dashed box.

The distribution of megablocks aligned in long chains within the palaeo shelf sediments, and these chains being parallel to MSGLS indicate clearly that the chains of blocks and rafts were formed by a fast-flowing ice stream. An additional argument for a sub-glacial genesis of the megablocks and rafts is their spatial relationship with the mega-scale glacial lineations. The RMS attribute map of 100 ms window around GII a horizon (Fig 3.21 B) shows elongation of the accumulations of sediment blocks and rafts in to directions. The two sets of MSGLS on the underlying horizon R5 (Fig. 3.12) and on the overlying horizon GII a (Fig. 3.21) are parallel with the elongated accumulations of sediment blocks and rafts. A similar relationship between MSGLS and chains of megablocks and rafts is also documented for several other stratigraphic levels of glacial sequences GII and GIII (Andreassen et al., 2004; Andreassen et al., 2007,b).

3.3.2 Circular depressions on the horizon R5

Description of circular depressions

The R5 horizon in the western end of the EL0001 Veslemøy 3D survey reveals large-scale sub-circular and ellipsoid depressions (Fig. 3.22). Six such depressions are observed, three of them are of outstanding size and three others of a smaller scale.

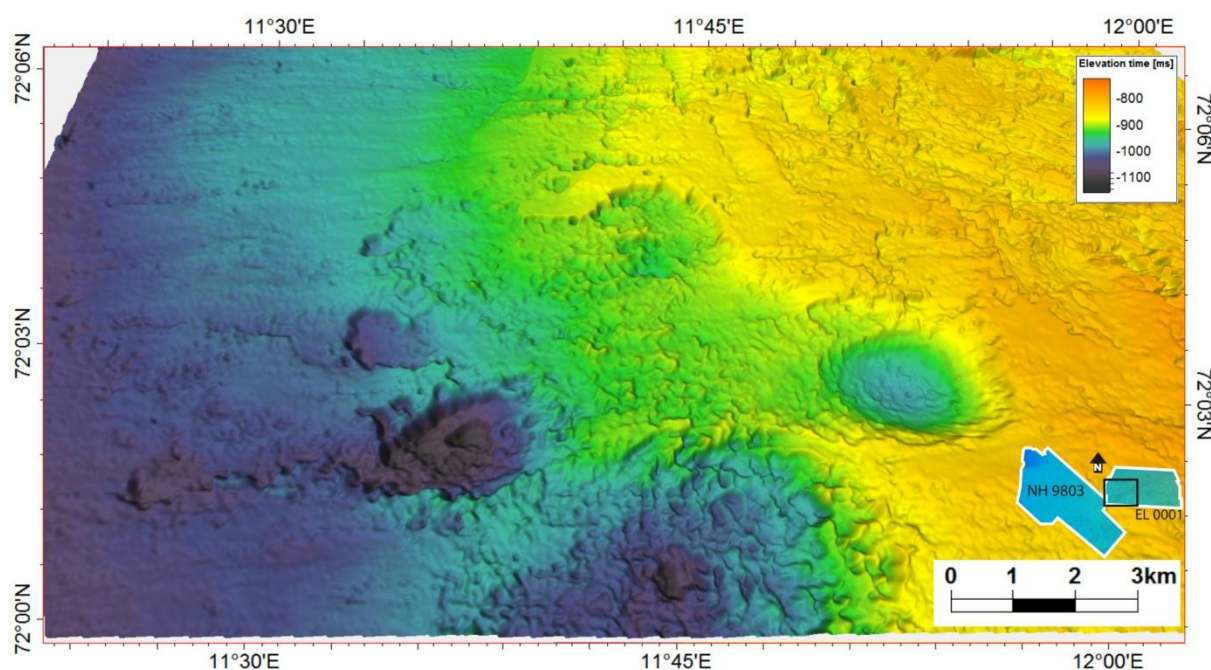


Figure 3.22 Shaded time map of the horizon R5 within SW limit of the EL0001 Veslemøy 3D survey showing distinct over-deepened depressions of semi-circular shape on its surface.

Results

The most distinct depression I (Fig.3.23) of semi-circular shape has a well-developed floor and flanks and represented by strong reflection on seismic profiles (Fig. 3.24C). The seismic reflection of depression I reveal parabolic-shaped segments that are carved into its floor (Fig. 3.24C), and shows irregular ridges on time map of NW-SE orientation (Fig. 3.23). Depression I is the easternmost of the depressions on R5, and it has a diameter of 3.5 km and 2.7 km in WE and NS directions respectively. The depth of the depression from the upper eastern edge to the bottom is 180 m, assuming sound velocity of 1960 m/s. The largest of the observed depressions, number II has an elliptical shape and is elongated in the WE direction (Fig. 3.23). It is 5.5 km in diameter along the WE axis and about 3.5 km along the short NNW-SSE axis and its southern extent is limited by the survey boundary. Depression II is about 190m deep and it is characterized by a chaotic seismic reflection pattern and irregular flanks (Fig.3.24 D). The depression III is similar in size and shape to depression I and is 180 m deep. On the time map irregular surface is observed to the west of the depression (Fig.3.23) and it is expressed as disturbed reflection R5 on the seismic profiles (Fig 3.24 C).

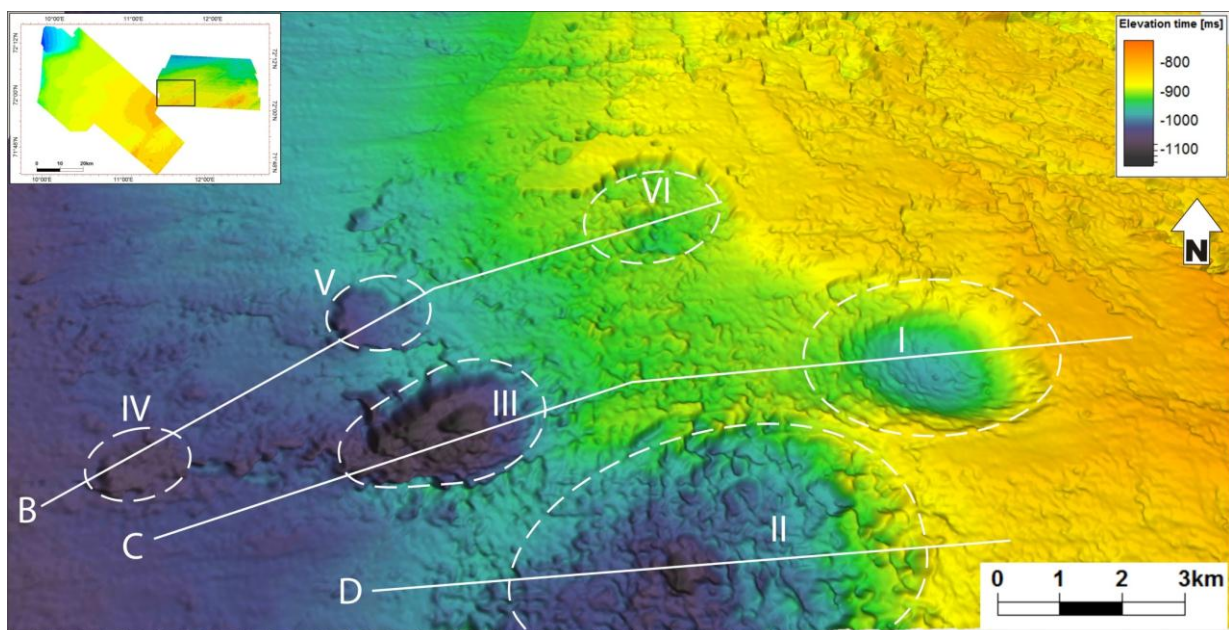


Figure 3.23 Perspective view of the R5 time map showing distribution and morphology of the six interpreted depressions. Diagram in the upper left corner shows location of the area within EL0001 Veslemøy survey. B, C & D indicate location of seismic profiles shown in Fig. 3.24. Note the approximately same WWS orientation of the long axes of three largest depressions I-III, and irregular surface down-stream of depression I, III and V expressed also on the seismic profiles in Fig.3.24.

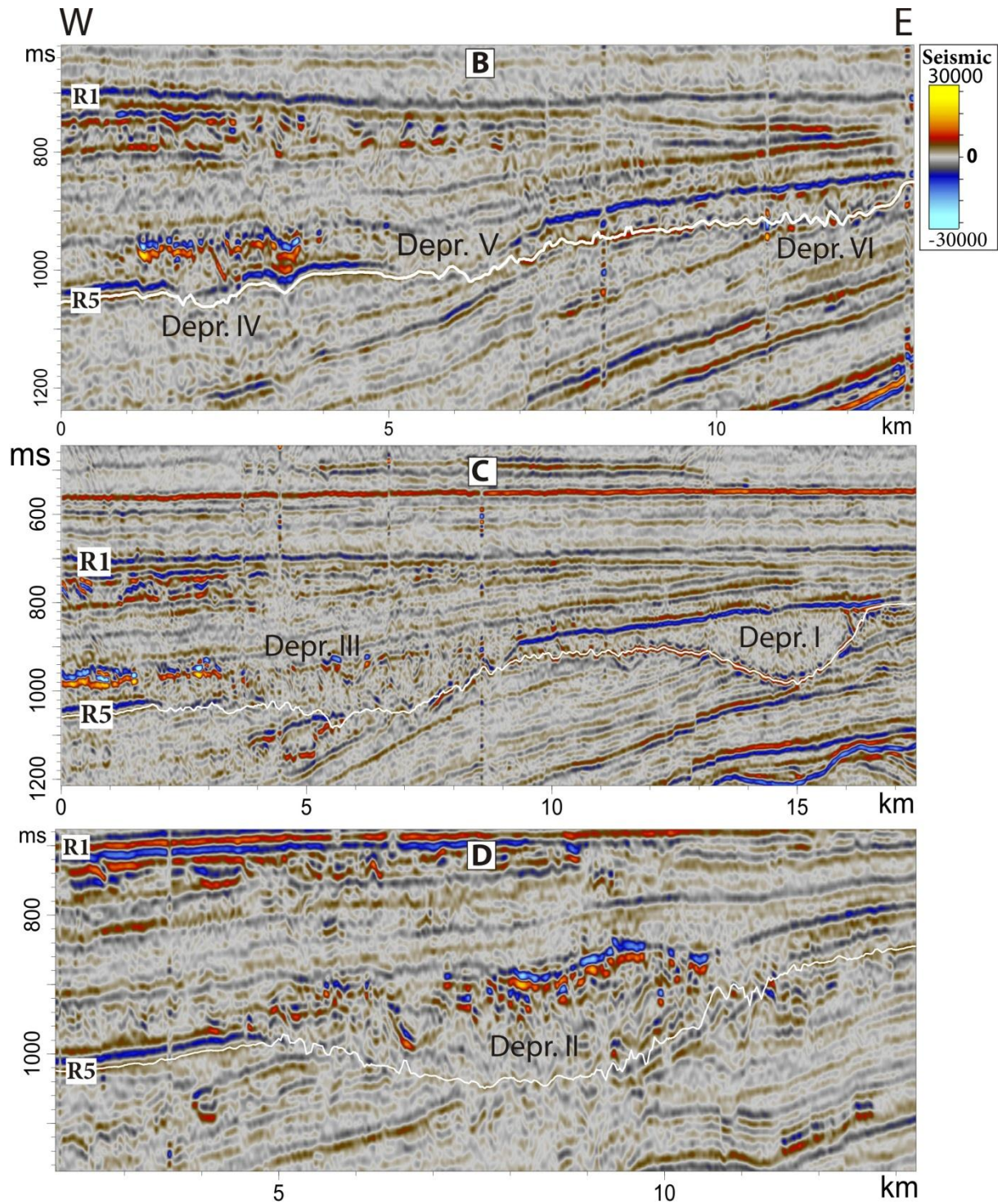


Figure 3.24 Seismic sections across interpreted depressions from I to VI showing their interior. Location of the profiles is indicated in Fig 3.23. Profiles show two different seismic facies of the depressions infill: a) chaotic and low-amplitude semi-transparent infill of the depressions I and V; b) chaotic reflections with tilted high-amplitude seismic anomalies in II, III and IV.

The elongated axes of the depression on R5 are pointing westwards (they become narrower towards the west), and they all seem to be open towards the west (Fig. 3.23) they also all

Results

have steeper eastern flanks and more gentle western ones. Seismic profiles show possibly two generations of the depressions formation expressed on the horizon R5 (Fig. 3.24 C).

The R5 horizon (which the depressions are eroded into) are also characterized by mega-scale glacial lineations of an EW orientation, suggesting an ice flow in the same direction as the elongated axes of the depressions (Fig. 3.26 A). Well-developed grooves appear also on the surface of the horizon GII located above the depressions (Fig 3.11 & 4.1). On seismic profiles the sediment infill of the depressions has chaotic seismic reflection configuration (Fig. 3.24) and low amplitude, although depressions II and III also contain tilted, high-amplitude seismic anomalies within their interior (Fig. 3.24 C, D). The depressions on R5 are eroded into the underlying dipping units of the G1 package and are bounded at their top by the erosional surface exhibiting well developed MSGLs (Fig.3.21 A). Thrusting in the westward direction is observed within depressions I, III and V and emphasized by the high amplitude segments varying from about 100 m to 1000 m in size (Fig. 3.25). Internal infill of the depressions in general expressed as chaotic seismic reflections of irregular configuration otherwise showing westward tilted weak sub vertical reflections (Fig. 3.25).

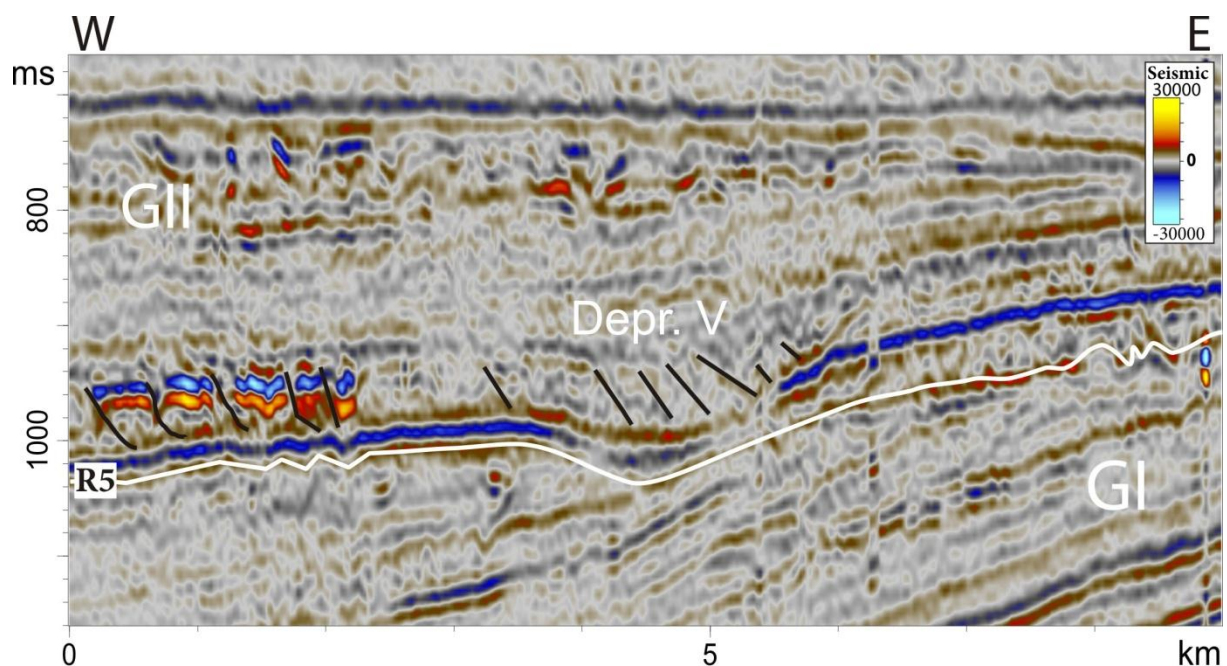


Figure 3.25 Arbitrary seismic profile along the elongated axis of the depression V shows inclined towards west vertical reflections interpreted as thrust planes. High-amplitude anomalies are observed immediately above R5 horizon down-stream from depression. Black lines are indicating interpreted discontinuities.

Interpretation of the semi-circular depressions

Distinct sub circular, large depressions like those observed on R5 in Veslemøy 3D survey area can be produced by a range of processes, volcanic eruptions, meteorite impact, collapse structures, melt water discharge or over-pressured fluid expulsion. The size of the depressions is much larger than assigned for the pockmarks or even pock mark craters described in the literature and most likely involve other formation mechanisms. Based on the distinct incision into underlying sediments and alignment of the long axes parallel to the palaeo ice stream direction (Fig. 3.26), the depressions on R5 are interpreted to be formed by erosional processes at the base of the palaeo ice streams likely draining Fennoscandian Ice Sheet.

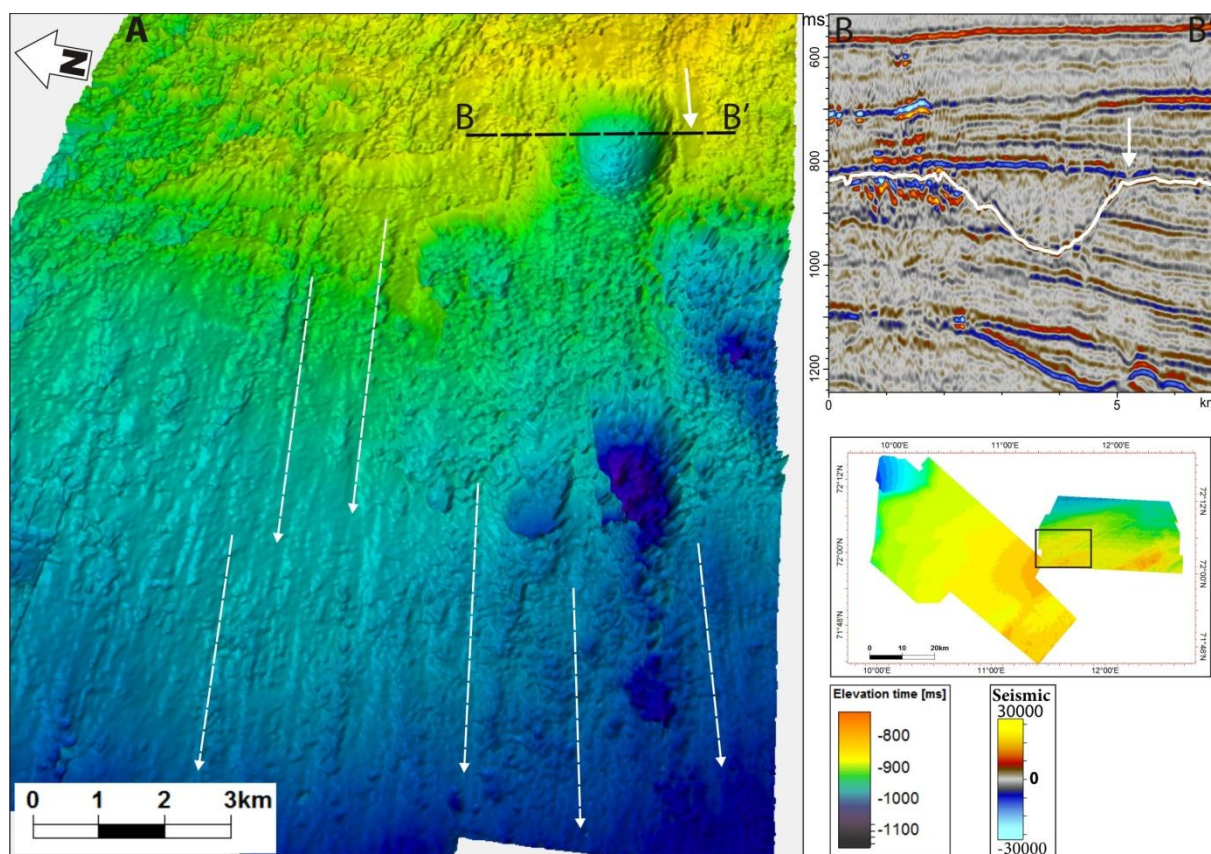


Figure 3.26 A) Perspective view from the west on the time map of horizon R5 within Veslemøy 3D survey. Stippled white arrows show interpreted buried MSGLs and palaeo ice flow direction. Note elongation and “opening” of the depressions in the same westward direction. **B)** Seismic profile across Depression I and adjacent mega-scale lineation pointed by white arrow. Note seismically transparent infill of the depression and stacked high-amplitude anomalies immediately to the north adjacent to the depression.

Dislocation of sediments from the depressions in one direction, occurrence of MSGs and occurrence of gas related amplitude anomalies, formation of the depressions. Fluid expulsion or glaciotectonic dislocation, or combination of both is likely erosional agents responsible.

Possible mechanisms and a conceptual model for formation of the depressions is a key aspect of this study and are addressed in more details in the discussion (Chapter 4).

3.4 Fluid flow migration pathways

Interpretation of the attributes of several horizons within two 3D surveys Sørvestsnaget and Veslemøy High, as well as studies of the seismic profiles give sufficient grounds for evaluation of potential fluid flow pathways. The EL0001 seismic survey covers the well-defined Veslemøy structural high surrounded by the Sørvestsnaget Basin from the western side and the Tromsø Basin from the eastern side (Fig. 3.26). Such geological architecture might lead to the migration buoyant fluids towards apex of the structural high along the permeable onlapping strata. Just the most representative and important amplitude anomalies for this study are covered in this chapter with consecutive evaluation of fluid migration pathways and shallow gas accumulations from the western and eastern basins. Seismic lines across the Sørvestsnaget Basin towards the Veslemøy High show numerous high-amplitude anomalies mainly within the Plio-Pleistocene glacigenic packages GI, GII and Pleistocene succession GIII. The Plio-Pleistocene wedge is comprised of oblique westward dipping reflections of about 2.5 degrees and extends beyond the limits of two 3D surveys. The upper part of the sediment package GII is marked by the erosional horizon R1 to the west and URU to the east, which truncates underlying dipping reflections (Fig. 3.26). The overlaying Pleistocene glacigenic package GIII is comprised of sub-horizontal parallel reflections starting to dip gently at the western extent of the NH9803 3D survey (Fig. 3.26) marking onset of the shelf break. Succession, despite of two strong internal reflectors, is comprised of generally low continuity and amplitude reflections with bright spots dominantly occurring above Veslemøy High (Fig. 3.26).

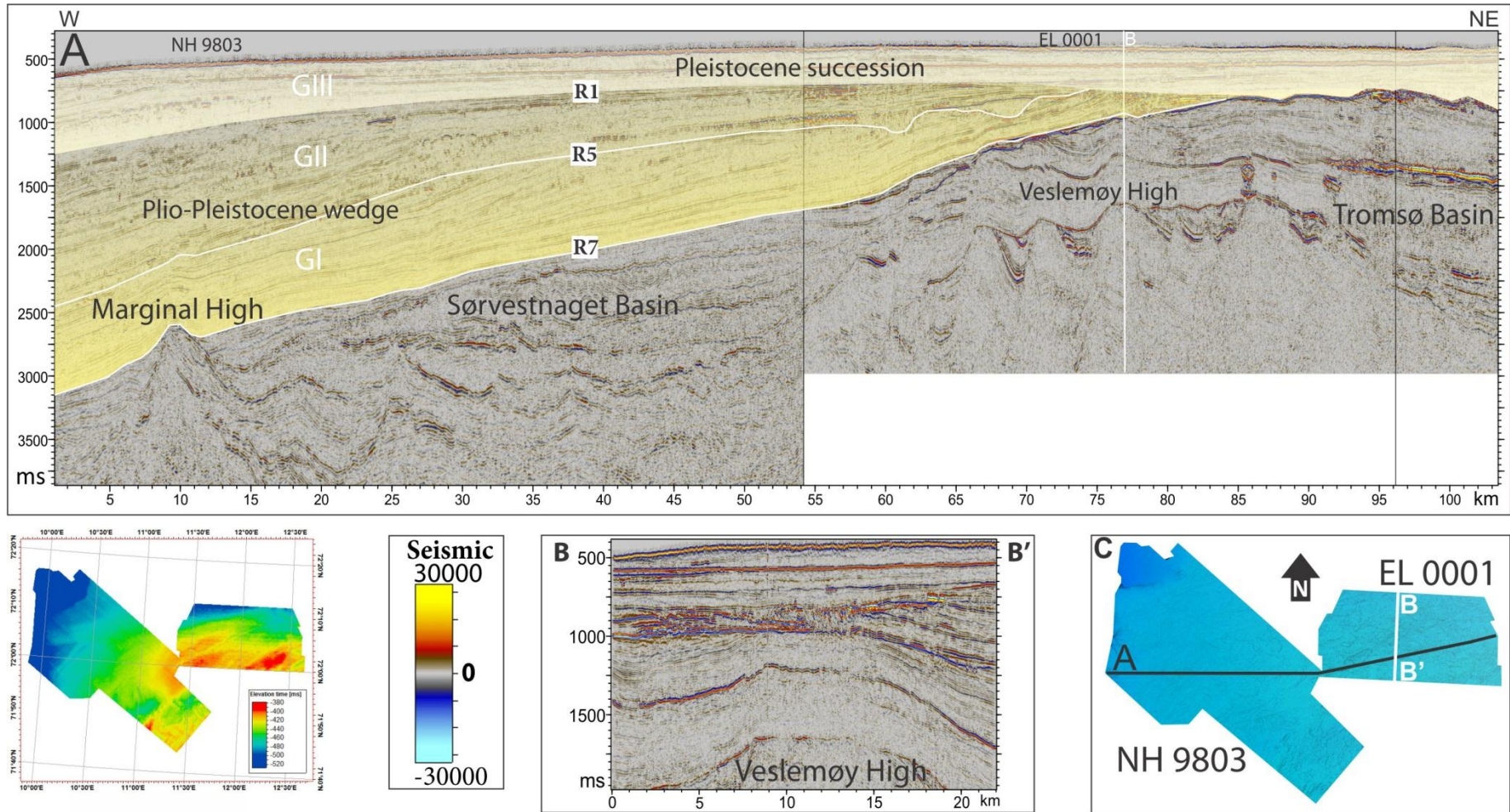


Figure 3.26 Seismic profiles showing structural and stratigraphic architecture of the Veslemøy High and surrounding basins. **A)** Composite seismic section across NH9803 and EL0001 seismic surveys indicating main structural elements of the study area, location of the profile shown in C. **B)** Seismic profile of the cross-line 1938 in the EL0001 3D survey showing cross-section of the Veslemøy high in a NS direction, where location of the profile is indicated in C.

3.4.1 Indications of the fluid flow from the Sørvestnaget Basin

An RMS map of the 120 ms window below R5 within EL0001 3D survey shows elongated groups of high-amplitude anomalies of elongated shape and trending in a NW-SE direction (Fig. 3.27).

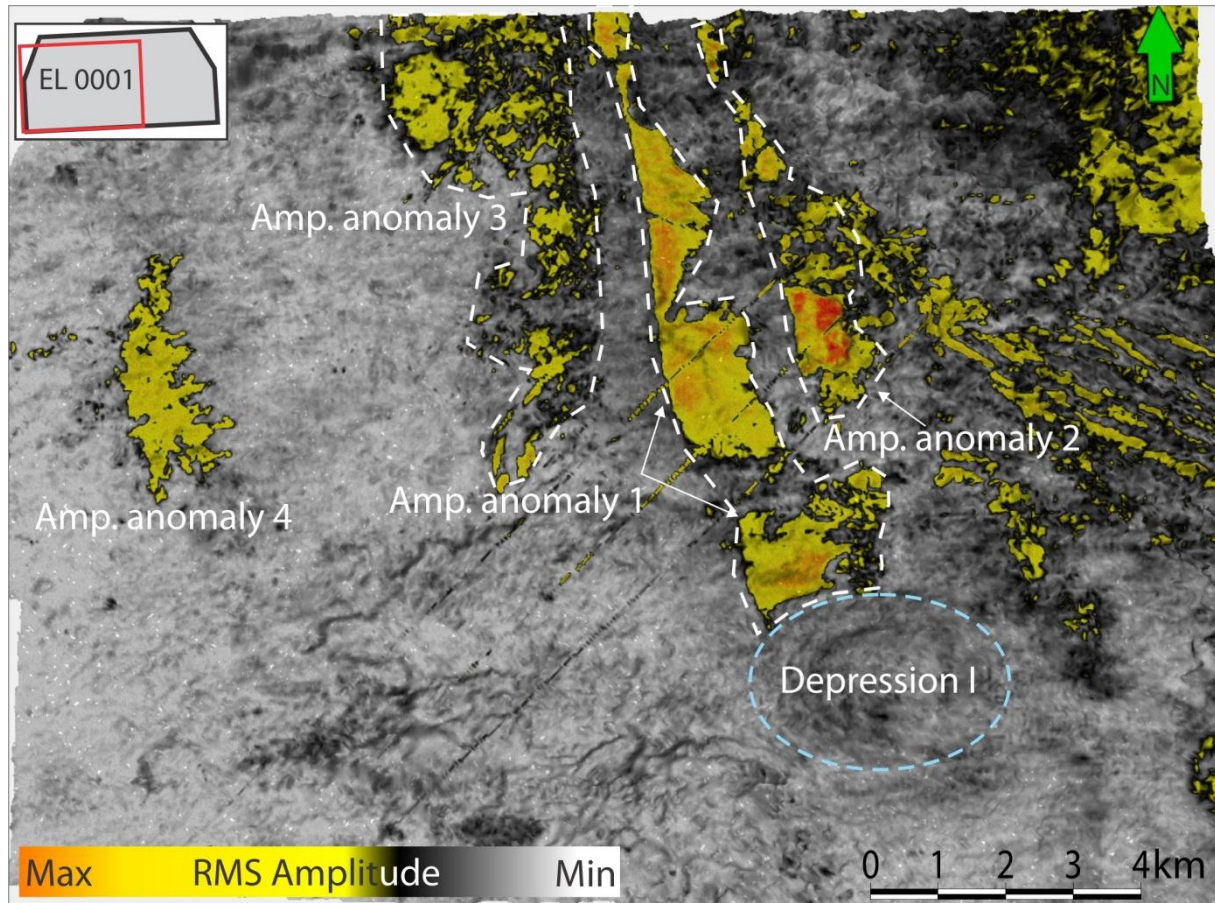


Figure 3.27 RMS amplitude map of the 120 ms window below R5 horizon with indicated high-amplitude anomalies. Vertical extent of the RMS window is shown on the profiles in Fig.3.31 White dashed lines indicate extent of interpreted anomalies, where blue line show extent of depression 1. Note the sharp western boundary of amplitude anomalies 1 and 2.

Description of seismic high-amplitude anomalies

Amplitude anomaly 1 is a group of high-amplitude anomalies (Fig. 3.28) aligned in the same NNW-SSE trend around 11.5 km long and up to 1.8 km wide in the map view (Fig. 3.27). The southern limit of this anomaly has a sharp boundary termination at the flank of the Depression 1 (Fig. 3.31B). On seismic profiles *Anomaly 1* is truncated by the overlying R1

reflector and has a gentle dip in the NW direction. It shows reversed polarity of the reflection compared to the seafloor.

Amplitude anomaly 2 has a lateral extent of 7.5 to 1.4 km and has the same trend on the map view as anomaly 1 (Fig. 3.27). On seismic sections this anomaly is associated with two adjacent subcropping reflectors stacked upon each other which have reversed polarity and pull-down effect and slight acoustic masking underneath (Fig. 3.28). Therefore the highest RMS amplitude values observed at the southern part of this anomaly are attributed to the sum of values from both reflections. The eastern limit of Anomaly 2 shows acoustic masking and pull-down effect on the underlying seismic reflections (Fig. 3.28 & Fig.3.31 C).

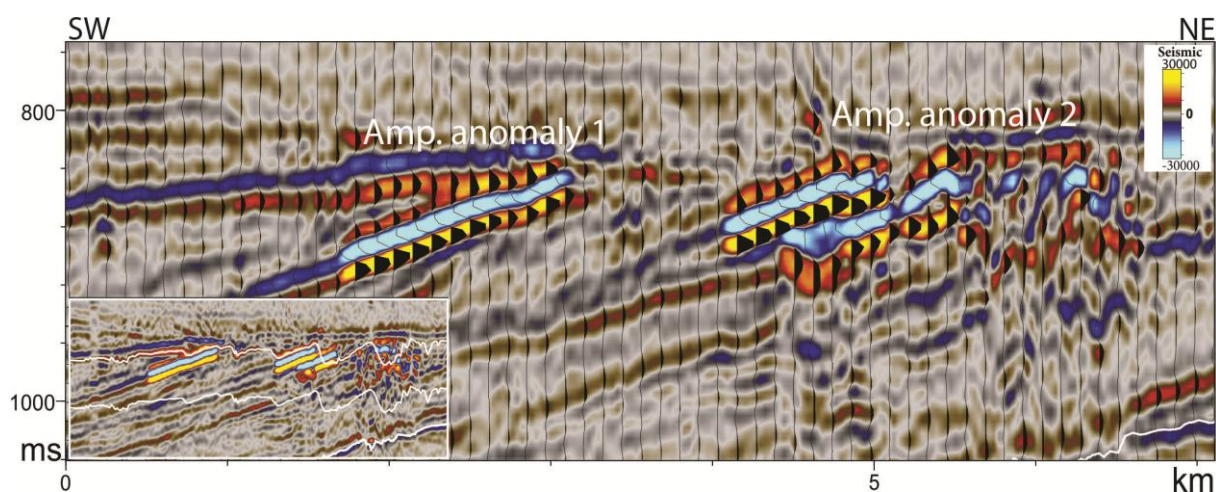


Figure 3.28 Seismic section with wiggles-trace display across the amplitude Anomalies 1 & 2 showing reversed polarity of the anomalies. The anomalies are associated with subcropping strata under the erosional unconformity. White lines in profile at the lower left corner show vertical extent of the RMS window used in Fig.3.27. Location of the section is shown in Fig. 3.31 as Profile 3

The western limits of the two groups of amplitude anomalies 1 and 2 show strikingly sharp boundaries, otherwise showing chaotic pattern at the eastern extents (Fig. 3.27). Seismic profiles across these anomalies show their alignment with dipping sedimentary beds and reveal abrupt termination of the down dip boundaries of anomalies (Fig 3.31 C, Fig 3.28)

Amplitude anomaly 3 is located to the west of the aforementioned anomalies and has an irregular shape on the RMS amplitude map, consisting of chaotically distributed smaller anomalies (Fig. 3.27). It covers an area of approximately 20 km² and is elongated in the same NW-SE direction as anomalies 1 and 2. Seismic profiles across Anomaly 3 show subcropping

Results

high-amplitude anomaly with polarity reversal (Fig. 3.29). Good continuity of the reflection at the lower part gradually changes to chaotic, discontinuous amplitude reflections towards toplap unconformity R1. Pull-down effect and acoustic masking are observed on the reflections beneath the amplitude anomaly 3 (Fig. 3.29).

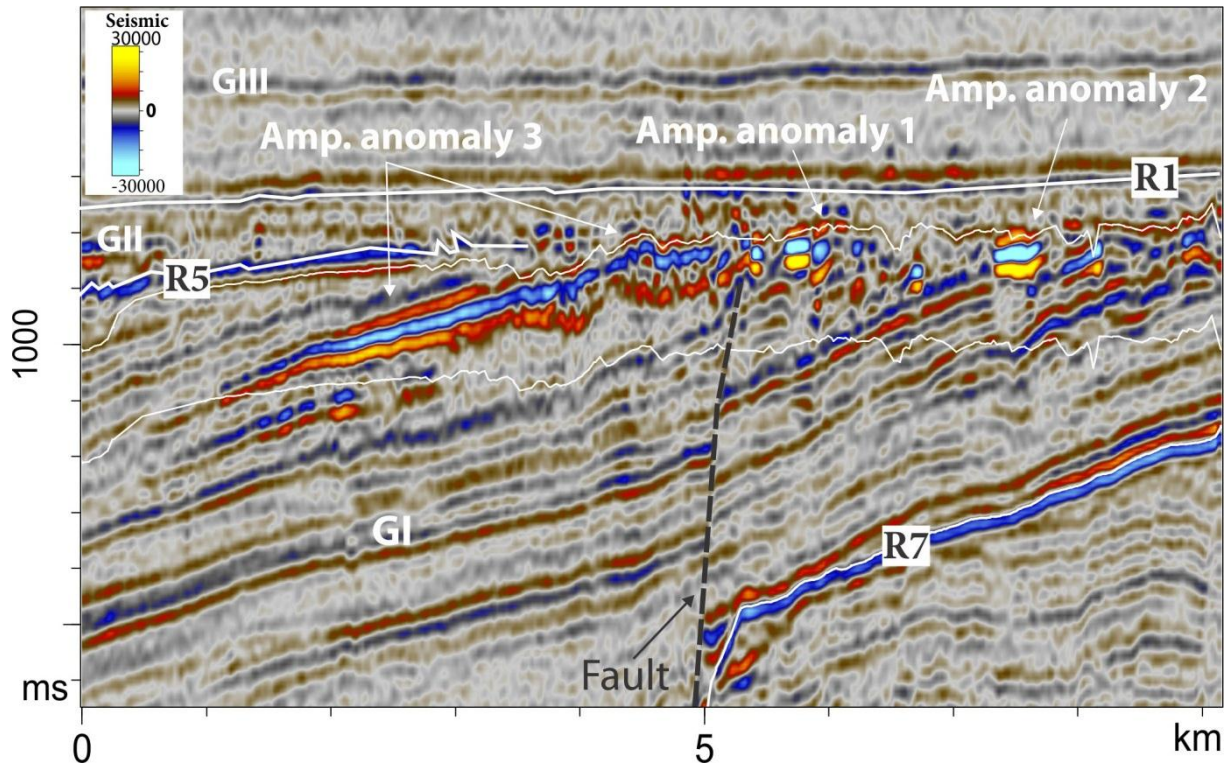


Figure 3.29 Seismic profile showing cross-section of the amplitude anomaly 3, 1 and 2. Lateral changes in reflection continuity occur toward the erosional unconformity R1 and low-frequency zone under anomaly is observed. Thin white lines show the RMS window used in Fig.3.27 and black dashed line indicates deep sided fault. Location of the section is shown in Fig. 3.31 as Profile 4.

Amplitude anomaly 4 is observed within the EL0001 3D survey's Pleistocene glacial package GIII and it is associated to the GIII a horizon. It is 5.8 km long in the NE-SW direction and up to 3.8km in the N-S, and it covers an area of about 21 km². Anomaly 4 has an irregular shape on the RMS amplitude map, but sub-circular trends occur in the high-amplitude values in the central part of the anomaly (Fig. 3.30 B). This sub-circular anomaly is the largest among a group of 14 smaller anomalies, observed at the GIII a level which aligned in roughly NW-SE trend. Seismic profiles across Anomaly 4 show its connection with the underlying anomaly 1 and anomaly 5 above it, expressed in the vertical zone of seismic signal distortions (Fig 3.30 A)

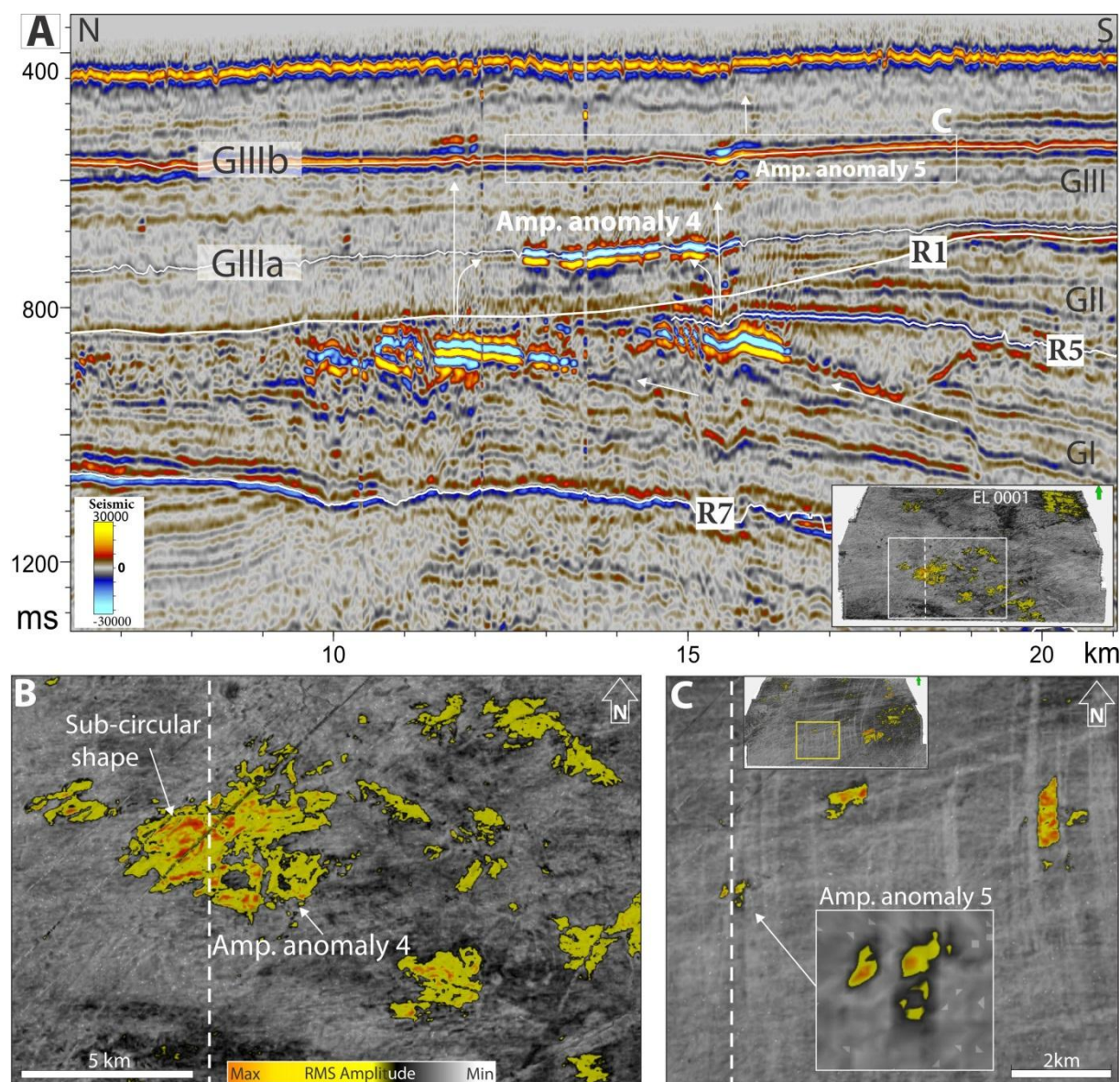


Figure 3.30 A) Seismic profile of the cross-line 1570 in the EL0001 3D survey, showing lateral and vertical fluid migration path ways within sediment packages GI-GIII. White arrows indicate potential fluid flow path and location of the section shown with dashed line in B & C. **B)** RMS amplitude map of the Pleistocene Intra 1 reflector showing lateral distribution of amplitude anomalies, location of figure within EL0001 survey indicated in A. **C)** RMS amplitude map of the Pleistocene Intra 2 reflector showing location and details of amplitude anomaly 5, note circular dim spot in south lower part of anomaly shown in zoomed box. Vertical extent is indicated by white box in A.

Amplitude anomaly 5 is observed within the Pleistocene Intra GIII2 reflector at the upper part of the succession GIII (Fig.3.30 C). This anomaly is located right above the southern limit of anomaly 4 (Figs 3.30 A and 3.30 C) and show a polarity reversal compared with the sea floor reflection (Fig. 3.30 A). Anomaly 5 is 0.5 km by 0.6 km large and has larger satellite

Results

anomalies at the same stratigraphic level (Fig. 3.30 C). At the southern part of anomaly 5 a circular shaped seismic low-amplitude core is surrounded by high-amplitude values (Fig. 3.30 C). On seismic profiles acoustic masking appears under anomaly 5, as well as vertical stack of higher amplitude values continuing also above anomaly (fig. 3.30 A).

Interpretation of seismic amplitude anomalies 1-5

High-amplitude anomalies indicating accumulations of the potential free gas in the sediments or gas charged fluids are interpreted. The seismic *high-amplitude anomalies 1-5* in the study area suggest that accumulations of free gas exist in the pore space of the sediments. Tuning effect on origin of anomalies is excluded due to the thickness of anomalies is exhibit vertical resolution of the 3D seismic data.

The seismic high-amplitude anomalies 1-3 are interpreted to represent free gas accumulations in the sediment layers subcropping the erosional unconformity of R5 (Fig. 3.29), accumulating and under low-permeability beds,. The western boundaries of these seismic anomalies are interpreted to represent the free gas - water contact (Figs. 3.31A and 3.31C), commonly referred to as a flat spot. Likely fluid migration path-ways within the Plio-Pleistocene glacial packages G1 and GII are permeable beds within the successions, where fluids would migrate towards elevated structural high and accumulate under the overlying erosional unconformity of R5.

Further vertical migration have taken place in GIII units, where sealing capacity of the beds is breached and fluids are trapped under the internal Intra GIII a and Intra GIII b horizons (e.g. Fig. 3.30 A) or may have seeped to the seafloor. The *amplitude anomalies 4 and 5* are thus interpreted as free gas accumulations within the GIII unit radially dispersed around vertical fluid flow conduits penetrating more permeable layers or by means of overpressure fracturing (e.g. Figs. 3.30A and 3.31).

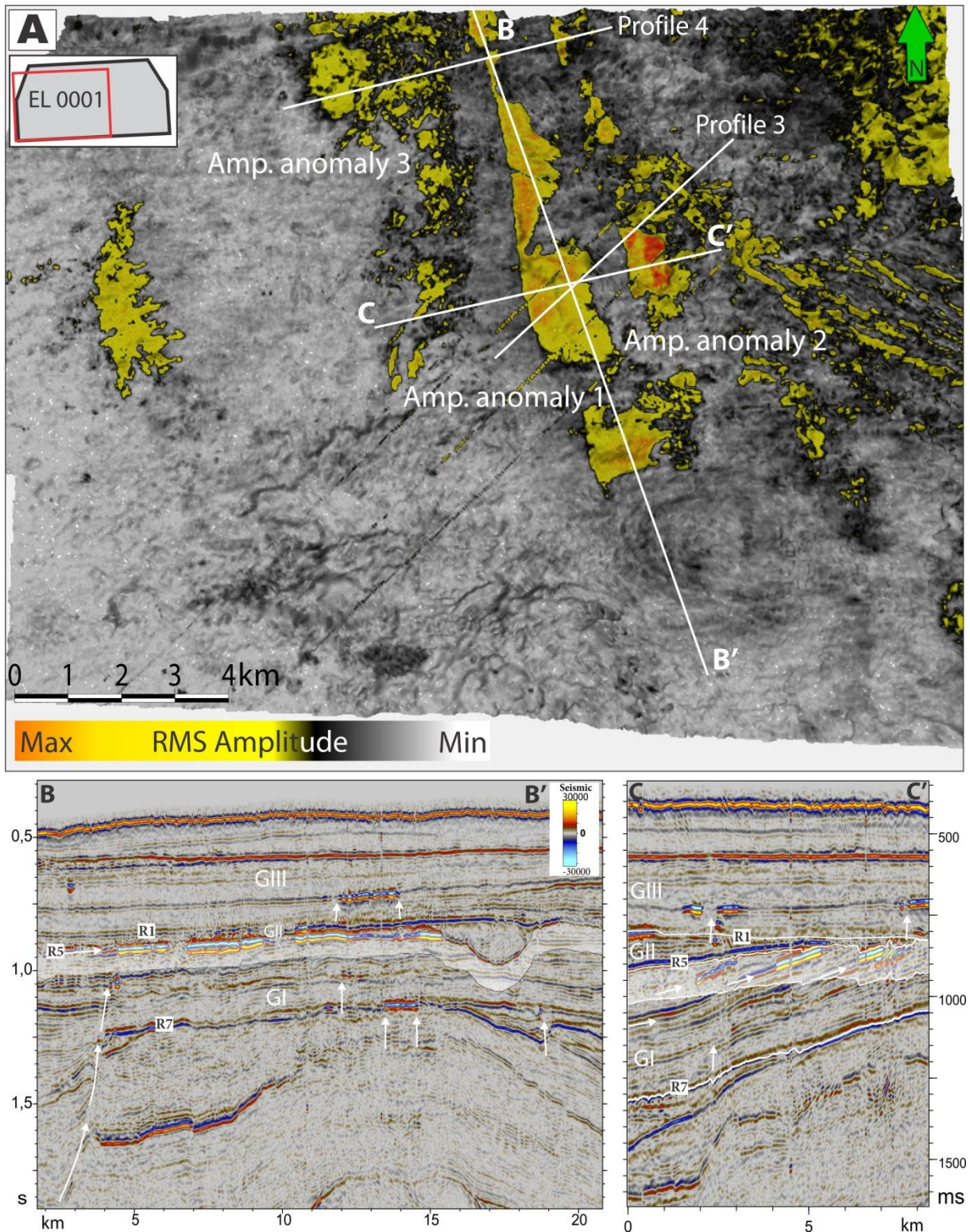


Figure 3.31 **A)** RMS Amplitude map of 120 ms window below R5 shows distribution of the seismic profiles over amplitude anomalies. **B)** Seismic profile along largest anomaly showing its stratigraphic position and abrupt termination towards depression up-dip. **C)** Seismic section across three anomalies shows their alignment with the subcropping layers under horizon R5. White shading indicates RMS Attribute window used in A, where white arrows show the interpreted fluid migration pathways.

3.4.2 Fluid migration from the Tromsø Basin

The eastern part of the EL0001 3D survey covers part of the Tromsø Basin located southeast of the Veslemøy High (Fig. 3.26, Fig. 3.32 A).

The large *amplitude anomaly 6* appears within Eocene units (Fig. 3.32). The polarity at the central part of anomaly is obscured by interference but it is evident that the polarity is reversed at the flanks of the anomaly (Figs. 3.32A and 3.32C). Anomaly 6 measures 7.5 km in NW-SE direction and about 14 km in NE-SW. It consists of several layers with high-amplitude intersecting and interfering with each other (Fig. 3.32C). The anomaly is dipping in SE direction parallel to the Eocene sediment layers and a zone of acoustic masking is observed below it (Fig. 3.32).

Another vertical feature different from the vertical artifacts is observed in the upper part of the cross-section piercing through the Pleistocene succession GIII (Fig. 3.32A). This *feature 1* is expressed as narrow vertical zone of chaotic reflections with low amplitude in the central part and associated bright spots at the bottom and top of it. The feature is about 450 ms high and 600 m in diameter and appears to connect two high-amplitude anomalies one at the R1 level and another at GIII b.

Amplitude anomaly 6 based on its polarity and strong acoustic masking effect is interpreted as free gas accumulation within more porous sedimentary beds of Eocene succession probably related to the submarine fan or sand injections.

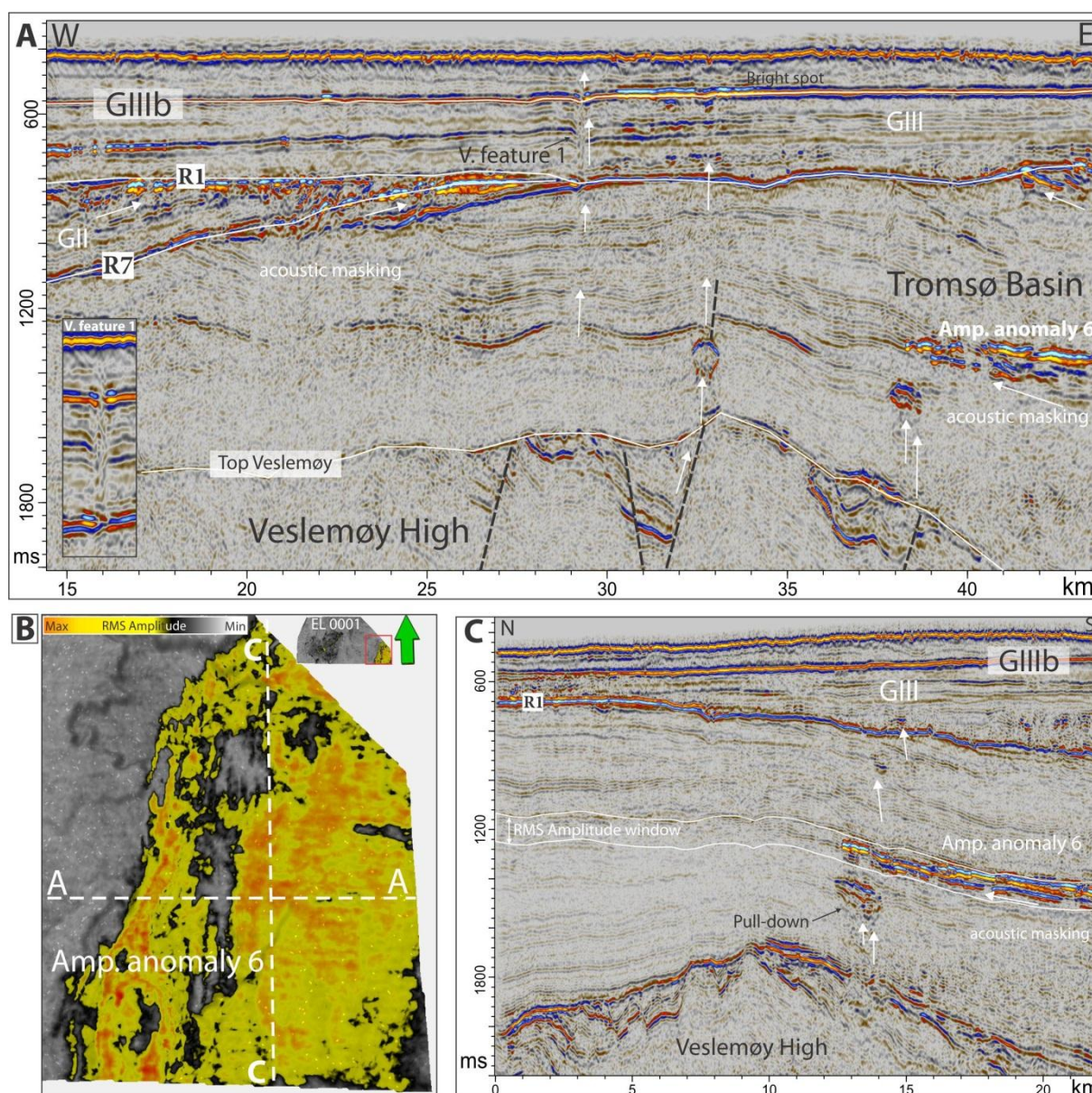


Figure 3.32 A) Seismic profile of inline 806 showing high-amplitude anomalies observed within Tromsø Basin and indicate interpreted fluid migration paths (white arrows). Zoom on vertical feature 1 is shown in lower left corner. **B)** RMS Amplitude map showing amplitude anomaly 6 and location of the profiles. RMS volume window of 150 ms is used and it is extent indicated in C. **C)** Profile of the cross-line 3506 show amplitude anomaly 6 at the eastern limit of the Veslemøy 3D survey and interpreted fluid migration pathways.

Vertical *feature 1* is interpreted as vertical conduit formed by upward focused migration of the over-pressured fluids, bypassing the Pleistocene sealing unit GIII by means of hydrofracturing.

Results

Based on distribution of high-amplitude anomalies interpreted as a free gas accumulations and vertical zones of chaotic reflections, interpreted as vertical conduits of focused fluid flow. There was created a conceptual model showing potential fluid flow migration pathways within Veslemøy High area (Fig. 3.33).

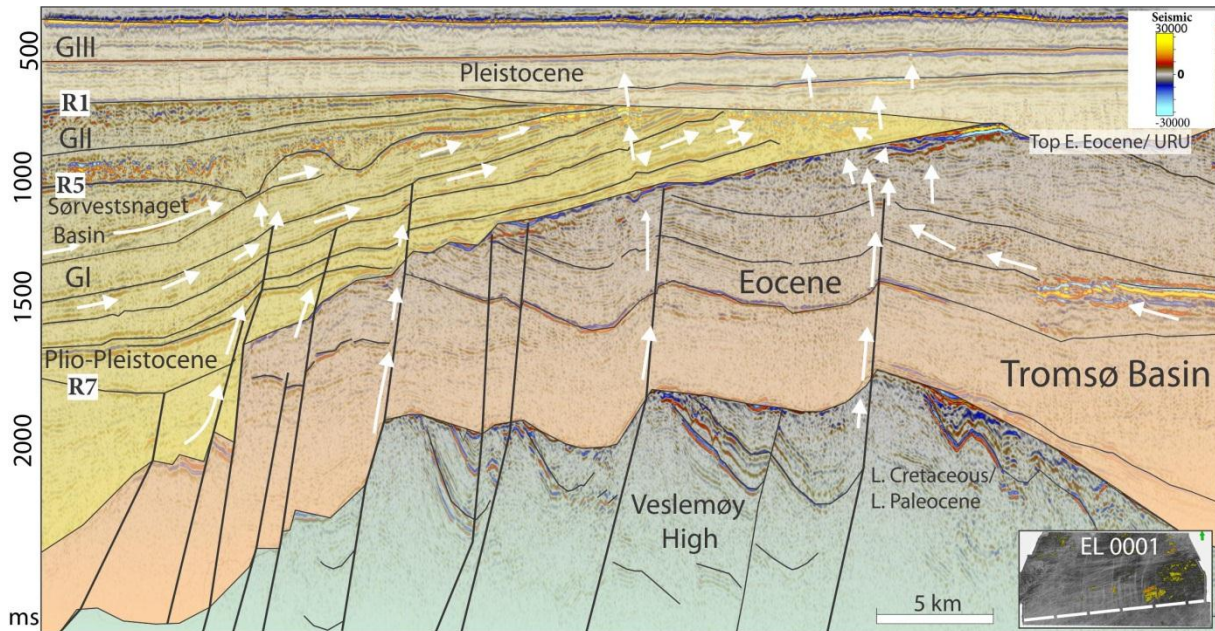


Figure 3.33 Conceptual model indicating potential fluid migration pathways within the Veslemøy High area. Tertiary boundaries are from Ryseth et al. (2003) and Plio-Pleistocene from Butt et al. (2000). The interpreted fluid migration pathways are indicated by the white arrows.

Observed geological architecture might lead to the migration of formation gas-rich fluids towards apex of the structural high along the permeable onlapping strata. Appearance of polygonal faulting, zones of vertical acoustic masking, amplitude anomalies related to gas charged fluids and presence of palaeo and present day pockmarks show evidence of active fluid migration systems in the study area. Accumulations of shallow gas above and in the vicinity of the Veslemøy High is evident from higher concentration of high-amplitude seismic anomalies are located above deep-seated faults and above the apexes of rotated fault blocks within Mesozoic rocks (Fig. 3.33).

3.5 Gas hydrate stability zone (GHSZ) modeling

A thorough evaluation of the NH9803 and EL0001 3D seismic surveys did not reveal presence of a bottom simulating reflector (BSR) within the study area. Occurrence of methane hydrates within the study area is disregarded by the presence of high-amplitude anomalies interpreted as free gas accumulations in the sediments. In addition, water depth of around 300 m at the location is indirectly excluding the area out of stability field. Nevertheless, due to geological setting similar to those where hydrates are found worldwide (Max, 2003) and abundance of shallow gas accumulations inferred from 3D seismic datasets, favorable conditions for formation of the methane gas hydrates might have occurred in the geological history of the area.

For stability field predictions the CSMHYD program by Sloan (1998b) was used. The parameters used for modeling input were acquired from published literature, although assumption has been made that glacial conditions were similar to those of last glacial maximum (LGM). Water depth in the area of the buried depressions is around 300 m. The average annual sea bottom water temperature for the area is about + 3⁰ C and could vary due to complex ocean current patterns (<http://data.nodc.noaa.gov/temperature>). A geothermal gradient of 34⁰ C/km is indicated in the exploration well 7216\11-1S (NPD, 2011) located in the central part of the Sørvestnaget 3D survey (Fig 2.12). As a higher temperature gradient is expected over Veslemøy structural high and the adjacent salt dome (Bugge et al., 2002) a gradient of 38⁰ C/km was used for the calculations. Composition of the supplied gas towards the seabed from underlying sources is vital, because even small amount of higher hydrocarbon gasses will significantly thicken the GHSZ (Sloan Jr, 1998a; Chand et al., 2008).

The following gas compositions were assumed for the modeling of GHSZ:

Type I: 99% Methane, 1% Ethane

Type II: 95% Methane, 3% Ethane, 2% Propane

GHSZ modeling results are plotted in the graphs which indicate hydrate stability to the left of the curve and water and gas to the right. The point where the gas hydrate stability curve crosses the geothermal gradient marks the modeled base of the gas hydrate stability zone (BGHSZ).

Results

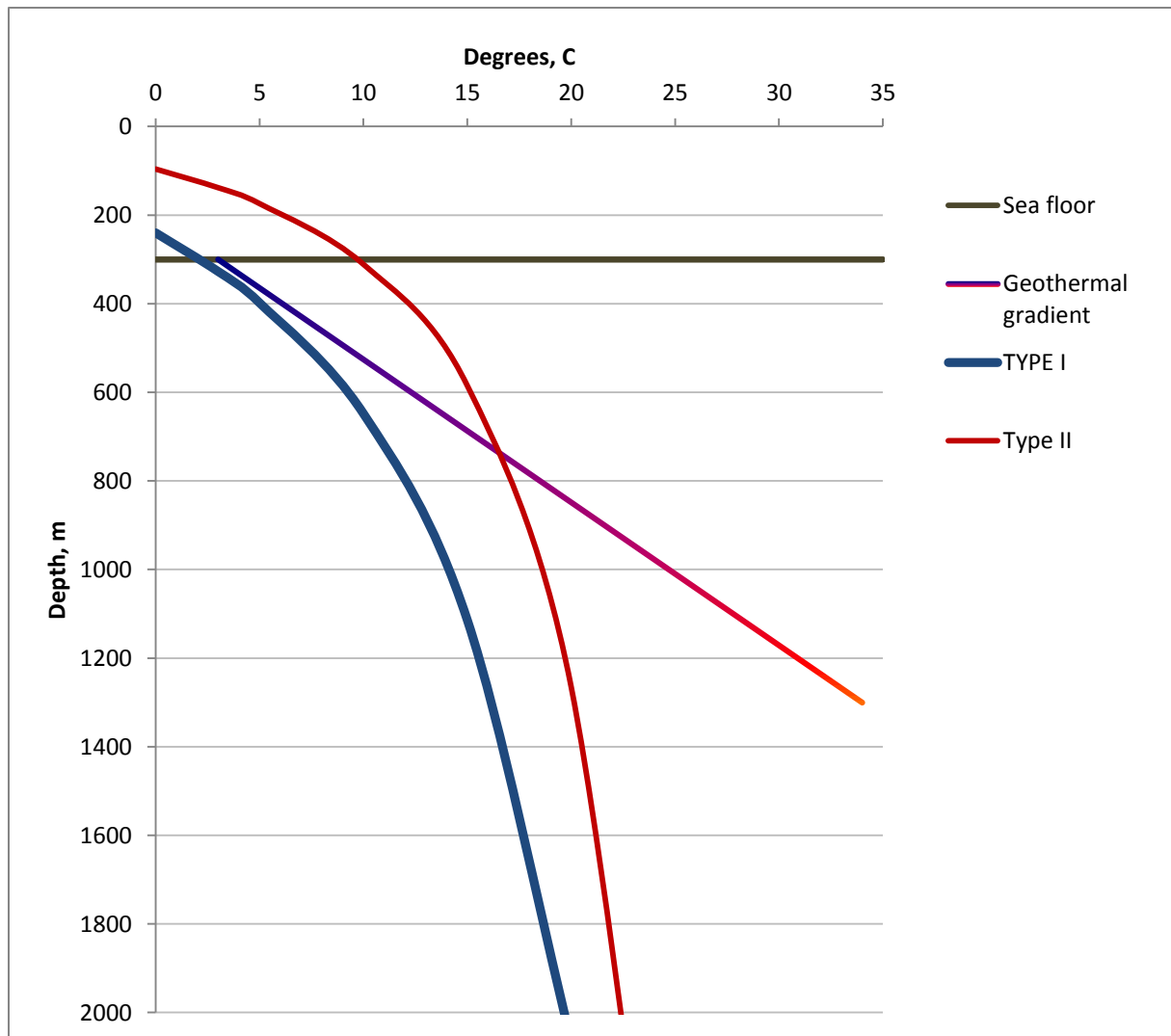


Figure 3.34 Diagram of GHSZ curves for two gas compositions, Type I (99% Methane, 1% Ethane) and Type II (95% Methane, 3% Ethane, 2% Propane) and calculated with the CSMHYD program (Sloan, 1998b). The geothermal gradient of 38°C/km is used in the plot and pressure gradient at the present day conditions.

Modeling of the GHSZ reveals that present day conditions at the study area are unfavorable for the formation of pure methane hydrate composition of Type I (Fig.3.34). Gas composition of the Type II may give rise for GHSZ of up to 420 m thick, given all the other parameters unchanged.

Calculations of the GHSZ are performed for glacial conditions in the area, first for an ice sheet cover (Fig. 3.35) which could be as thick as 1000 m at the margin (Siegert et al., 2001). A cold based ice sheet is interpreted to have a bottom temperature of -1.5 °C (Chand et al., 2008). The second model (Fig. 3.36) is constrained for ice stream conditions, where thickness

of a fast flowing ice stream is expected to be about 500 m (Siegert et al., 2001) and, in case of warm-based ice, assumed to have a bottom temperature of $+2^{\circ}\text{C}$ (Benn and Evans, 2010).

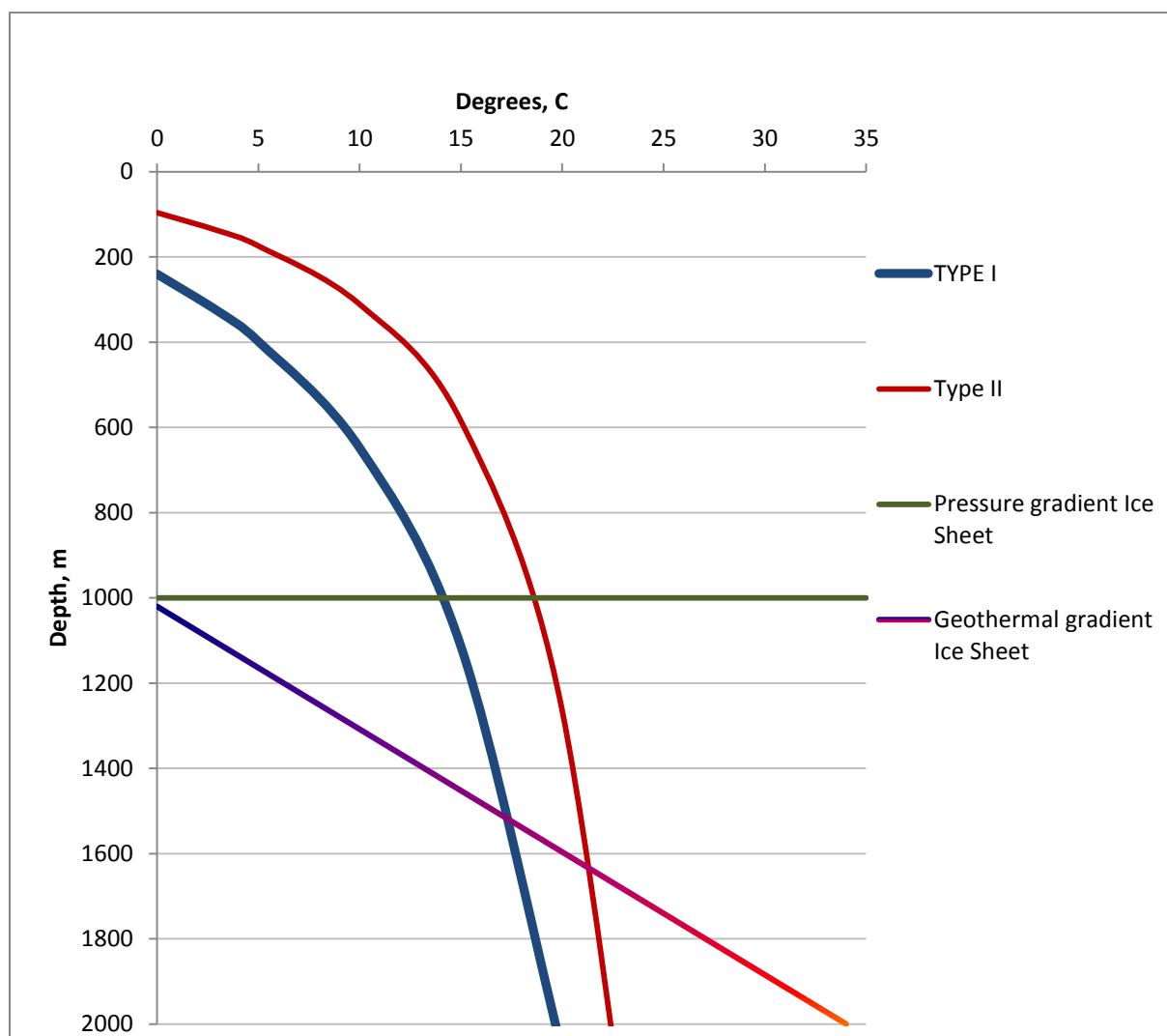


Figure 3.35 Diagram showing GHSZ for the gas composition of Type I (99% Methane, 1% Ethane) and Type II (95% Methane, 3% Ethane, 2% Propane) for the conditions of Ice Sheet cover of about 1000 m thick. The geothermal gradient used for the modeling is $38^{\circ}\text{C}/\text{km}$ and ice sheet bottom temperature is assumed to be -1.5°C .

Modeling results for the conditions of an ice sheet covering the Veslemøy High area give a GHSZ thickness of 500 m for the Type I composition below the base of ice, and a 630 m thick GHSZ is modeled for the Type II gas composition.

Calculations performed for ice stream conditions give a thickness of methane hydrate stability zone of 220 m for the Type I gas composition, 530 m for the Type II hydrate.

Results

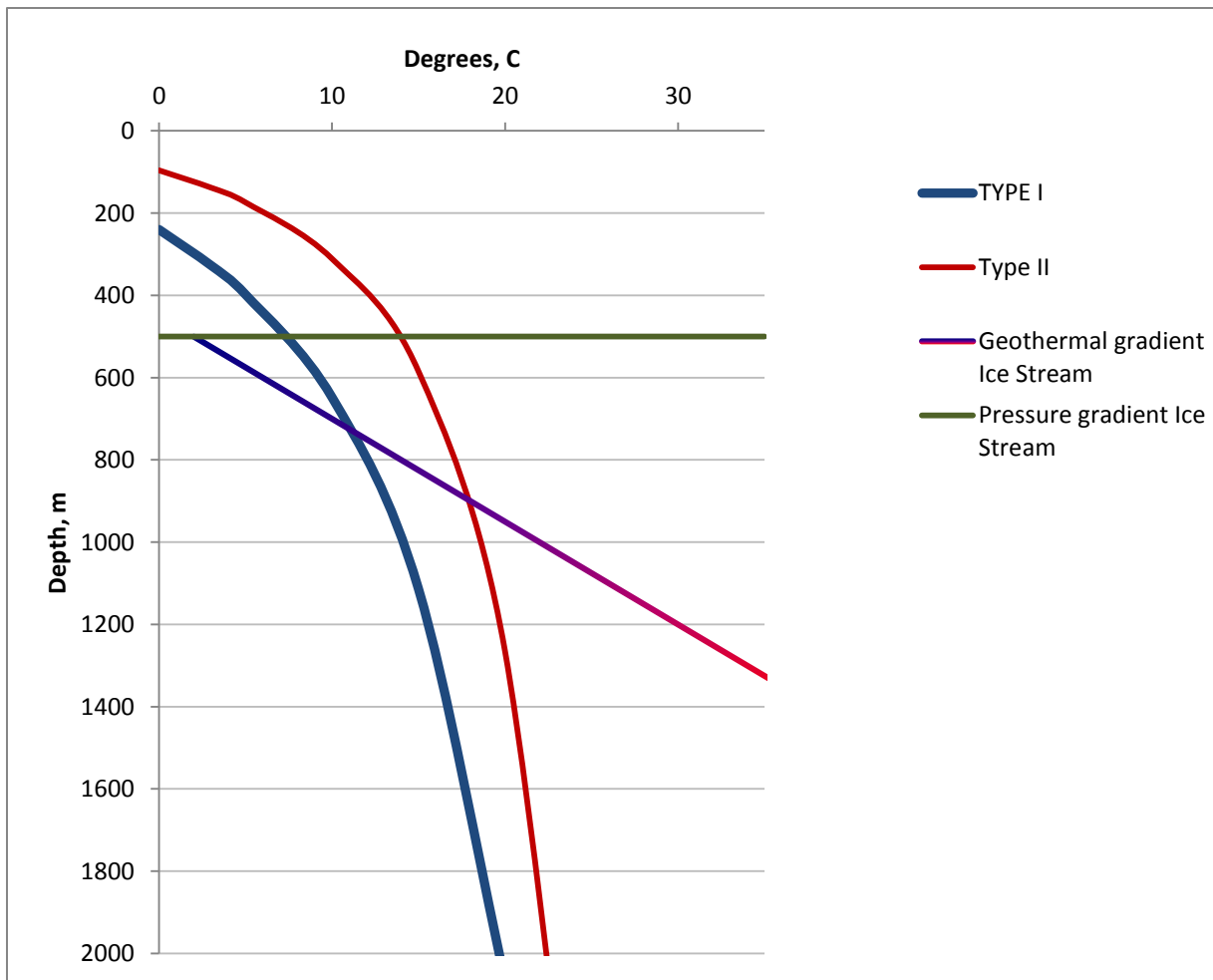


Figure 3.36 Diagram showing GHSZ modeling for the Type I and II gas compositions for conditions under the ice stream. The thickness of ice is used in calculations equal to 500 m and ice stream bottom temperature is assumed to be +2⁰ C.

Based on the GHSZ modeling results, it is inferred that methane hydrate might have been stable under glacial conditions and would dissociate during interstadials.

4 Discussion

The discussion of this study is focusing on the relationship between buried geomorphologic erosional features and fluid migration observed in the surveys NH9803 and EL0001. An attempt is made to identify geological processes which control the glaciotectonic erosion and formation of the depressions. Observations and interpretation made in the result part of the thesis lead to several topics for the discussion. First, the relationship between palaeo ice flow direction and sediment blocks and rafts will be discussed. Second, evaluation of the relationship between sediment blocks and depressions is going to be made. Third relationship between depressions and gas accumulations, as well as fluid flow pathways will be evaluated. The gas hydrate stability zone modelling results will be assessed in terms of potential hydrate formation and dissociation processes effect on the sediments. Finally, models for formation of the depressions and sediment block will be evaluated.

4.1 Relationship between palaeo ice stream flow and sediment blocks.

The evidence of the grounding ice sheet reaching the palaeo shelf edge in the study area is shown by the Andreassen et al. (2004). The morphological features observed on the interpreted erosional surfaces of glacial packages GII and GIII, suggest that glacial erosion and deposition were common processes since the R5 time. The units are subdivided by the erosional surfaces which earlier were interpreted to be formed by subglacial erosion (Andreassen et al., 2004; Andreassen et al., 2007,b). The interpreted horizons R5, GIIa, Pleistocene Intra 1 & 2 and seafloor reveal sub-parallel lineations of up to 75 km long, which are interpreted as mega-scale glacial lineations (Clark, 1993; Stokes and Clark, 2002), formed under the former ice streams and indicating palaeo ice flow direction (Rafaelsen et al., 2002; Andreassen et al., 2004). There is an open discussion in regard to the formation processes of MSGs either they formed by erosion (Tulaczyk et al., 2001; Clark et al., 2003) or by the deposition (Clark, 1993; Canals et al., 2000). There is an open discussion on the formation processes of MSGs, whether they are formed by erosion (Tulaczyk et al., 2001; Clark et al., 2003) or by the deposition (Clark, 1993; Canals et al., 2000). The MSGs interpreted in this study show clear evidence of erosional genesis at the lower stratigraphic levels example GIIa horizon (Fig 4.1, Fig3.5). But at the higher stratigraphic level, within a GIII glacial unit and at the seafloor, are interpreted to be formed by the deposition expressed as positive

Discussion

features (i.e. Fig.3. The MSGLs often indicate several ice flow directions at the same surface which can be attributed to switching of ice-stream flow direction at different stages of glaciation (Winsborrow et al., 2011).

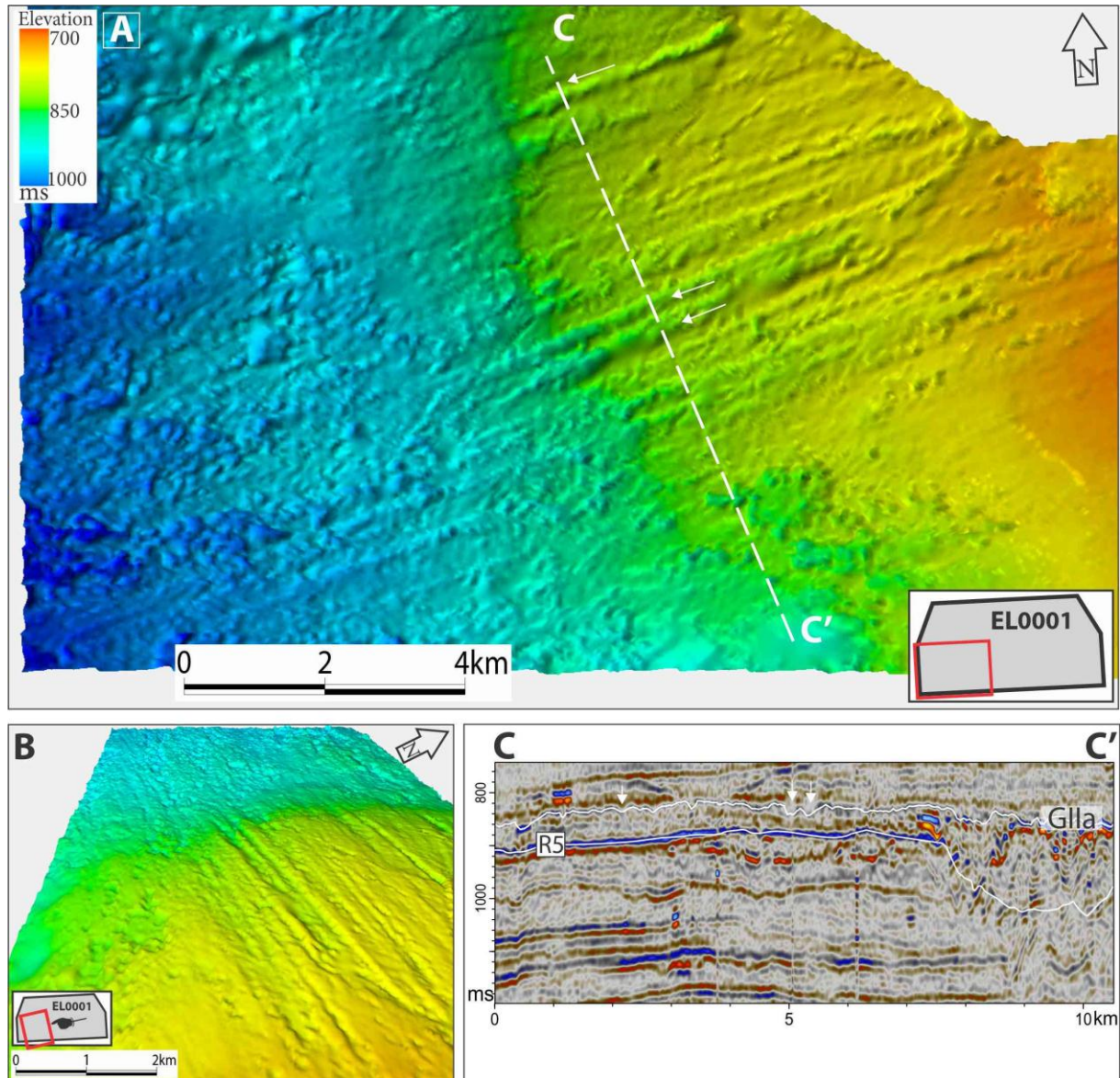


Figure 4.1 A) Shaded relief time map of the GII a reflection showing well developed MSGLs of W-E direction of clear erosional nature. **B)** The illuminated perspective view from the east of the same horizon as in A, showing erosional surface over the interpreted sediment blocks. **C)** Seismic profile shown in A, which indicates location of the GIIa surface and incised MSGLs marked with white arrows.

Several areas with high-amplitude anomalies are observed within the Plio-Pleistocene package GII and Pleistocene succession GIII of both 3D surveys. These high- amplitude reflections are interpreted as sediment blocks and rafts of different composition compared

with the surrounding sediments and appear to be common features within these successions. Glacial megablocks and rafts are documented from other formerly glaciated areas (Aber et al., 1989) and from the NH9803 Sørvestsnaget 3D survey (Andreassen et al., 2004; Andreassen et al., 2007,b), where they are interpreted to be subglacially eroded and deposited. The volumetric 3D seismic attributes in combination with shaded relief time maps show a clear relationship between sediment blocks and glacial streamlined features in the study area.

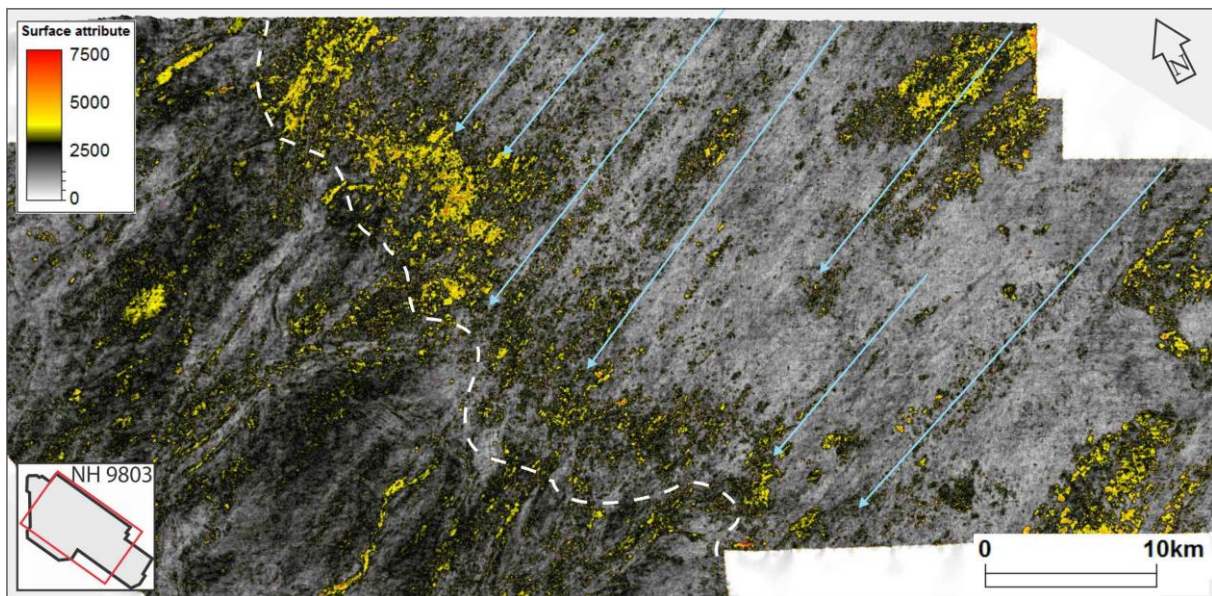


Figure 4.2 RMS Attribute map of 100 ms window above horizon R5 showing alignment of the sediment blocks with palaeo ice flow direction indicated by blue arrows. White dashed line is indicates position of the interpreted ice grounding line.

The alignment of the sediment blocks in chains with dominantly east-west orientation is consistent with the palaeo ice flow direction inferred from MSGLs (Fig. 4.2, Fig4.3). Thus alignment of the sediment blocks and rafts in chains is interpreted to be parallel to the palaeo Ice streams draining the Barents Sea and Fennoscandian ice sheets. This is in accordance with previous studies (Andreassen et al., 2004; Aber and Ber, 2007; Andreassen et al., 2007,b), and documented in this study. The sediment blocks are therefore inferred to be eroded and deposited by the ice streams.

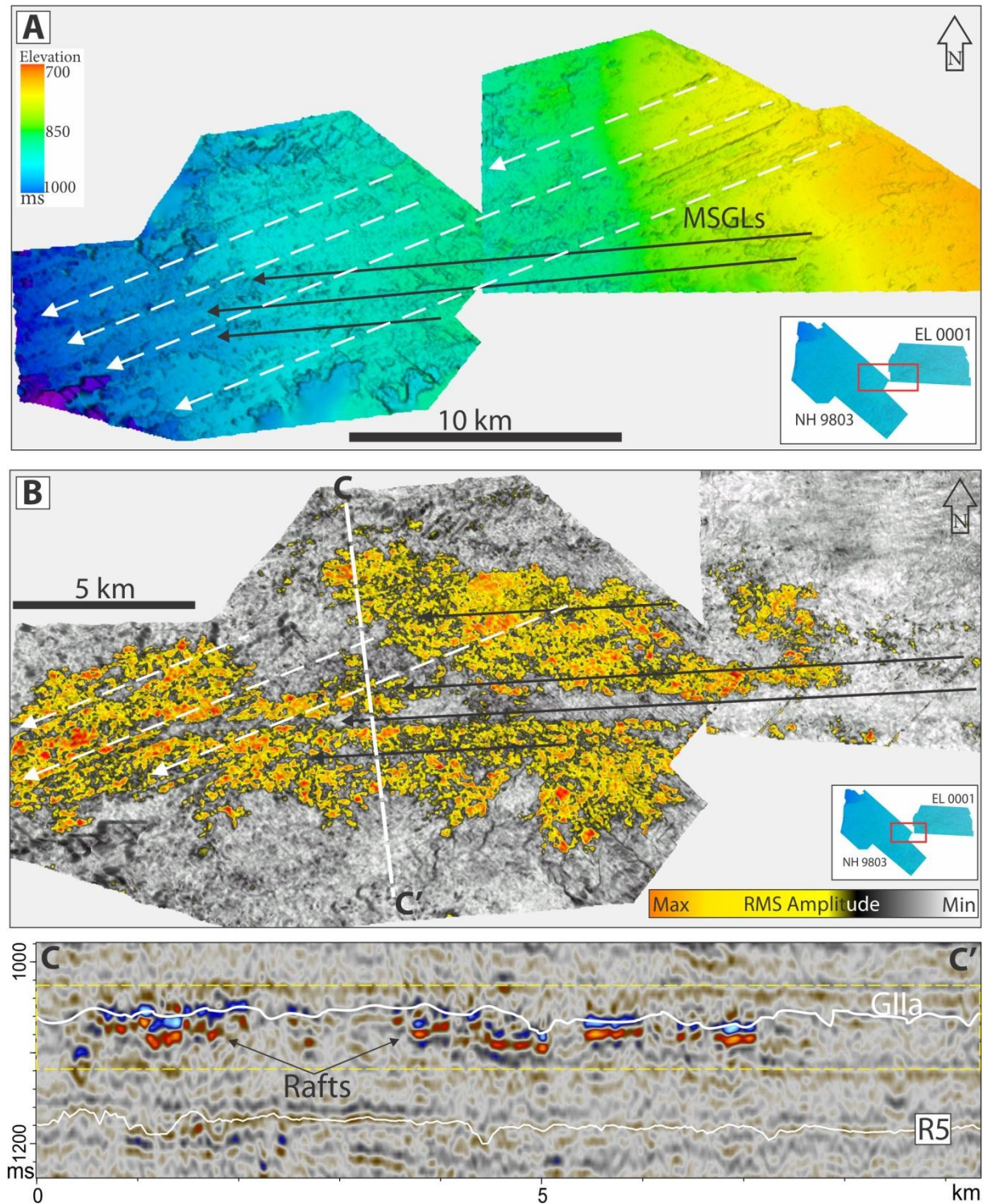


Figure 4.3 **A)** Illuminated time map of the Glla horizon showing two sets of mega-scale glacial lineations indicated by arrows of the south-west and western orientation. **B)** RMS amplitude map of Glla horizon displaying the lateral distribution of sediment blocks and their relation to the MSGLs indicated by black and white arrows. **C)** Arbitrary seismic profile showing location of the horizon Glla and extent of the RMS amplitude volume indicated by a yellow dashed box.

4.2 Relationship between the sediment blocks and depressions

The most distinct geomorphologic features observed on interpreted horizons are the large scale erosional depressions. The five depressions of semi-circular shape are located within western part of the EL0001 Veslemøy 3D seismic survey. The similar depressions of comparable scale were described from the other parts of the Barents Sea (Sættem, 1990; Solheim and Elverhøi, 1993; Rafaelsen et al., 2002), from the North Sea (Heggland, 1998; Fichler et al., 2005) and from the Norwegian Sea and Svalbard (Ottesen et al., 2005). This indicates common appearance of the sub circular depression on the continental shelf offshore Norway. Nevertheless, authors discuss different mechanisms for the formation of the depressions and in each case either glacial erosion or fluid expulsion is inferred. Horizon R5, on which depressions are exposed, also show evidence of erosion by fast-flowing ice indicated from the MSGLs (Fig.4.4).

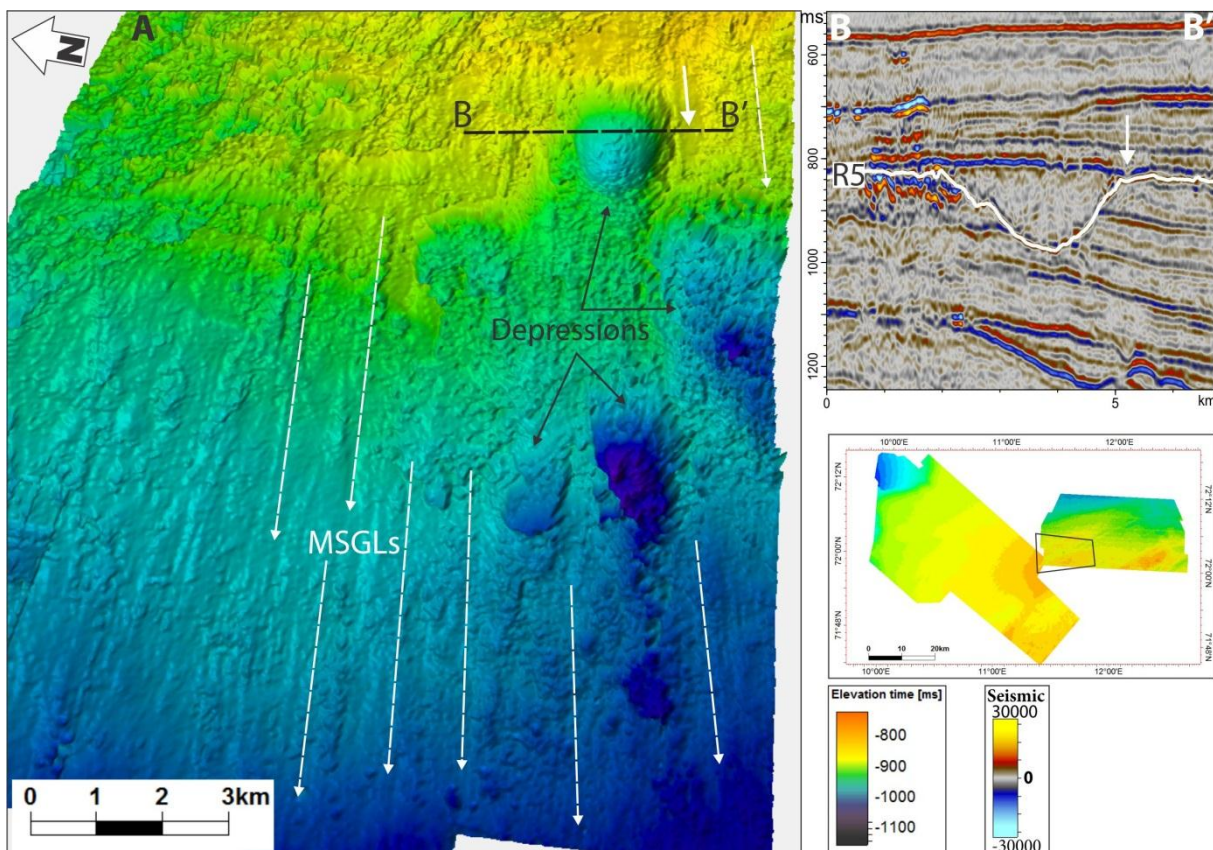


Figure 4.4 Perspective view of the shaded relief time map of horizon R5 which shows a relation between the MSGLs and depressions. B) Seismic profile across the depression 1 and showing location of horizon R5, white arrow indicates location of the well-developed MSGL visible in A.

MSGs appear adjacent to the depressions, and have the same orientation as the long axes of the depressions, suggesting that also the depressions were formed by ice streams.

Andreassen et al. (2004) suggested that chains of sediment blocks in Sørvestnaget survey were eroded and deposited by fast-flowing ice streams. Based on the morphology of chains they suggested that the source of the blocks material most probably was a point or line source. This study provides evidence for such source areas present within the Veslemøy 3D survey, attributed to the depressions observed here (Fig. 4.4, Fig. 4.5).

The chains of the sediment blocks and rafts in the eastern part of the NH9803 Sørvestnaget seismic survey appear just above the R5 horizon (Fig. 4.5). The continuation of these chains occurs in the western part of the Veslemøy High 3D survey at the same stratigraphic level (Fig. 4.5). Furthermore, the sediment blocks seem to terminate right at the eastern limits or within the depressions on horizon R5. On seismic profiles the depressions II, III and IV show high-amplitude anomalies inside them (Fig. 3.24, Fig. 4.5), interpreted to be displaced sediment blocks which have not been transported away from the depressions. Chains of sediment megablocks and rafts are aligned parallel to the MSGs observed on the R5 and GIIa horizons and at several locations show imbrication perpendicular to the inferred ice flow direction (Fig. 3.17, Fig. 3.21). Interpretation of the mega-blocks and rafts to be deposited by grounded ice is in agreement with Andreassen et al. (2004, 2007b), which had inferred that they are products of fast-flowing ice streams. The fact that long axes of the depression are parallel to the palaeo ice flow direction indicates that depressions have been formed by subglacial erosion or modified by subglacial processes.

All discussed observations provide evidence for the provenance area for the sediment megablocks and rafts within the lower part of the GII package. The depressions are therefore interpreted to be likely source areas for the sediment mega-blocks and rafts observed downstream in the GII succession above the R5 horizon. The mechanisms and processes involved into the displacement, transport and deposition of the sediment blocks appear to be complex, and hypotheses will be discussed in chapter 4.4.

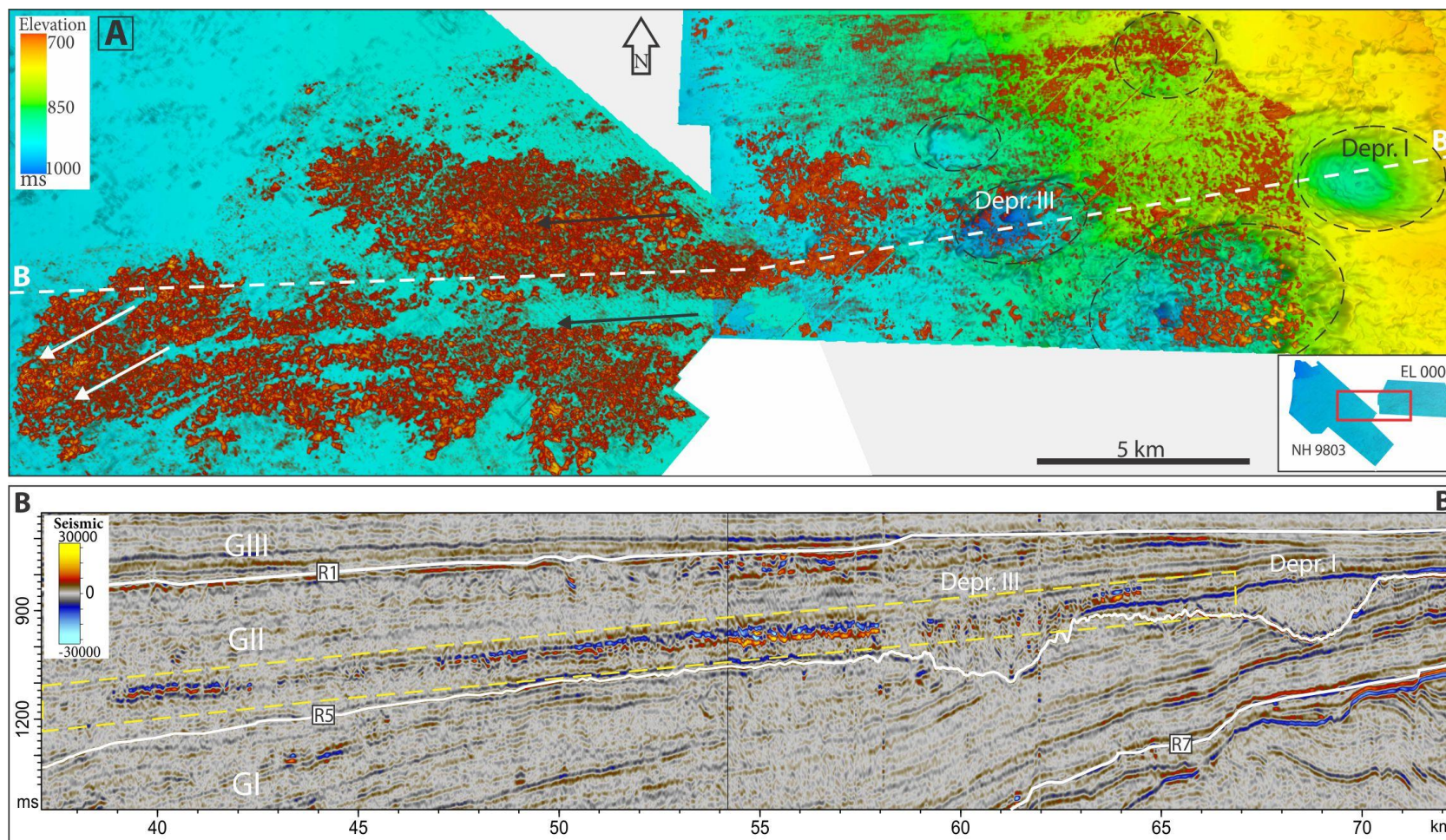


Figure 4.5 A) Shaded relief time map of the horizon R5 at the intersection of the two 3D surveys, combined with the volume render and showing spatial relationship between blocks and depressions. Arrows indicate two sets of the MSGLs and circles outline location of the depressions. **B)** Seismic profile shows relationship between sediment blocks at the lower part of the GII unit and erosional depressions on horizon R5. Yellow dashed box shows the extent of volume render used in A.

4.3 Relationship between the depressions and indications of fluid migration

Relationship between indications of fluid migration and depressions (pockmarks) observed on the sea floor has been well documented (Hovland and Judd, 1988; Solheim and Elverhøi, 1993; Long et al., 1998; Fichler et al., 2005). The results of this study discuss relationship between potential fluid flow path ways and buried erosional depressions. Several observations suggest that there is such a relationship. First of all the observed group of depressions is concentrated in one particular area and stratigraphic level of the Veslemøy 3D survey. Some of the depressions are observed adjacent to, or in contact with gas accumulations inferred from high-amplitude anomalies (Fig.3.27). These anomalies occur at the subcropping layers of the succession GI and show evidence of vertical fluid migration through the Pleistocene glacigenic succession GIII (Fig. 3.30, Fig.3.31, Fig. 3.33).

In addition, indications of former fluid expulsions are documented on the sea floor and palaeo horizons in form of giant pockmarks, which often associated with the gas charged fluid expulsions (Hovland and Judd, 1988; Solheim and Elverhøi, 1993). It is worth mentioning that three giant pockmark craters are concentrated in the area above the buried depressions (Fig. 4.6). This observation indicates that an active fluid flow system has persisted in this area for an extended time, probably since the deposition of the glacigenic package GI. The preservation of the pockmarks on the erosional horizons is showing evidence that they were likely formed right after grounded ice retreat. They most likely have been active for a short time after the deglaciation and no or minimum seepage occurs at the present time. This upper relative time limit is evident from the iceberg plough marks which are overprinting on the flanks and bottom of the pockmarks (Fig. 4.6). This observed relationship between the glacigenic land forms and giant pockmarks, suggests that the fluid flow expulsion most likely took place during initial phase of the deglaciation and was related to the processes active during this phase. This interpretation is in line with several publications (Solheim and Elverhøi, 1993; Long et al., 1998; Bünz et al., 2003; Fichler et al., 2005; Andreassen et al., 2007,a), where authors associate deglaciation phase with increased fluid migration and expulsions.

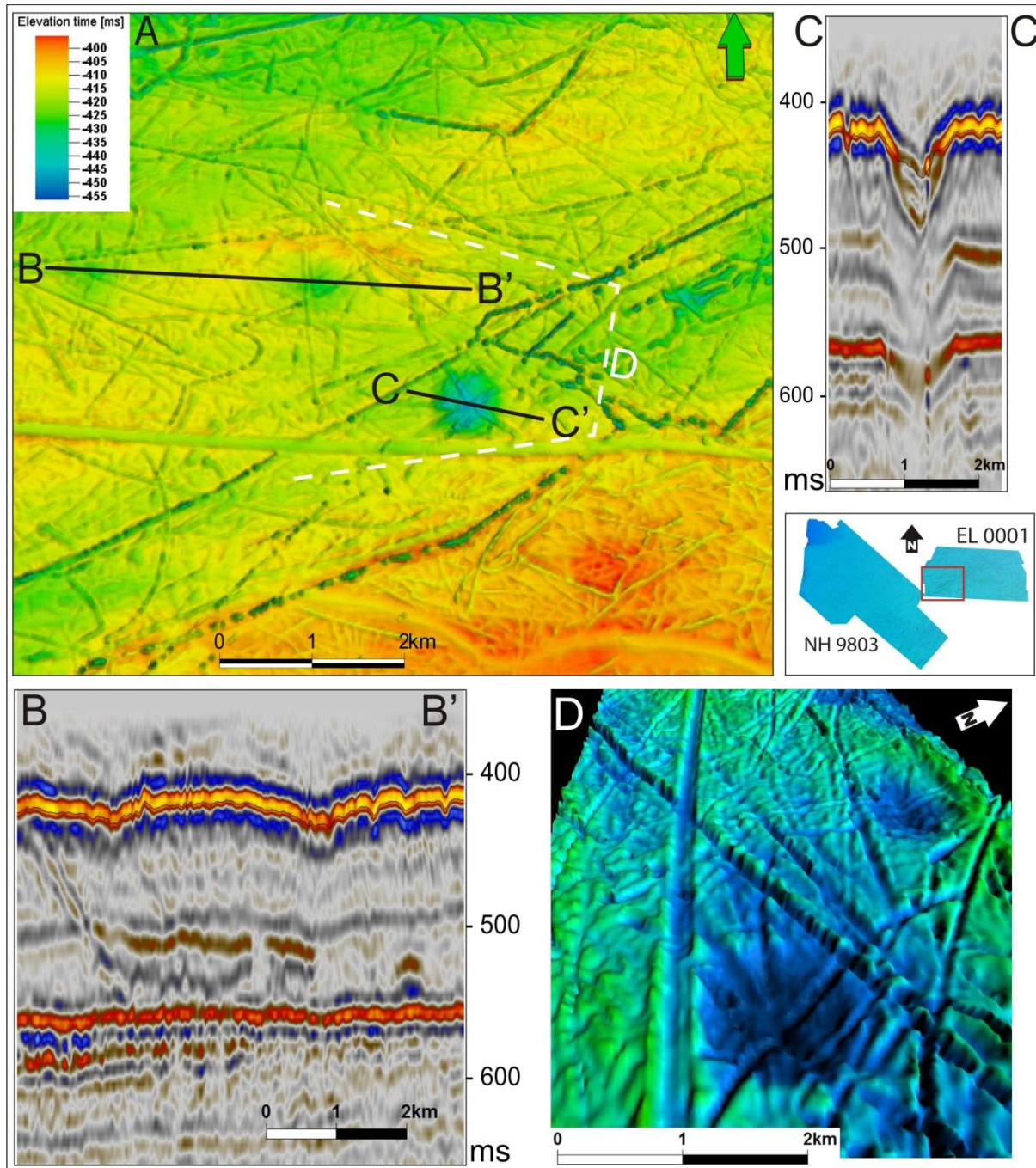


Figure 4.6 **A)** Illuminated time map of the seafloor horizon in the south-western part of the Veslemøy 3D survey, showing three giant pockmark craters. **B)** and **C)** are showing seismic profiles across the giant pockmarks indicated in **A)**. **D)** Perspective view of the seafloor from the east showing elevated rims around giant pockmarks and iceberg ploughmarks overprinting bottom and flanks of depressions.

Discussion

The buried depressions are observed right above deep-seated listric faults marking the western flank of the Veslemøy High (Fig. 4.7). Faults are known to be acting as conduits for the fluids, creating a seal by-pass system, which may develop even in sediments with low permeability (Cartwright et al., 2007). However, flow through faults and fractures might not be sustainable over geological time scale and it often has episodic character associated with the active phase of the fault growth or the over-pressurized fluid escape (Hooper, 1991). The seismic profiles show evidence of reactivation along the deep-sited faults underneath the depressions during the R5 time (Fig 4.7). It is evident from displacement along the faults to be less within Plio-Pleistocene than in Tertiary strata and their truncation by R5 unconformity (Fig. 4.7). These faults are developed within the G1 glacial unit and exhibit a throw of about 20 m and terminate within erosional depressions. Correlation between fault trends and giant pockmark craters has been also documented by Lammers et al. (1995) and Long et al. (1998) farther north in Bjørnøyrenna, as well as in the North Sea (Fichler et al., 2005), where authors indicate gas migration along the faults from the greater depth.

Although observations do not show evidence for present day fluid migration through the deep-seated faults or large accumulations of the gas above them, this migration might have been short-lived event persisted in the past. Indications of past vertical fluid migration are observed within succession GIII. These are documented in form of acoustic pipes and presence of the pockmarks on buried horizon and on the seafloor (Fig. 3.8, Fig. 4.6). Moreover, faults in the fine-grained sediments are known to be sealed quick after the movement along the fault plain has sized (Cartwright et al., 2007).

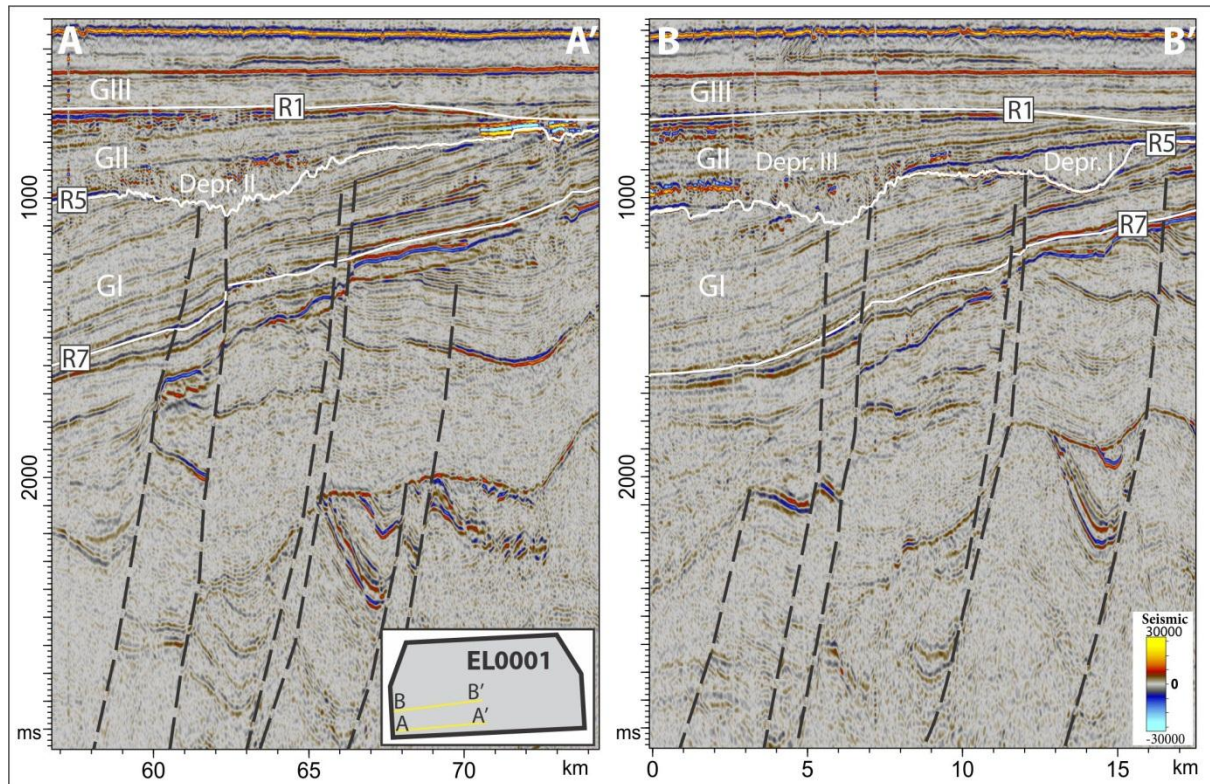


Figure 4.7 A) An arbitrary seismic profile showing the deep-sited faults at the western part of the EL0001 Veslemøy 3D survey and extending to the R5 reflection. Note termination of the faults within the Depression II. **B)** Arbitrary seismic line across the depressions I and III showing their relationship with underlying deep-sited faults. Location of the profiles is indicated in lower right corner in A.

These acoustic pipes are interpreted to be formed by the short lived fluid expulsion events which are able to transport gas-charged fluids to the seabed (Cartwright et al., 2007). Also formation of the buried depressions them self is might be related, in a certain way, to the gas charged fluid expulsion.

Another explanation for the fluid escape is lying in the erosional nature of the glacial horizons. The potential gas accumulations within the glacial packages GI - GIII would have been affected by the presence of the grounded ice. In the first place glacier would act as an erosional agent removing sediments down to shallow gas accumulations and may cause fluid escape into the sub-glacial environment. On the other hand, gas hydrate stability zone modelling results show that the methane hydrate stability zone would be up to 630 m thick during glacial conditions, assuming an ice thickness of 1000 m. Deglaciation would have caused

rapid dissociation of the hydrates which might have led to upward migration of gas and sediment instability at the continental margins (Mienert et al., 1998; Bünz et al., 2005).

Andreassen et al. (2007a) inferred that repeated cycles of the Plio-Pleistocene glaciations and interstadials most likely caused cycles of fluid expulsion and fluid migration in the Sørvestnaget part of the study area.

4.4 Hypothesis for the formation of the buried depressions

There are several mechanisms that can produce sub-circular depressions of the large size as those observed in the study area. In the following part of the discussion different actual processes are evaluated and, based on this evaluation, a conceptual model explaining formation of the depressions is proposed.

4.4.1 Pure glaciotectonic dislocation hypothesis

There are several published studies addressing depressions formed by the glaciotectonic processes (Aber et al., 1989; Sættem, 1990; Sættem et al., 1994; Aber and Ber, 2007). The shape and dimensions of the observed depressions on the R5 horizon at the south-western part of the E10001 Veslemøy survey have many similarities to depressions described as hill-hole pairs. A hill-hole pair is described by Bluemle and Clayton (1984) as “ *a discrete hill of ice-thrust material, often slightly crumpled, situated a short distance down glacier from a depression of similar size and shape*”(Bluemle and Clayton, 1984). Hill-hole pairs have documented in marine settings in the SW Barents Sea (Sættem, 1990; Sættem et al., 1994; Rafaelsen et al., 2002), on the Mid-Norwegian shelf and offshore Svalbard (Ottesen et al., 2005). The depressions in my study area do not show well-developed hills associated with them, but it has been inferred that such depressions may also occur without hills (Sættem, 1990) or that the hills might be located up to 5 km down-stream from the source depressions (Benn and Evans, 2010).

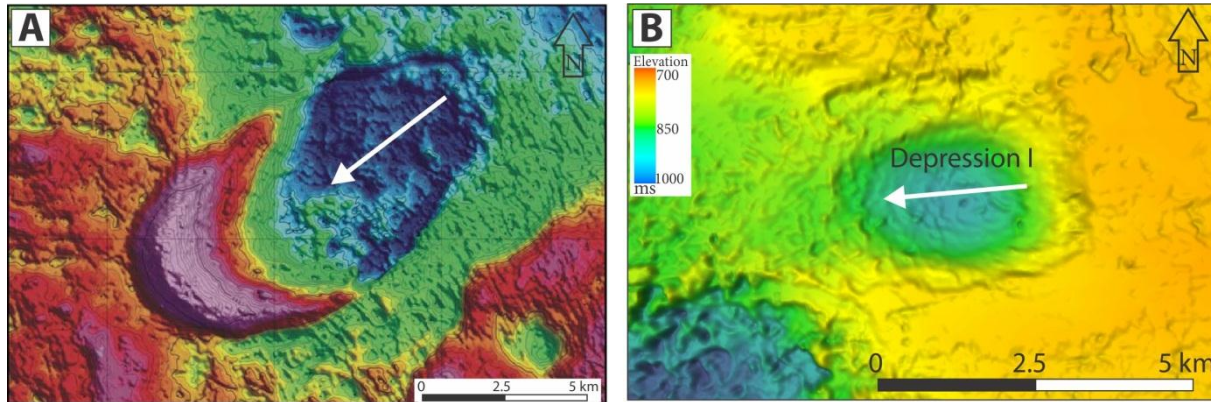


Figure 4.8 Shaded relief images showing comparison of one hill-hole pair observed on the seafloor by Ottesen et al. (2005) in A, and one of the depressions on R5 in this study in B, located within EL0001 3D seismic survey. White arrows indicate inferred direction of the palaeo ice flow. Note absence of the hill immediately downstream from the depression I and its steeper upstream flank (see also Fig. 4.9 B).

A characteristic morphological feature of a hill-hole pair is a steeper slope on the downglacier side (Benn and Evans, 2010), but the opposite is observed for the depressions in this study (Fig. 4.8 and 4.9). The results presented in this thesis reveal that high amounts of sediment blocks and rafts have been deposited down-stream of the depressions above the R5 horizon in succession GII (Fig. 4.5, Fig. 3.18 and Fig. 3.21). The sediment blocks and rafts extend for up to 20 km down-stream of the depressions into the NH9803 Sørvestnaget 3D survey (Fig 4.5). These sediment blocks and rafts are therefore interpreted to be eroded and transported subglacially from the source depressions in the south-western part of the EL0001 Veslemøy seismic survey. It seems likely that erosion, transport and deposition may have occurred in several stages and that displaced sediments have been overridden by the ice stream re-advance. This is evident from the two sets of the chains of sediment blocks with different orientation (Fig 4.3, Fig. 4.5, and Fig. 3.24). This is in line with the previous works in the area (Sanchez-Borgue, 2009).

A pure glaciotectonic hypothesis for formation of the depressions in the study area does, however not explain the localized appearance of the depressions and the observed relationship of these and indications of fluid migration. Therefore alternative mechanisms for formation the depressions is discussed further.

4.4.2 Gas-charged fluid expulsion hypothesis

There are numerous publications describing a relationship between gas-charged fluid escape and formation of sub-circular depressions on the seafloor (Hovland and Judd, 1988; Solheim and Elverhøi, 1993; Sun et al., 2011) and on buried horizons (Heggland, 1998; Max, 2003; Fichler et al., 2005). Genesis of the depressions is likely to be associated with processes that were commonly taking place during the Plio-Pleistocene glaciations, and here the waxing and waning of glaciers might be of importance. Such processes, among others, are gas hydrate formation (Long et al., 1998) and dissociation and hydrocarbon migration related to gas expansion and reservoir tilting (Andreassen et al., 2007,a). Craters on the seafloor was documented from the northern flank of the Bear Island Trough (Lammers et al., 1995; Long et al., 1998), where distribution of the craters is attributed to the underlying faults (Fig 4.10 A). Long et al. (1998) suggesting origin of these craters from the gas blowout associated with the dissociation of the gas hydrates. Similarly, the distribution of the depressions observed in this study is appearing to be associated with the fault structures below. Another group of buried craters comparable in size is documented from the North Sea (Fichler et al., 2005) and suggested to be generated by gas expulsion from gas-hydrate dissociation in combination with melt-water erosion. Another observation supporting active fluid expulsion in the past is the presence of giant pockmarks on the seafloor and located above buried depressions (Fig.4.6). In addition pockmark is observed within the depression I located on its bottom (Fig. 4.9). These are inferred to be indicative of fluid expulsion persistent in this particular area shortly after last deglaciation and interpreted to originate from the melting gas hydrate. Since hydrate stability zone is confined to upper part of the sediment column the hydrates are expected to be accumulate. Trapping of the hydrate under till layers might cause overpressure during hydrate dissociation and will drive pore fluids towards the seabed.

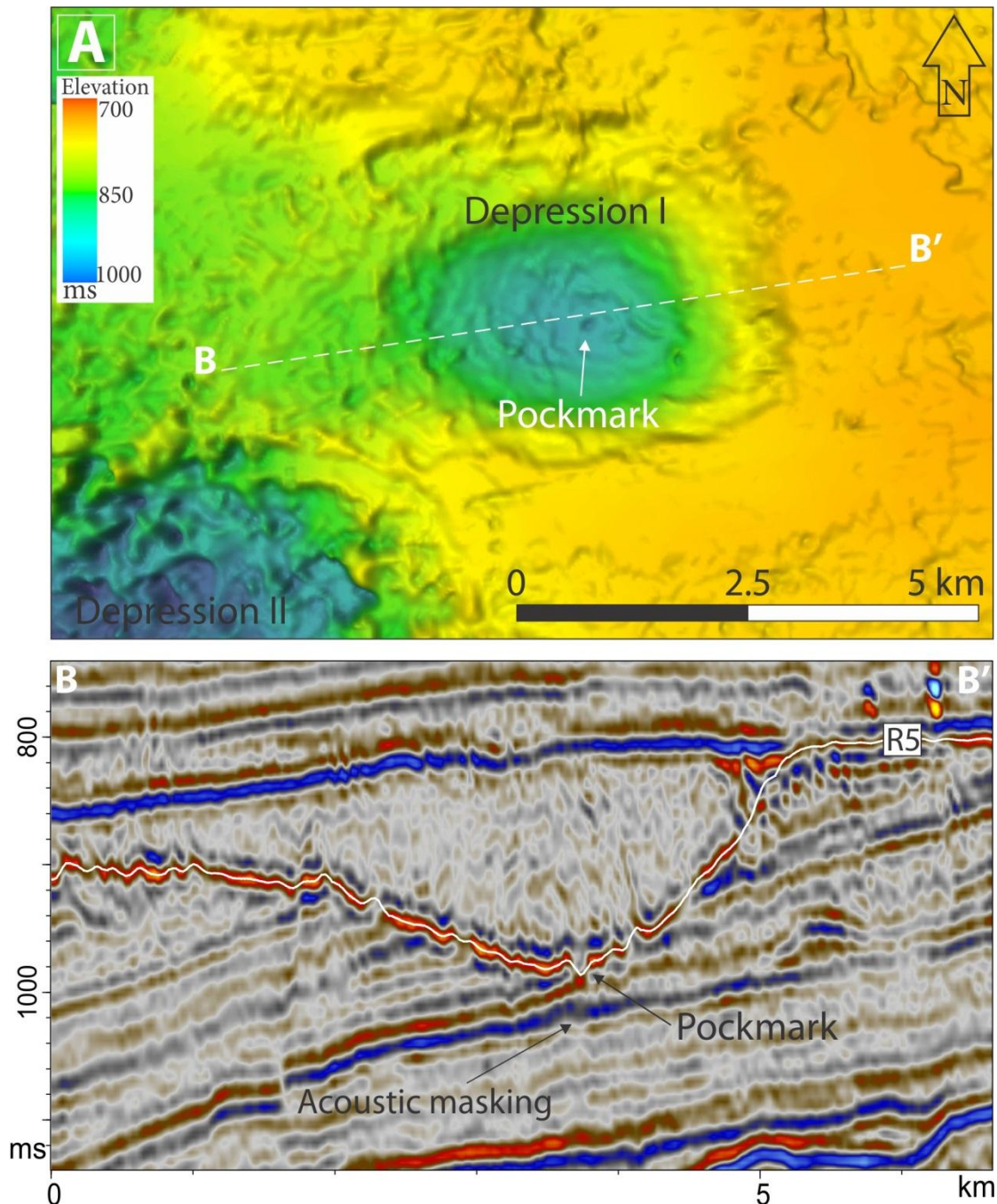


Figure 4.9 **A)** Shaded time map of horizon R5 showing the geomorphology of depression I and the pockmark observed on its floor. **B)** Arbitrary seismic profile indicated in A and showing sediment infill of depression I with acoustically chaotic reflection configuration. A pockmark associated with vertical zone of weak acoustic masking appears within the depression.

The observation of a small pockmark at the bottom of depression I (Fig. 4.9) is also suggesting fluid escape from the underlying strata within the depressions. Overpressure from dissociating

Discussion

gas hydrates may build up under sealing glacial till units or permafrost layers (Fichler et al., 2005; Max and Johnson, 2011) and consequently might escape to the sea-bed when the seal capacity is breached, in extreme cases causing blowout events. This will in turn lead to erosion of the sediments by venting fluids. Dissociation of the hydrates was inferred for the formation of expulsion features such as collapse structures creating rough-floored depression (Dillon et al., 1998; Max, 2003).

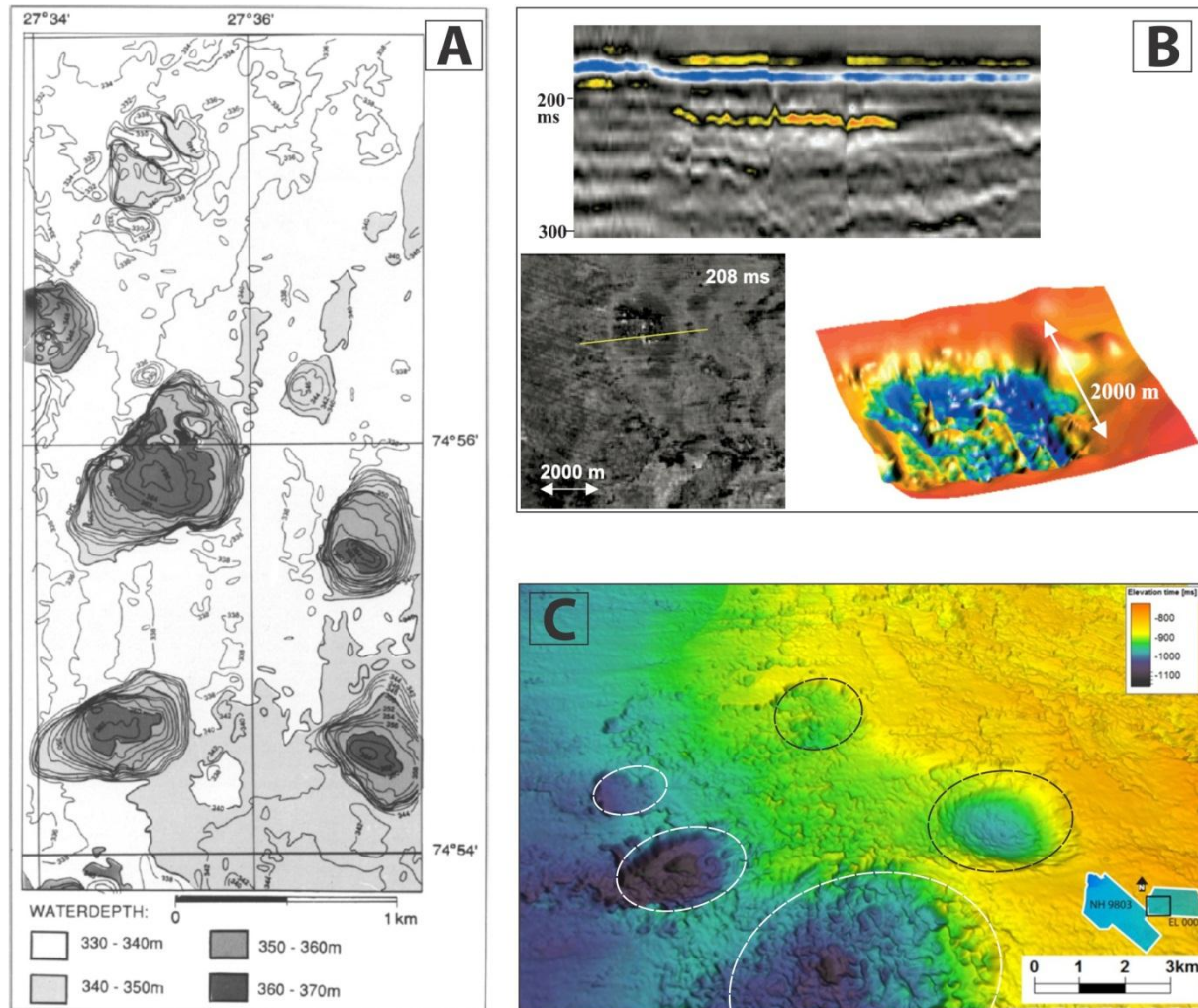


Figure 4.10 Maps showing comparison of the depressions documented on the seabed and buried horizons. **A)** Multibeam bathymetric map showing the blowout craters in the central Barents Sea from Solheim and Elverhøi (1993). **B)** Seismic profile and map of the buried craters related to gas expulsion documented from the North Sea, from Fichler et al. (2005). **C)** Shaded time map showing buried depressions on the R5 horizon outlined by dashed lines, interpreted in this study.

Abundant accumulations of shallow gas accumulations and inferred fluid flow migration pathways, which likely sustained through the Quaternary, would have provided source for gas hydrate formation. The gas hydrate stability zone (GHSZ) modeling indicates existence of a gas hydrate stability zone of 220 m – 550 m thick depending on the Ice sheet thickness. Gas hydrates would otherwise have been unstable during deglaciation conditions, if those were similar to present day. Therefore, it is possible that formation of the buried depressions I-V is could be associated with a blowout event releasing over-pressured gas from dissociating gas hydrates, which were caused by ice sheet retreat.

4.4.3 Conceptual model for formation of glacial depressions and sediment blocks in GII unit

None of the hypotheses mentioned above can alone explain the complexity of the observed erosional features. However, a combination of fluid migration and glacial erosion seems to be the best model for explaining the observed features, and is therefore proposed for the formation of the depressions and sediment blocks within the study area.

A common explanation for glaciotectonic dislocation and glacial transport of t mega-blocks is related to freezing of sediments onto the glacier base (Aber et al., 1989). Over-consolidation of the sediments caused by the basal freezing (Sættem et al., 1996) might lead to dislocation of frozen sediment blocks along thrust planes formed at the base of the consolidated material (Andreassen et al., 2004; Andreassen and Winsborrow, 2009).

Since the glacial erosion of the large buried depressions in my study area seems to be associated with fluid flow and shallow gas accumulations an alternative mechanism is proposed for consolidation of the sediments and thereby generation of a weak layer. Gas hydrates cementing the sediment pore space will significantly increase the shear strength of the sediments, since hydrates are documented to be 20- 30 times stronger than ice (Durham et al., 2003). In addition, gas hydrate formation will withdraw pore water and free gas, if present, from sediments, contributing to their compaction. The presence of gas hydrate in the sediments is ruled mainly by the hydrostatic pressure and geothermal gradient, and does not require freezing temperatures at the glacier base (Figs. 3.34-3.36). Also, several observations indicate that basal processes can remain active at freezing temperatures, contributing to extensive

erosion (Bennett et al., 2003). Andreassen et al. (2007, a) has interpreted the GI succession as shelf margin deltaic facies deposited in a glacial marine environment. In the GI unit minor sand layers were encountered in the well 7216/11-1S (Ryseth et al., 2003), which is located within the Sørvestsnaget 3D survey. It is suggested here that clinofolds will contain more sands and silt towards the provenance area closer to the palaeo shelf break. This is also inferred in the Fig. 4.11 & 3.31 C, where present day shallow gas accumulations are confined to the dipping sedimentary beds.

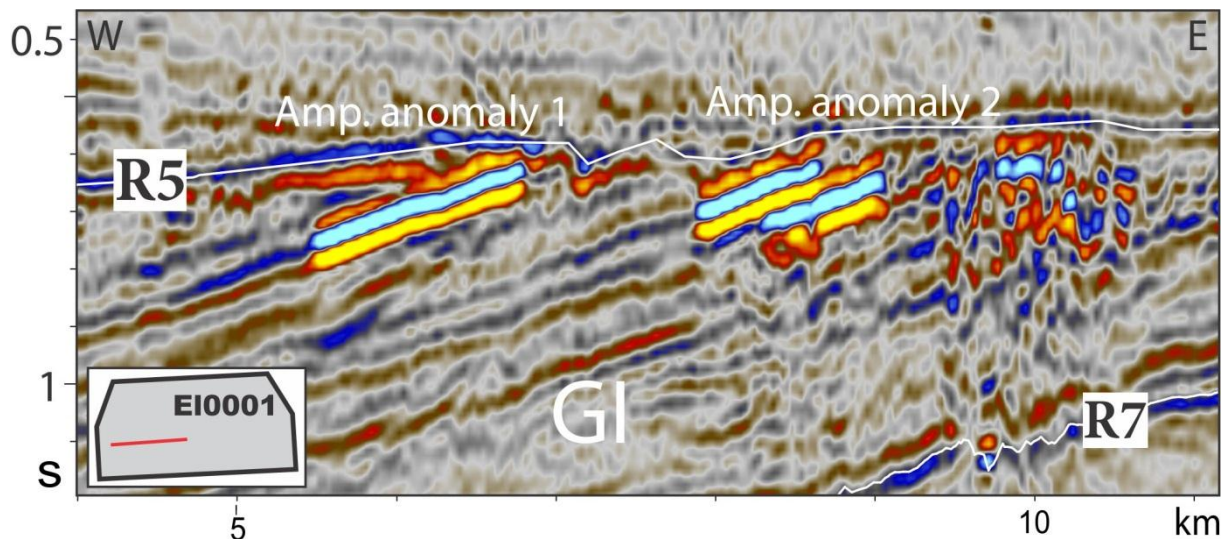


Figure 4.11 Seismic profile showing shallow gas accumulations confined to the dipping beds subcropping erosional horizon R5. Location of the line is shown in lower left corner.

It has been suggested from other studies and areas that high grade gas hydrate accumulations will be confined to permeable beds, when such are present (Bünz et al., 2003; Max et al., 2006; Hustoft et al., 2007; Max and Johnson, 2011), ultimately increasing the sediment shear strength. In my study area, glacial erosion could have been more active at locations where such hydrate-cemented beds are subcropping the glacier base, eventually leading to glaciotectonic excavation and transport of sediment blocks. The decollement surface in this case is most likely located at the bottom of gas hydrate stability zone (BGHSZ), where the contrasts of the mechanical properties between hydrate cemented sediments and underlying over-pressured gas-bearing sediments will be at its maximum.

A three-stage conceptual model is proposed of the formation for the depressions in the R5 horizon, exemplified on a geo-seismic profile across the NH9803 and EL0001 seismic surveys (Fig. 4.12).

The first stage (Fig 4.12 A) is marked by the first advance of the Barents Sea Ice sheet towards the shelf break, probably in the form of a slow-moving ice sheet. This ice sheet is assumed to build up a thickness of 1 km during glaciation (Siegert et al., 2001) and significantly increase lithostatic pressure under the ice sheet. This consequently lead to the thickening of the methane gas hydrate stability zone, which based on the modeling will be up to 500 m thick (Chapter 3.5, Fig. 3.35). Given constant supply of gas and water, gas hydrates are assumed to have formed during this stage within GHSZ, where high-grade gas hydrates would be confined to the permeable beds. Migration of gas-charged fluids is suggested to be from deeper reservoirs along the deep-seated and polygonal faults and along the permeable beds in the Plio-Pleistocene succession.

The second stage (Fig 4.12 B) is attributed to the late glaciation phase when fast flowing ice streams start to drain the BSIS causing thinning of the ice sheet to about 500 m (Siegert et al., 2001). The subglacial erosion is suggested to be especially high at the locations where constant fluid flow has produced high grade gas hydrate deposits. Thinning of the Ice will inevitably lead to the hydrostatic pressure decrease. In turn this will cause upward shift of the BGHSZ, and modeling shows that it will be located at 220 m below the base of the ice stream (Chapter 3.5, Fig. 3.36). This depth correlates well with the depth of the largest depressions I, II and III (Figs. 3.24 & 4.9 B). An upward shift of the BGHSZ will cause dissociation of the hydrates below it and might lead to pore-pressure increase, which also would contribute to high contrasts in mechanical properties. It is therefore suggested that a decollement surface for glaciotectionic sediment dislocation was associated with the BGHSZ, or its changes. The ice stream would have acted as an erosional agent, dislocating hydrate-cemented sediments as blocks and rafts by englacial thrusting (Bluemle and Clayton, 1984; Hambrey et al., 1997) and re-depositing them in elongated chains farther downstream.

Discussion

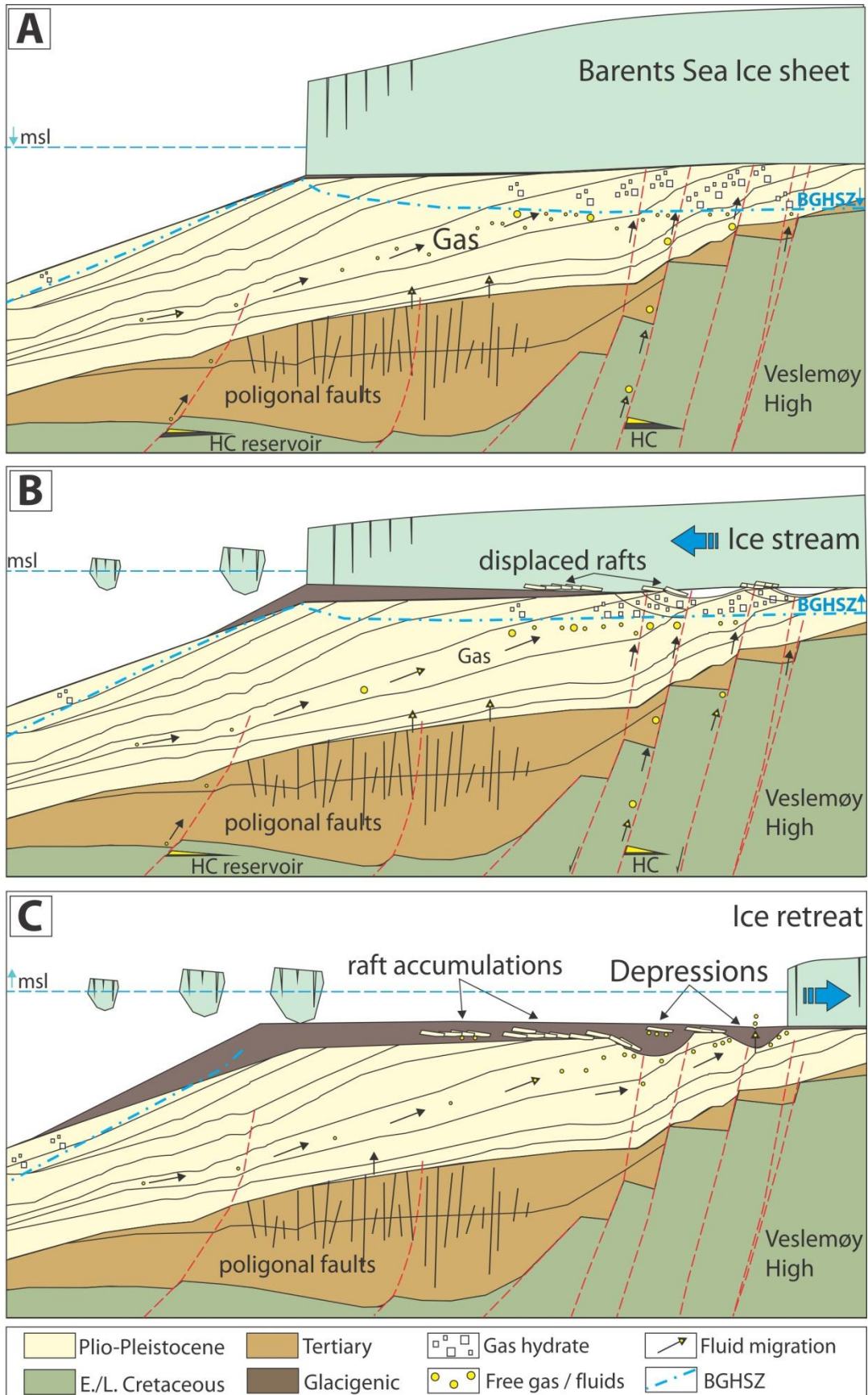
The third stage of the conceptual model (Fig. 4.12 C) is related to the deglaciation phase and glacier retreat. At this stage sediment blocks and rafts being buried within the till unit and erosional depressions are infilled with glacial sediments. Ice stream retreat would cause pressure decrease in underlying sediments and the palaeo shelf area would be outside the gas hydrate stability zone. Remaining gas hydrates would likely dissociate. This eventually could have caused fluid migration and potentially have contributed to reworking of the depressions by fluid expulsion.

Consequent subsidence of the Sørvestsnaget Basin and western Barents Sea margin within study area has led to burial and preservation of the sequence in geological record.

Remarks

Indication of gas hydrate accumulations (interpreted from BSR formed as patches (Chand et al., 2012) above the hydrocarbon field is confirmed by the recent discoveries Skrugård and Havis east from study area. It is therefore suggested that observed depressions might be indicative for the presence of underlying hydrocarbon accumulations, this is in line with Fichler et al. (2005) indicating higher concentrations of craters above the Tertiary hydrocarbon discoveries.

The exploration well is planned to be spudded in the area during late 2012/early 2013 and will test hydrocarbon potential of the Veslemøy High area.



Discussion

Figure 4.12 Conceptual model showing suggested mechanisms involved in formation of the depressions on the R5 horizon in the study area. **A)** Initial stage of the glaciation when a slowly-moving ice sheet advances to the SW Barents Sea palaeo shelf break. **B)** Sketch showing the second stage of ice streaming associated with thinning of the glacier and an upward shift of the BGHSZ. Active erosion of the depressions and dislocation of sediment blocks and rafts is inferred. **C)** Deglaciation stage associated with rapid ice stream retreat and expulsion of the remaining fluids onto the seabed. Red dashed lines indicate deep-seated faults; HC is indicating deep hydrocarbon reservoirs; msl stands for the mean sea level and BGHSZ is indicating the base of the gas hydrate stability zone.

5 Conclusions

- Three-dimensional (3D) seismic techniques have allowed visualizing of buried geomorphologic features in great details in the Sørvestsnaget-Veslemøy area of the southwestern Barents Sea. Large sub-circular depressions and fluid migration pathways are imaged, as well as glacial sediment blocks and rafts.
- Several interpreted horizons reveal their glacial nature and inferred to be formed by grounded ice reaching study area and the shelf break during Pleistocene glaciations. Mega scale glacial lineations (MSGs) were formed on the buried horizons since the R5 time and are indicative for fast-flowing ice streams.
- Volumetric attributes reveal the presence of megablocks and rafts aligned in chains and lobes within the glacial packages GII and GIII between glacially eroded surfaces. A glacial origin is inferred for the megablocks and rafts based on their relationship with MSGs indicating high glaciogenic activity of the former ice streams.
- Six large-scale semi-circular depressions up to 270 m deep are mapped on the buried R5 horizon, formed during the first advance of the ice sheet to the shelf break. The elongated axes of the depressions are aligned with the orientation of the palaeo ice flow indicated from mega-scale glacial lineations on the same horizon.
- A relationship between glacial sediment blocks and depressions on the R5 horizon is inferred from long chains of sediment blocks emerging immediately downstream of or within interior of the depressions. The depressions are inferred to be sources for the removal of sediment mega-blocks and rafts in the lower part of the GII succession, eroded from the R5 horizon.
- Mapped fluid migration pathways and shallow gas accumulations show evidence of an active fluid migration system, and its spatial relationship with the erosional depressions is documented. Both vertical migration along faults and lateral migration along permeable beds is inferred from the 3D seismic data.
- Gas hydrate stability zone (GHSZ) modeling suggest repeated cycles of methane hydrate formation and dissociation associated with the glacial-interstadial periods. Hydrate

Conclusions

dissociation after the transition from a thick ice sheet to thinner, fast-flowing ice streams, as well as after deglaciation suggests increase in pore pressure leading to fluid expulsions. High-grade gas hydrate accumulations are suggested to be formed within permeable beds of the westward dipping GI unit, hence promoting their consolidation.

- A three stage model is proposed for the formation of large depressions on the buried R5 horizon. Brittle glaciotectionic deformation along a weak layer at the base of gas hydrate-cemented sediments is proposed, leading to subglacial erosion of the depressions and deposition of sediment blocks and raft accumulations downstream. Subsequent expulsion of gas-rich fluids is assumed to have followed deglaciation which might further have reworked the depressions.

6 References

- Aber, J. S., and Ber, A., 2007, *Glaciotectonism*, Elsevier Science, 243 p.:
- Aber, J. S., Croot, D. G., and Fenton, M. M., 1989, *Glaciotectonic landforms and structures*, Kluwer Academic Publishers.
- Andreassen, K., 1995, *Seismic reflections associated with submarine gas hydrates*. Doctor scientiarum thesis: University of Tromsø, 98 p.
- Andreassen, K., Laberg, J. S., and Vorren, T. O., 2008, Seafloor geomorphology of the SW Barents Sea and its glaci-dynamic implications: *Geomorphology*, v. 97, no. 1-2, p. 157-177.
- Andreassen, K., Nilssen, E. G., and Ødegaard, C. M., 2007,a, Analysis of shallow gas and fluid migration within the Plio-Pleistocene sedimentary succession of the SW Barents Sea continental margin using 3D seismic data: *Geo-Marine Letters*, v. 27, no. 2, p. 155-171.
- Andreassen, K., Nilssen, L. C., Rafaelsen, B., and Kuilman, L., 2004, Three-dimensional seismic data from the Barents Sea margin reveal evidence of past ice streams and their dynamics: *Geology*, v. 32, no. 8, p. 729.
- Andreassen, K., and Winsborrow, M., 2009, Signature of ice streaming in Bjornoyrenna, Polar North Atlantic, through the Pleistocene and implications for ice-stream dynamics: *Annals of Glaciology*, v. 50, no. 52, p. 17-26.
- Andreassen, K., Ødegaard, C., and Rafaelsen, B., 2007,b, Imprints of former ice streams, imaged and interpreted using industry three-dimensional seismic data from the south-western Barents Sea: Geological Society, London, Special Publications, v. 277, no. 1, p. 151-169.
- Badley, M. E., 1985, *Practical seismic interpretation*: , no. D. Reidel, Dordrecht (1985),, p. p. 266.
- Benn, D. I., and Evans, D. J. A., 2010, *Glaciers and glaciation*, Hodder Education.
- Bennett, M. R., Waller, R. I., Midgley, N. G., Huddart, D., Gonzalez, S., Cook, S. J., and Tomio, A., 2003, Subglacial deformation at sub-freezing temperatures? Evidence from Hagafellsjökull-Eystri, Iceland: *Quaternary Science Reviews*, v. 22, no. 8-9, p. 915-923.
- Bjørlykke, K., 2010, *Sequence Stratigraphy, Seismic Stratigraphy and Basin Analysis: Petroleum Geoscience*, p. 235-251.
- Bluemle, J. P., and Clayton, L. E. E., 1984, Large-scale glacial thrusting and related processes in North Dakota: *Boreas*, v. 13, no. 3, p. 279-299.
- Breivik, A. J., Faleide, J. I., and Gudlaugsson, S. T., 1998, Southwestern Barents Sea margin: late Mesozoic sedimentary basins and crustal extension: *Tectonophysics*, v. 293, no. 1-2, p. 21-44.
- Brown, A. R., 1999 *Interpretation of Three-Dimensional Seismic Data.: AAPG Memoir 42. SEG Investigations in Geophysics 9.*
- Brown, A. R., 2004, *Interpretation of three-dimensional seismic data*, Soc of Exploration Geophysicists.
- Bugge, T., Elvebakk, G., Fanavoll, S., Mangerud, G., Smelror, M., Weiss, H. M., Gjelberg, J., Kristensen, S. E., and Nilssen, K., 2002, Shallow stratigraphic drilling applied in hydrocarbon exploration of the Nordkapp Basin, Barents Sea: *Marine and Petroleum Geology*, v. 19, no. 1, p. 13-37.
- Bulat, J., 2005, Some considerations on the interpretation of seabed images based on commercial 3D seismic in the Faroe-Shetland Channel: *Basin Research*, v. 17, no. 1, p. 21-42.
- Butt, F. A., Drange, H., Elverhøi, A., Otterå, O. H., and Solheim, A., 2002, Modelling Late Cenozoic isostatic elevation changes in the Barents Sea and their implications for oceanic and climatic regimes: preliminary results: *Quaternary Science Reviews*, v. 21, no. 14-15, p. 1643-1660.
- Bünz, S., Mienert, J., and Berndt, C., 2003, Geological controls on the Storegga gas-hydrate system of the mid-Norwegian continental margin: *Earth and Planetary Science Letters*, v. 209, no. 3-4, p. 291-307.

References

- Bünz, S., Mienert, J., Bryn, P., and Berg, K., 2005, Fluid flow impact on slope failure from 3D seismic data: a case study in the Storegga Slide: *Basin Research*, v. 17, no. 1, p. 109-122.
- Canals, M., Urgeles, R., and Calafat, A. M., 2000, Deep sea-floor evidence of past ice streams off the Antarctic Peninsula: *Geology*, v. 28, no. 1, p. 31-34.
- Cartwright, J., Huuse, M., and Aplin, A., 2007, Seal bypass systems: *AAPG bulletin*, v. 91, no. 8, p. 1141.
- Chand, S., Mienert, J., Andreassen, K., Knies, J., Plassen, L., and Fotland, B., 2008, Gas hydrate stability zone modelling in areas of salt tectonics and pockmarks of the Barents Sea suggests an active hydrocarbon venting system: *Marine and Petroleum Geology*, v. 25, no. 7, p. 625-636.
- Chand, S., Thorsnes, T., Rise, L., Brunstad, H., Stoddart, D., Bøe, R., Lågstad, P., and Svolsbru, T., 2012, Multiple episodes of fluid flow in the SW Barents Sea (Loppa High) evidenced by gas flares, pockmarks and gas hydrate accumulation: *Earth and Planetary Science Letters*, v. 331–332, no. 0, p. 305-314.
- Clark, C. D., 1993, Mega-scale glacial lineations and cross-cutting ice-flow landforms: *Earth Surface Processes and Landforms*, v. 18, no. 1, p. 1-29.
- Clark, C. D., Tulaczyk, S. M., Stokes, C. R., and Canals, M., 2003, A groove-ploughing theory for the production of mega-scale glacial lineations, and implications for ice-stream mechanics: *Journal of Glaciology*, v. 49, no. 165, p. 240-256.
- Cofaigh, C. Ó., Taylor, J., Dowdeswell, J. A., and Pudsey, C. J., 2003, Palaeo-ice streams, trough mouth fans and high-latitude continental slope sedimentation: *Boreas*, v. 32, no. 1, p. 37-55.
- Crutchley, G., Gorman, A., Pecher, I., Toulmin, S., and Henrys, S., 2011, Geological controls on focused fluid flow through the gas hydrate stability zone on the southern Hikurangi Margin of New Zealand, evidenced from multi-channel seismic data: *Marine and Petroleum Geology*.
- Dalland, A., D., W., and K., O., 1988, A lithostratigraphic scheme for the Mesozoic succession offshore mid- and northern Norway.: *NPD-bulletin no.4*, v. 4, p. 87.
- Dillon, W., Danforth, W., Hutchinson, D., Drury, R., Taylor, M., and Booth, J., 1998, Evidence for faulting related to dissociation of gas hydrate and release of methane off the southeastern United States: *Geological Society, London, Special Publications*, v. 137, no. 1, p. 293-302.
- Durham, W. B., Kirby, S. H., Stern, L. A., and Zhang, W., 2003, The strength and rheology of methane clathrate hydrate: *J. Geophys. Res.*, v. 108, no. 2182, p. 1–11.
- Elverhøi, A., Dowdeswell, J. A., Funder, S., Mangerud, J., and Stein, R., 1998, Glacial and oceanic history of the polar North Atlantic margins: an overview: *Quaternary Science Reviews*, v. 17, no. 1-3, p. 1-10.
- Faleide, J., Gudlaugsson, S., Eldholm, O., Myhre, A., and Jackson, H., 1991, Deep seismic transects across the sheared western Barents Sea-Svalbard continental margin: *Tectonophysics*, v. 189, no. 1-4, p. 73-89.
- Faleide, J. I., Gudlaugsson, S. T., and Jacquart, G., 1984, Evolution of the western Barents Sea: *Marine and Petroleum Geology*, v. 1, no. 2, p. 123-150.
- Faleide, J. I., Solheim, A., Fiedler, A., Hjelstuen, B. O., Andersen, E. S., and Vanneste, K., 1996, Late Cenozoic evolution of the western Barents Sea-Svalbard continental margin: *Global and Planetary Change*, v. 12, no. 1-4, p. 53-74.
- Faleide, J. I., Tsikalas, F., Breivik, A. J., Mjelde, R., Ritzmann, O., Engen, O., Wilson, J., and Eldholm, O., 2008, Structure and evolution of the continental margin off Norway and the Barents Sea: *Episodes-Newsmagazine of the International Union of Geological Sciences*, v. 31, no. 1, p. 82-91.
- Faleide, J. I., Vagnes, E., and Gudlaugsson, S. T., 1993, Late Mesozoic-Cenozoic evolution of the south-western Barents Sea in a regional rift-shear tectonic setting: *Marine and Petroleum Geology*, v. 10, no. 3, p. 186-214.

- Fichler, C., Henriksen, S., Rueslaatten, H., and Hovland, M., 2005, North Sea Quaternary morphology from seismic and magnetic data: indications for gas hydrates during glaciation?: *Petroleum Geoscience*, v. 11, no. 4, p. 331-337.
- Fiedler, A., and Faleide, J. I., 1996, Cenozoic sedimentation along the southwestern Barents Sea margin in relation to uplift and erosion of the shelf: *Global and Planetary Change*, v. 12, no. 1-4, p. 75-93.
- Fisher, Q. J., Casey, M., Harris, S. D., and Knipe, R. J., 2003, Fluid-flow properties of faults in sandstone: the importance of temperature history: *Geology*, v. 31, no. 11, p. 965-968.
- Gabrielsen, R. H., Færseth, R. B., Jensen, L. N., Kalheim, J. E. a., and Riis, F., 1990, Structural elements of the Norwegian continental shelf, Part I. The Barents Sea Region: *Norwegian Petroleum Directorate Bulletin*, 6, p. 33.
- Glørstad-Clark, E., Faleide, J. I., Lundschieen, B. A., and Nystuen, J. P., 2010, Triassic seismic sequence stratigraphy and paleogeography of the western Barents Sea area: *Marine and Petroleum Geology*, v. 27, no. 7, p. 1448-1475.
- Gudlaugsson, S., Faleide, J., Johansen, S., and Breivik, A., 1998, Late Palaeozoic structural development of the south-western Barents Sea: *Marine and Petroleum Geology*, v. 15, no. 1, p. 73-102.
- Hambrey, M. J., Huddart, D., Bennet, M. R., and Glasser, N. F., 1997, Genesis of 'hummocky moraines' by thrusting in glacier ice: evidence from Svalbard and Britain: *Journal of the Geological Society*, v. 154, no. 4, p. 623-632.
- Heggland, R., 1998, Gas seepage as an indicator of deeper prospective reservoirs. A study based on exploration 3D seismic data: *Marine and Petroleum Geology*, v. 15, no. 1, p. 1-9.
- Henriksen, E., Bjørnseth, H., Hals, T., Heide, T., Kiryukhina, T., Kløvjan, O., Larssen, G., Ryseth, A., Rønning, K., and Sollid, K., 2011a, Uplift and erosion of the greater Barents Sea: impact on prospectivity and petroleum systems: *Geological Society, London, Memoirs*, v. 35, no. 1, p. 271-281.
- Henriksen, E., Ryseth, A., Larssen, G., Heide, T., Rønning, K., Sollid, K., and Stoupakova, A., 2011b, Tectonostratigraphy of the greater Barents Sea: implications for petroleum systems: *Geological Society, London, Memoirs*, v. 35, no. 1, p. 163-195.
- Hooper, E., 1991, Fluid migration along growth faults in compacting sediments: *Journal of Petroleum Geology*, v. 14, p. 161-180.
- Hovland, M., 1981, Characteristics of pockmarks in the Norwegian Trench: *Marine Geology*, v. 39, no. 1-2, p. 103-117.
- Hovland, M., Gardner, J. V., and Judd, A. G., 2002, The significance of pockmarks to understanding fluid flow processes and geohazards: *Geofluids*, v. 2, no. 2, p. 127-136.
- Hovland, M., and Judd, A. G., 1988, Seabed pockmarks and sepages: London, Graham & Trotman, p. 283.
- Hustoft, S., Dugan, B., and Mienert, J., 2009, Effects of rapid sedimentation on developing the Nyegga pockmark field: Constraints from hydrological modeling and 3-D seismic data, offshore mid-Norway: *Geochemistry Geophysics Geosystems*, v. 10, no. 6, p. Q06012.
- Hustoft, S., Mienert, J., Bünz, S., and Nouzé, H., 2007, High-resolution 3D-seismic data indicate focussed fluid migration pathways above polygonal fault systems of the mid-Norwegian margin: *Marine Geology*, v. 245, no. 1-4, p. 89-106.
- Judd, A., Hovland, M., Dimitrov, L., Garcia Gil, S., and Jukes, V., 2002, The geological methane budget at continental margins and its influence on climate change: *Geofluids*, v. 2, no. 2, p. 109-126.
- Judd, A. G., and Hovland, M., 1992, The evidence of shallow gas in marine sediments: *Continental Shelf Research*, v. 12, no. 10, p. 1081-1095.
- Judd, A. G., and Hovland, M., 2007, Seabed fluid flow: the impact of geology, biology and the marine environment, Cambridge Univ Pr.

References

- Knies, J., Matthiessen, J., Mackensen, A., Stein, R., Vogt, C., Frederichs, T., and Nam, S. I., 2007, Effects of Arctic freshwater forcing on thermohaline circulation during the Pleistocene: *Geology*, v. 35, no. 12, p. 1075.
- Knies, J., Matthiessen, J., Vogt, C., Laberg, J. S., Hjelstuen, B. O., Smelror, M., and Larsen, E., 2009, The Plio-Pleistocene glaciation of the Barents Sea-Svalbard region: a new model based on revised chronostratigraphy: *Quaternary Science Reviews*, v. 28, no. 9-10, p. 812-829.
- Kvenvolden, K. A., 1998, A primer on the geological occurrence of gas hydrate: Geological Society, London, Special Publications, v. 137, no. 1, p. 9-30.
- Laberg, J., Andreassen, K., and Knutsen, S. M., 1998, Inferred gas hydrate on the Barents Sea shelf—a model for its formation and a volume estimate: *Geo-Marine Letters*, v. 18, no. 1, p. 26-33.
- Laberg, J., and Vorren, T., 1993, A late Pleistocene submarine slide on the Bear Island trough mouth fan: *Geo-marine letters*, v. 13, no. 4, p. 227-234.
- Laberg, J., and Vorren, T., 1996, The Middle and Late Pleistocene evolution and the Bear Island Trough Mouth Fan: *Global and Planetary Change*, v. 12, no. 1-4, p. 309-330.
- Laberg, J. S., and Andreassen, K., 1996, Gas hydrate and free gas indications within the Cenozoic succession of the Bjørnøya Basin, western Barents Sea: *Marine and Petroleum Geology*, v. 13, no. 8, p. 921-940.
- Lammers, S., Suess, E., and Hovland, M., 1995, A large methane plume east of Bear Island (Barents Sea): implications for the marine methane cycle: *Geologische Rundschau*, v. 84, no. 1, p. 59-66.
- Larsen, E., Andreassen, K., Nilssen, L., and Raundalen, S., 2003, The prospectivity of the Barents Sea: Ice ages, erosion and tilting of traps.: NGU Report.
- Long, D., Lammers, S., and Linke, P., 1998, Possible hydrate mounds within large sea-floor craters in the Barents Sea: Geological Society, London, Special Publications, v. 137, no. 1, p. 223-237.
- Løseth, H., Gading, M., and Wensaas, L., 2009, Hydrocarbon leakage interpreted on seismic data: *Marine and Petroleum Geology*, v. 26, no. 7, p. 1304-1319.
- Maslin, M., Owen, M., Betts, R., Day, S., Jones, T. D., and Ridgwell, A., 2010, Gas hydrates: past and future geohazard?: *Philosophical Transactions of the Royal Society A: Mathematical, Physical and Engineering Sciences*, v. 368, no. 1919, p. 2369-2393.
- Max, M., and Johnson, A., 2011, Hydrate petroleum system approach to natural gas hydrate exploration ICGH 2011, p. 12.
- Max, M. D., 2003, *Natural gas hydrate in oceanic and permafrost environments*, Springer.
- Max, M. D., Johnson, A. H., and Dillon, W. P., 2006, *Economic geology of natural gas hydrate*, Kluwer Academic Pub.
- Mienert, J., Posewang, J., and Baumann, M., 1998, Gas hydrates along the northeastern Atlantic margin: possible hydrate-bound margin instabilities and possible release of methane: Geological Society, London, Special Publications, v. 137, no. 1, p. 275-291.
- Nilsen, E. G., 2006, 3D seismic interpretation of gas indications in Pliio-Pleistocene sediments at the Barents Sea margin: University of Tromsø, 131 p.
- NPD, 2011, <http://npdmap1.npd.no/website/npdgis/viewer.htm>, Volume 2011: ww.npd.no.
- Ottesen, D., Dowdeswell, J. A., and Rise, L., 2005, Submarine landforms and the reconstruction of fast-flowing ice streams within a large Quaternary ice sheet: The 2500-km-long Norwegian-Svalbard margin (57°–80°N): *Geological Society of America Bulletin*, v. 117, no. 7-8, p. 1033-1050.
- Perrodon, A., 1983, *Dynamics of oil and gas accumulations*, Editions TECHNIP.
- Pless, G., 2009, Occurrence of free gas and focused fluid systems in the Veslemøy High area, SW Barents Sea. Unpublished Master's thesis: University of Tromsø.
- Rafaelsen, B., Andreassen, K., Kuilman, L. W., Lebesbye, E., Hogstad, K., and Midtbø, M., 2002, Geomorphology of buried glacial horizons in the Barents Sea from three-dimensional seismic data: Geological Society, London, Special Publications, v. 203, no. 1, p. 259-276.

- Ryseth, A., Augustson, J. H., Charnock, M., Haugerud, O., Knutsen, S.-M., Midbøe, P. S., Opsal, J. G., and Sundsbø, G., 2003, Cenozoic stratigraphy and evolution of the Sørvestsnaget Basin, southwestern Barents Sea: *Norwegian Journal of Geology*, v. 83, p. 107-130.
- Sanchez-Borgue, J., 2009, Late Cenozoic paleoenvironments in the Veslemøy High area, SW Barents Sea based on 3D- and 2D- seismic data, unpublished Master thesis: University of Tromsø, 129 p.
- Schlumberger, 2010, *Interpreter's Guide to Seismic Attributes*.
- Selley, R. C., 1998, *Elements of petroleum geology*. San Diego, Academic Press Ltd.
- Sheriff, R. E., 2002, *Encyclopedic dictionary of applied geophysics*, Society of exploration geophysicists.
- Siebert, M. J., Dowdeswell, J. A., Hald, M., and Svendsen, J. I., 2001, Modelling the Eurasian Ice Sheet through a full (Weichselian) glacial cycle: *Global and Planetary Change*, v. 31, no. 1, p. 367-385.
- Sloan, E. D., and Koh, C. A., 2008, *Clathrate Hydrates of Natural Gases*: CRC Press, Boca Raton, FL.
- Sloan Jr, E., 1998a, Physical/chemical properties of gas hydrates and application to world margin stability and climatic change: *Geological Society, London, Special Publications*, v. 137, no. 1, p. 31-50.
- Sloan Jr, E. D., 1998b, *Clathrate hydrates of natural gases*, Marcel Dekker, New York, p. 641.
- Sloan Jr, E. D., 1998c, Gas hydrates: review of physical/chemical properties: *Energy & Fuels*, v. 12, no. 2, p. 191-196.
- Smelror, M., Petrov, O., Larssen, G. B., and Werner, S., 2009, *Geological History of the Barents Sea*: Geological Survey of Norway, Trondheim.
- Solheim, A., and Elverhøi, A., 1993, Gas-related sea floor craters in the Barents Sea: *Geo-Marine Letters*, v. 13, no. 4, p. 235-243.
- Solheim, A., Russwurm, L., Elverhøi, A., and Nyland Berg, M., 1990, Glacial geomorphic features in the northern Barents Sea: direct evidence for grounded ice and implications for the pattern of deglaciation and late glacial sedimentation: *Geological Society, London, Special Publications*, v. 53, no. 1, p. 253-268.
- Stoker, M. S., and Long, D., 1984, A relict ice-scoured erosion surface in the central North Sea: *Marine Geology*, v. 61, no. 1, p. 85-93.
- Stokes, C. R., and Clark, C. D., 1999, Geomorphological criteria for identifying Pleistocene ice streams: *Annals of Glaciology*, v. 28, no. 1, p. 67-74.
- Stokes, C. R., and Clark, C. D., 2002, Are long subglacial bedforms indicative of fast ice flow?: *Boreas*, v. 31, no. 3, p. 239-249.
- Sun, Q., Wu, S., Hovland, M., Luo, P., Lu, Y., and Qu, T., 2011, The morphologies and genesis of mega-pockmarks near the Xisha Uplift, South China Sea: *Marine and Petroleum Geology*.
- Sættem, J., 1990, Glaciotectonic forms and structures on the Norwegian continental shelf: observations, processes and implications: *Norsk geologisk tidsskrift*, v. 70, no. 2, p. 81-94.
- Sættem, J., Bugge, T., Fanavoll, S., Goll, R., Mork, A., Mork, M., Smelror, M., and Verdenius, J., 1994, Cenozoic margin development and erosion of the Barents Sea: Core evidence from southwest of Bjørnøya: *Marine Geology*, v. 118, no. 3-4, p. 257-281.
- Sættem, J., Poole, D., Ellingsen, L., and Sejrup, H., 1992, Glacial geology of outer Bjørnøyrenna, southwestern Barents Sea: *Marine Geology*, v. 103, no. 1-3, p. 15-51.
- Sættem, J., Rise, L., Rokoengen, K., and By, T., 1996, Soil investigations, offshore mid Norway: A case study of glacial influence on geotechnical properties: *Global and Planetary Change*, v. 12, no. 1, p. 271-285.
- Tulaczyk, S. M., Scherer, R. P., and Clark, C. D., 2001, A ploughing model for the origin of weak tills beneath ice streams: a qualitative treatment: *Quaternary International*, v. 86, no. 1, p. 59-70.
- Vorren, T. O., Hald, M., and Lebesbye, E., 1988, Late Cenozoic environments in the Barents Sea: *Paleoceanography*, v. 3, no. 5, p. 601-612.
- Vorren, T. O., and Laberg, J. S., 1997, Trough mouth fans--palaeoclimate and ice-sheet monitors: *Quaternary Science Reviews*, v. 16, no. 8, p. 865-881.

References

- Vorren, T. O., Richardsen, G., Knutsen, S. M., and Henriksen, E., 1991, Cenozoic erosion and sedimentation in the western Barents Sea: *Marine and Petroleum Geology*, v. 8, no. 3, p. 317-340.
- Winsborrow, M., Andreassen, K., Corner, G. D., and Laberg, J. S., 2010, Deglaciation of a marine-based ice sheet: Late Weichselian palaeo-ice dynamics and retreat in the southern Barents Sea reconstructed from onshore and offshore glacial geomorphology: *Quaternary Science Reviews*, v. 29, no. 3-4, p. 424-442.
- Winsborrow, M. C. M., Stokes, C. R., and Andreassen, K., 2011, Ice-stream flow switching during deglaciation of the southwestern Barents Sea: *Geological Society of America Bulletin*.